

2
AFML-TR-79-4173

LEVEL III

(2)

DISK RESIDUAL LIFE STUDIES

AD A089791

PART 1: F100 1ST-STAGE TURBINE DISK (IN100)

J. S. Cargill, J. K. Malpani, Y. W. Cheng

Pratt & Whitney Aircraft Group
Government Products Division
West Palm Beach, Florida 33402

SDTIC
ELECTED
OCT 1 1980

December 1979

Technical Report AFML-TR-79-4173, Part 1
Final Report for Period 1 April 1976 through 30 June 1979

Approved for public release; distribution unlimited

Prepared for
AIR FORCE MATERIALS LABORATORY
AIR FORCE WRIGHT AERONAUTICAL LABORATORIES
AIR FORCE SYSTEMS COMMAND
WRIGHT-PATTERSON AIR FORCE BASE, OHIO

FILE COPY

80 9 30 040

621021F

NOTICE

When Government drawings, specifications, or other data are used for any purpose other than in connection with a definitely related Government procurement operation, the United States Government thereby incurs no responsibility nor any obligation whatsoever; and the fact that the government may have formulated, furnished, or in any way supplied the said drawings, specifications, or other data, is not to be regarded by implication or otherwise as in any manner licensing the holder or any other person or corporation, or conveying any rights or permission to manufacture, use, or sell any patented invention that may in any way be related thereto.

This report has been reviewed by the Information Office (OI) and is releasable to the National Technical Information Service (NTIS). At NTIS, it will be available to the general public, including foreign nations.

This technical report has been reviewed and is approved for publication.



DR. W. REIMANN
Metals Behavior Branch
Metals and Ceramics Division



NATHAN G. TIPPER, Chief
Metals Behavior Branch
Metals and Ceramics Division

If your address has changed, if you wish to be removed from our mailing list, or if the addressee is no longer employed by your organization please notify AFVAL/MLLN, W-PAFB, OH 45433 to help us maintain a current mailing list.

Copies of this report should not be returned unless return is required by security considerations, contractual obligations, or notice on a specific document.

UNCLASSIFIED

SECURITY CLASSIFICATION OF THIS PAGE (When Data Entered)

UNCLASSIFIED SECURITY CLASSIFICATION OF THIS PAGE (When Data Entered)		REPORT DOCUMENTATION PAGE		READ INSTRUCTIONS BEFORE COMPLETING FORM	
1	REPORT NUMBER	2	GOVT ACCESSION NO.	3	RECIPIENT'S CATALOG NUMBER
(18)	AFML TR-79-4173-PM-1		AD-A089 791		
4	TITLE (and Subtitle)		5 TYPE OF REPORT & PERIOD COVERED		
(6)	DISK RESIDUAL LIFE STUDIES. Part I. F100 1st Stage Turbine Disk (CENT-100)		Final Report 1 Apr 1976-30 June 1979 PERFORMING ORGANIZATION REPORT NUMBER PWA-FR-11878-701-1		
(10)	J. S. Cargill, J. K. Malpani, Y. W. Cheng		(15) F33615-76-C-5172		
9	PERFORMING ORGANIZATION NAME AND ADDRESS		10 PROGRAM ELEMENT PROJECT, TASK AREA & WORK UNIT NUMBERS		
	Pratt & Whitney Aircraft Group Government Products Division West Palm Beach, FL. 33402		(16) 735106 C1 (17) 06		
11	CONTROLLING OFFICE NAME AND ADDRESS		12 REPORT DATE		
	Air Force Materials Laboratory (LLN) Air Force Wright Aeronautical Laboratories, AFSC Wright-Patterson AFB, OH		(11) December 1979		
14	MONITORING AGENCY NAME & ADDRESS (if different from Controlling Office)		13 NUMBER OF PAGES		
	(12) 112		102		
			15 SECURITY CLASS (of this report)		
			Unclassified		
			15a DECLASSIFICATION/DOWNGRADING SCHEDULE		
16	DISTRIBUTION STATEMENT (of this Report)				
	Approved for public release; distribution unlimited.				
17	DISTRIBUTION STATEMENT (of the abstract entered in Block 20, if different from Report)				
18	SUPPLEMENTARY NOTES				
19	KEY WORDS (Continue on reverse side if necessary and identify by block number)				
	Turbine engine disks Eddy current Nondestructive evaluation Fluorescent penetrant Fracture mechanics Acoustic emission				
23	ABSTRACT (Continue on reverse side if necessary and identify by block number)				
	A residual fatigue life prediction method, suitable for Retirement-for-Cause application, has been developed for two P&WA turbine disks: the F100 1st-stage high pressure turbine disk and the TF50 10th-stage compressor disk. The method is based upon interaction of fracture mechanics crack propagation modeling concepts with laboratory nondestructive evaluation (NDE) techniques. Fracture mechanics life models were developed using the GPD hyperbolic sine (SINH) model refined during an earlier Air Force Materials Laboratory (AFML) program. Stress intensity (K) solutions for the engine components were based upon experimental effective K determinations made during full-scale component fatigue tests. The NDE techniques developed for disk inspections included acoustic emission (AE), eddy current (EC), and fluorescent penetrants (FP). Stress-enhanced penetrant and semi-automated rotating probe EC techniques were developed as periodic inspections, while the AE time-domain technique was developed as a real-time inspection tool.				

DD FORM 1 JAN 73 1473 EDITION OF 1 NOV 65 IS OBSOLETE

UNCLASSIFIED

SECURITY CLASSIFICATION OF THIS PAGE (When Data Entered)

392887

B

FOREWORD

This is the final report for Contract F33615-76-C-5172, Disk Residual Life Studies, covering the period 1 April 1976 to 30 June 1979. It is divided into two parts relating to specific engine disk applications. Part 1 deals with F100 1st-stage turbine disk, while the subject of Part 2 is the TF30 10th-stage compressor disk. A third part is scheduled to be published in 1980 as the final report for an additional study entitled, "Concept Definition: Retirement-for-Cause of F100 Rotor Disks." The first two parts are being submitted in December 1979.

The Air Force Project Engineer is Dr. W. H. Reimann, AFML/LLN, Wright-Patterson AFB, Ohio. The Responsible Engineer/Program Manager is J. S. Cargill, reporting through J. A. Harris, Jr. to M. C. VanWanderham, General Supervisor, Mechanics of Materials and Structures, Pratt & Whitney Aircraft Group/Government Products Division, (P&WA/GPD) West Palm Beach, Florida 33402.

The authors wish to acknowledge the contributions to this program made by R. M. Wallace, former Program Manager, prior to his reassignment to his present position at the P&WA Dayton field office.

Accession For	
NTIS GEMM	<input checked="" type="checkbox"/>
DTIC TAB	<input type="checkbox"/>
Unannounced	<input type="checkbox"/>
Justification	<input type="checkbox"/>
By _____	
Distribution/	
Availability Codes	
Dist	Avail and/or Special
A	

CONTENTS

<i>Section</i>	<i>Page</i>
I INTRODUCTION	1
Phase I	3
Phase II	3
Phase III	3
Phase IV	4
Phase V	5
II EXPERIMENTAL METHODS	6
Laboratory Apparatus	6
Test Procedures	17
Acoustic Emission Inspection Procedures	19
Eddy Current Inspection Procedures	22
Fluorescent Penetrant Inspection Procedures	24
III TEST RESULTS	25
Strain-Controlled LCF	25
Fracture Mechanics Testing	29
Dovetail Specimens	35
Bolthole Specimens	41
Disk Inspections (Phase III)	49
Spin Study (Phase III)	56
Residual Life Studies (Phase IV)	58
IV DISCUSSION	63
Phase I — Acoustic Emission Fatigue Characterization	63
Stage I — Nucleation	63
Stage II — Microcrack Initiation	63
Stage III — Transition	63
Stage IV — Macrocrack Propagation	64
Phase II (Nondestructive Evaluation of Complex Geometry Specimens)	64
Phase III (NDE of the Turbine Disk)	66
Phase IV (Disk Residual Life Studies)	67
V CONCLUSIONS	81
Acoustic Emission	82
Eddy Current	82
Wink Fluorescent Penetrant	82
Static Fluorescent Penetrant	82
Replication (Transfer of Inspection Surface Details to Acetate Film, Microscopic Examination of Acetate Replica)	84
APPENDIX — Acoustic Emission Analysis	85
REFERENCES	101 & 102

ILLUSTRATIONS

<i>Figure</i>		<i>Page</i>
1	Residual Life Prediction as Applied to Retirement-for-Cause	2
2	Constant Strain LCF Specimen	6
3	P&WA/ GPD Component Life Analysis Group Test Area	6
4	AE Monitoring Configuration for LCF Strain Control Testing of GATORIZED® IN100 (PWA 1073)	8
5	AE Laboratory Apparatus Used for Continuous Inspections During Fatigue Testing	9
6	Modified Compact Tension Specimen	10
7	Bolthole LCF Specimen FML 96308A	11
8	Dovetail Groove LCF Specimen PWA 1073 $K_1 = 2.0$	11
9	Circograph Model 6.230 Rotating Probe EC Inspection Instrument	12
10	Defectometer Model 2.164 EC Inspection Instrument With Fixtures and Probes	13
11	F100 1st-Stage High-Pressure Turbine Disk, Made of GATORIZED® P/M IN100	13
12	Structural Test Laboratory "Ferris Wheel" Facility	14
13	EC Probe for Firtree Inspection of F100 1st-Stage Turbine Disk	14
14	The MMT Spin Rig Showing Vacuum and Turbine Lubrication Pumps and Turbine Box	15
15	The MMT Spin Rig Basic Configuration Showing the Drive Schematic	16
16	The Dunegan/Endevco Model 1032 Computerized AE System	16
17	Two-Dimensional Crack Source Location System for Engine Disks	18
18	Classical Representation of an AE Event	19
19	Distribution Analyzer Histogram, Normal Output	21
20	Q-Meter Inspection System for Ferrite Toroids	22
21	EC Probe Designs Used for Bolthole, Cooling Hole and Groove Inspections ...	23
22	Defectometer Model 2.164 EC Inspection Instrument With a Bolthole Edge-Sensitive Probe	24
23	AE Multiparameter Distribution Model for Fatigue Damage in Elevated Temperature IN100	27
24	LCF Specimen 217-4	28
25	LCF Specimen 217-1	30
26	LCF Specimen Fractured After Multiple Macrocrack Indications	31
27	Crack Growth Characteristics of IN100 at 1000°F, R = 0.1, 10 cpm	32
28	Crack Growth Characteristics of IN100 at 1200°F, R = 0.1, 10 cpm	33
29	Crack Growth Characteristics of IN100 at Room Temperature, R = 0.1, 10 cpm	34
30	Stress Intensity vs Average AE Rate for IN100 MCT Specimens	35
31	Dovetail Groove LCF Specimen S/N D-1 EC Defectometer Records	38
32	Dovetail Groove LCF Specimen S/N D-1 AE Distribution Histogram Records	39
33	Dovetail Groove LCF Specimen S/N D-5 AE Distribution Histogram Records	40
34	LCF Bolthole Specimen BR-1, 15,000-cycle Circograph EC Inspection Record	45
35	LCF Bolthole Specimen BR-1 Fracture Surface	45
36	LCF Specimen BR-4, 15,000-cycle Circograph EC Inspection Record	46
37	LCF Bolthole Specimen S/N BR-5 Fracture Mechanics Macrocrack Propagation Life Analysis	47
38	LCF Bolthole Specimen BR-5 Circograph Records	47
39	LCF Bolthole Specimen BR-5 Distribution Analyzer Histogram Records	48

ILLUSTRATIONS (Continued)

<i>Figure</i>		<i>Page</i>
40	LCF Bolthole Specimen BR-5 Fracture Surface	49
41	F100 1st-Stage Turbine Disk S/N BDB 257 Strain Gage Locations for Experimental Stress Analysis	51
42	Source Locate Characterization F100 1st-Stage HPT Disk Radial Cooling Holes	53
43	Recommended EC Probe Fixture for Disk Lug Inspections	55
44	Dunegan/Endevco Model 1032 Computerized AE System Transducer Arrays	56
45	AE Characterization of F100 Balance Weight Snap Ring	57
46	1st-Stage Turbine Disk Fatigue Crack Measurements, Radial Cooling Hole	59
47	Front View Showing Crack from Axial Cooling Hole at "Failure" Condition	61
48	K/ϵ vs a Relationship for F100 1st-Stage Turbine Disk Radial Cooling Hole ...	68
49	The Effect of Frequency on Crack Growth Rate at 1200°F, R = 0.1	70
50	Effect of Frequency on Sinh Model Coefficients C_2 and C_4 at 1200°F, R = 0.1	71
51	Effect of Stress Ratio on Crack Growth Rate at 1200°F, 10 cpm	72
52	Effect of Stress Ratio, R, on Sinh Model Coefficient, C_3 at 1200°F	73
53	Crack Growth Models for Phase IV Turbine Disk Tests	74
54	1st-Stage Turbine Disk S/N BAA43, Actual vs Calculated Crack Length, Radial Cooling Hole	75
55	Effect of Temperature on Sinh Coefficients, 1000-1350°F, $\nu = 2$ Minute Dwell, R = 0.1	76
56	1st-Stage Turbine Disk S/N OZ7463 Radial Cooling Hole Residual Life Analysis	77
57	Effect of Temperature on Sinh Coefficients, 1000-1350°F, $\nu = 10$ cpm, R = 0.1	78
58	1st-Stage Turbine Disk S/N BDB 257 Radial Cooling Hole Residual Life Prediction	79
59	AE Response During Total Fatigue Life of Wrought GATORIZED® IN100	81
60	A Simple Picture of an Acoustic Emission Event	85
61	Test No. 00265: Cumulative Emissions and Emissions Rate vs Cycles	87
62	Schematic Representation of Components in Energy Measuring Device	89
63	Log Amplification Characteristics of Dunegan/Endevco 920/921 Amplitude Distribution Analyzer	91
64	Burst Time Pulse Width Composed of Signal Pulse Width Plus Envelope Time (Manually Selected as 50 μ sec, 100 μ sec, 1 msec, and 10 msec)	92
65	Acoustic Emission Configuration to Monitor Strain Control Tests. Phase I: Acoustic Emission Characterization of Fatigue Damage	93
66	Typical Frequency Response of a Dunegan/Endevco Model D750 Transducer	94
67	Distribution Analyzer Output Example	96

TABLES

<i>Table</i>		<i>Page</i>
1	Turbine Disks for Phase IV Studies	19
2	LCF Strain Control Testing of IN100	25
3	Phase I Crack Propagation Testing of Virgin IN100.....	31
4	IN100 Dovetail Groove Simulation LCF Specimens Fatigue Test Inspection Records	36
5	IN100 LCF Bolthole Specimens Fatigue Test Inspection Records	41
6	F100 1st-Stage HPT Disk S/N BDB 257 Room Temperature Strain Survey	50
7	Acoustic Emission Source Location Inspection F100 1st-Stage HPT Disk S/N BM 798	54
8	Phase III Disk Inspection Record F100 1st-Stage HPT Disk S/N BM 798	54
9	Electrical Noise Assessment from Spin Configuration	58
10	1st-Stage Turbine Disk S/N BDB 257 Ferris Wheel Program Inspection Record	62
11	Calculated Macrocrack Propagation Lives for Phase II Specimens	66
12	Demonstration of Residual Life Prediction Procedure	80

SUMMARY

A residual fatigue life prediction method, suitable for Retirement-for-Cause application, has been developed for two P&WA turbine engine disks: the F100 1st-stage high pressure turbine disk and the TF30 10th-stage compressor disk. The method is based upon interaction of fracture mechanics crack propagation modeling concepts with laboratory nondestructive evaluation (NDE) techniques. Fracture mechanics life models were developed using the GPD hyperbolic sine (SINH) model, refined during an earlier Air Force Materials Laboratory (AFML) program Stress intensity (K) solutions for the engine components were based upon experimental effective K determinations made during full-scale component fatigue tests. The NDE techniques developed for disk inspections included acoustic emission (AE), eddy current (EC), and fluorescent penetrants (FP). Stress-enhanced penetrant and semiautomated rotating probe EC techniques were developed as periodic inspections, while AE time-domain technique was developed as a real-time inspection tool, resulting in the following observations.

- AE inspection is sensitive to unexpected defects in the *entire component*, as well as those in primary fracture critical locations.
- AE inspection is *not* limited to surface or near-surface defects.
- Application of AE techniques to real-time component inspection of operating gas turbine engines may be feasible.

SECTION I INTRODUCTION

Current turbine engine design systems necessitate early retirement of all critical components due to uncertainties in material fatigue behavior and routine inspection capabilities. When some conservative life limitation is reached, the critical components are retired, although non-destructive inspection generally indicates structural integrity comparable to virgin components. In the case of Government-owned engine disks alone, it has been estimated that replacement costs of undamaged disks will reach \$100,000,000 in the 1980 to 1985 time period (Reference 1).

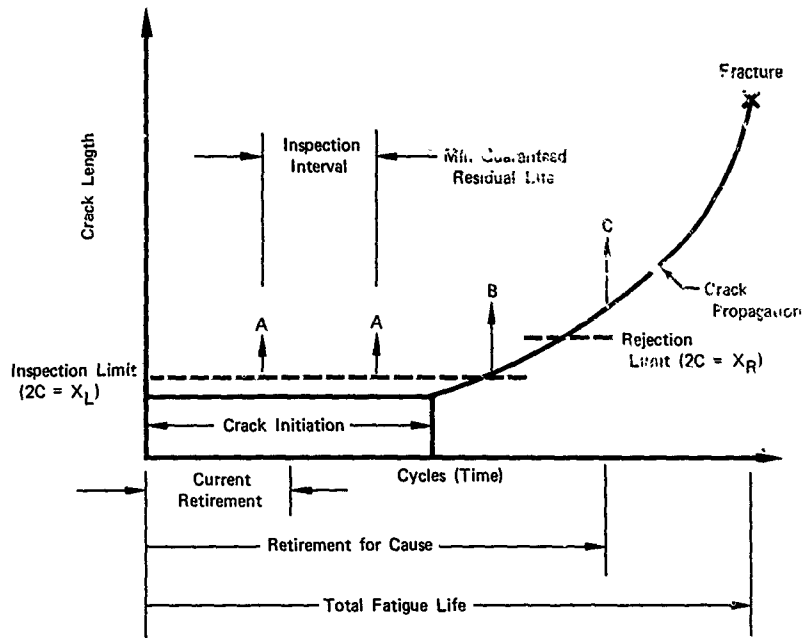
Increasing pressure at all Government levels to reduce costs and conserve basic materials and energy is resulting in major turbine engine assessment and redesign programs to better understand fatigue damage mechanisms and extend useful life of critical components through advanced design systems. In order to assure more economical engine operation, a primary segment of any advanced design system is NDE to reject potentially dangerous critical components and allow utilization of structurally sound components to the full extent of their design life. Buckley (Reference 2) researched the economic potential of advanced NDE techniques while employed by the AFML and concluded that "a synergism between the development of advanced NDE and the development of models to predict failure is essential for the realization of the overall economic potential that these fields offer."

The implication of *advanced NDE* has generally been *more sensitive techniques to detect small flaws*. However, D. P. Johnson (References 3 and 4) determined that cost-effectiveness of advanced NDE is a function of (1) the cost of manufacturing, (2) the cost of inspection, (3) the cost of failure, (4) the NDE rejection probability, (5) the flaw frequency, and (6) the probability of failure, given the fact that the material unit contains an imperfection of a given size. In other words, to establish the "optimum" NDE methodology for an advanced design system, there must be a consideration of economic factors, inspection uncertainties, and probability of component failure.

It was the intent of this program to establish a low-cycle fatigue (LCF) residual life prediction method for two engine disk components (the F100 1st-stage high pressure turbine disk and the TF30 10th-stage compressor disk) and project widespread, practical applications of the method. The results of this program will be instrumental in determination of the direction of a follow-on study, entitled "Concept Definition: Retirement-for-Cause of F100 Rotor Disks," through development and demonstration of a fracture mechanics minimum residual life prediction method which allows operation of critical engine components until quantifiable damage necessitates retirement. Fracture mechanics life predictions are based on the results of AFML Contract F33615-75-C-5097, "Applications of Advanced Fracture Mechanics Concepts to Crack Growth in Turbine Disks." These results have been published in three AFML Technical Reports and are listed as References 5, 6, and 7 in this report.

The optimum procedure for minimum residual LCF life prediction of the F100 1st-stage turbine disk has been determined to be an NDE methodology based on laboratory AE, EC, and FP inspections, combined with fracture mechanics and empirical modeling concepts. The concept of fracture mechanics/NDE-based Retirement-for-Cause is illustrated in Figure 1. Note that safety factors, such as multiple reinspections during a period of detectable subcritical crack growth, may be built into the system.

In applying this residual life prediction method to the TF30 10th-stage compressor disk, the procedure changed little. Periodic laboratory inspections were quantified according to reliability of fatigue crack detection in the primary critical location (axial bolthole).



- A - AE, EC, and FP Produce No Indications. Component Could Be Reinstalled
 B - AE, EC, and/or FP Produce Indication ($2C = X_i$), but $X_L \leq X_i < X_R$. Component Could Be Reinstalled
 C - AE, EC, and/or FP Produce Indication ($2C = X_{i+1}$), and $X_{i+1} \geq X_R$. Component Is Rejected

Note that the inspection interval could be chosen so that an undetected flaw would not propagate to failure in two periods between overhauls.

FD 148901

Figure 1. Residual Life Prediction as Applied to Retirement-for-Cause

The program technical approach consists of a five-phase effort including: (1) laboratory studies on simple specimen geometries, (2) laboratory studies to determine optimum inspection procedures for complex specimen geometries, (3) development of the optimum inspection procedure for the F100 1st-stage HPT disk, (4) demonstration of the residual life prediction procedure for the F100 1st-stage HPT disk and application methodology to a different disk material and geometry: the TF30 10th-stage compressor disk, and (5) the follow-on study "Concept Definition: Retirement-for-Cause of F100 Rotor Disks."

PHASE I

In the first phase of this program, laboratory studies on simple specimen geometries using AE multiparameter distributions, including signal pulse width, peak amplitude, and ringdown counts per event, were conducted during elevated temperature strain-control LCF testing of GATORIZED® IN100 to characterize the various stages of fatigue damage in the high-strength, powder-metallurgy nickel-base superalloy. The objectives of this phase were to characterize fatigue mechanisms in IN100 and establish the utility of AE for classifying these mechanisms. It was concluded from the test results that at least four different stages of fatigue damage in elevated temperature IN100 may be characterized using time-domain AE multiparameter distributions (Reference 8).

PHASE II

In the second phase, studies were performed to determine optimum inspection procedures for complex IN100 specimen geometries. Comparisons of inspection techniques included evaluations of the potential for Type I and Type II inspection errors. Remembering that it is a single crack size, a , that is being quantified (for the fracture mechanics analysis), the following definitions are made:

1. Type I errors include not detecting defects that are larger than a . These result in possible component failures.
2. Type II errors include identifying innocuous material anomalies or surface aberrations as real defects, thus creating high, costly rejection rates.

The FP, EC, and AE inspection techniques have been established as viable individual tools for detecting fatigue damage in turbine engine alloys (References 9 and 10), but the use of these three techniques (or any combination of techniques) as complementary inspections of complex engine component geometries has received little development. The primary impetus of Phase II research using complex geometry specimens was to establish the relative advantages and disadvantages of these various inspection techniques as applied to specific turbine engine disk fracture critical locations. Using Phase II results, an inspection methodology combining the three techniques as "complementary" inspections (each technique being used according to its particular set of advantages) was developed during Phase III for inspection of the F100 1st-stage HPT disk.

PHASE III

Phase III consisted of (1) development of the optimum inspection procedure for the F100 1st-stage HPT disk, (2) an experimental stress analysis of the disk, and (3) a study in the P&WA/GPD spin pit to determine feasibility of AE inspection during spin/proof testing of the disk.

An experimental stress analysis of the primary fracture critical location (radial cooling hole) was conducted using a strain gage survey. This stress analysis, along with an experimental fracture mechanics stress intensity determination, was used to form the basis for fracture mechanics residual life predictions. The experimental fracture mechanics stress intensity was determined from crack growth measurements taken during ferris wheel testing of a 1st-stage HPT disk. Crack growth/test cycle information was correlated with fracture mechanics specimen crack propagation rate (da/dN) data to produce an experimental stress intensity model for the disk region adjacent to the radial cooling hole.

Inspection procedures were refined and correlated using a fatigue-damaged subject disk. The disk was examined fractographically after Phase III NDE studies were complete to produce a baseline flaw detection/size determination for further correlation with inspection results.

The AE research in the P&WA/GPD spin pit was conducted using a computerized AE source location system and a simulated AE source to determine the feasibility of AE inspection of a rotating turbine engine component using state-of-the-art signal transfer and processing apparatus.

PHASE IV

Demonstration of the residual life prediction methodology for the F100 1st-stage HPT disk was performed on three engine-cycled disks, one of which was actually returned to an experimental engine for its minimum predicted residual fatigue life. Each disk was inspected using a combination AE, EC, and FP technique and fatigue-cycled to failure in the P&WA/GPD ferris wheel fixture. Fracture mechanics life characterizations were based upon the interpolative SINH model, and actual disk test conditions were modeled from specimen test data taken at various temperature, cyclic rate, and stress ratio conditions.

Application of the method to the TF30 10th-stage compressor disk was performed as a sister program with the Navy M-32 component life verification program. The Navy program funded the disk mechanical testing effort. Six TF30 compressor disks were subjected to engine-simulated fatigue damage in the MMT ferris wheel fixture, and residual life models were developed by MMT as periodic inspections were performed. GPD-Design is developing detailed fatigue models for this disk (under M-32 funding), but results are not yet available for comparison with MMT models.

The TF30 10th-stage compressor disk program will be discussed as Part 2 of this report to avoid possible confusion. Basic materials characterization, studies with complex geometry specimens, and fracture mechanics residual life models were developed for the compressor disk, as was performed for the F100 disks. The primary differences in the TF30 compressor disk program and the F100 turbine disk program include: (1) NDE reliability of periodic inspections was quantified for compressor disk laboratory inspections, and (2) fracture mechanics models were developed based upon simple cyclic testing of three disks and fracture mechanics specimens, and those models were projected to predict behavior of three additional disks tested to a duty-cycle simulation.

PHASE V (CONTRACT MODIFICATION, JUNE 1979)

The objective of this phase is to conduct a concept definition study of Retirement-for-Cause as it applies to the P&WA F100 turbofan gas turbine engine rotor disks. From this study, a means for developing a viable Retirement-for-Cause methodology, a means for determining a Return on Investment (ROI) for each component, an identification of required technology, and plans for acquisition, development, and implementation of Retirement-for-Cause techniques will be established. While the program is specifically directed at the F100 engine, an assessment of the applicability of Retirement-for-Cause to other P&WA engines such as the TF30, TF33, and J52 may be made. The P&WA Project Group will advise the Government in assessing applicability to other engines in the Government inventory.

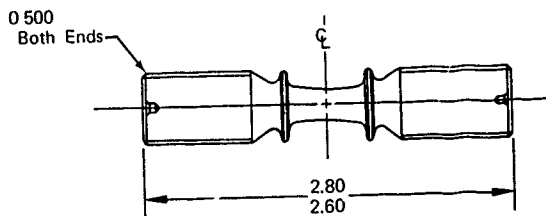
While the first four phases demonstrated feasibility of the Retirement-for-Cause concept from the laboratory life modeling/NDE standpoint, this concept definition phase will include factors which are crucial to field implementation. These factors include specialized field inspection problems, inspection economics, and possible fatigue situations (such as multiple initiations) which may not be accounted for in state-of-the-art fracture mechanics life models.

Results of "Concept Definition: Retirement-for-Cause of F100 Rotor Disks" will be published as Part 3 of this final report in mid-1980.

SECTION II EXPERIMENTAL METHODS

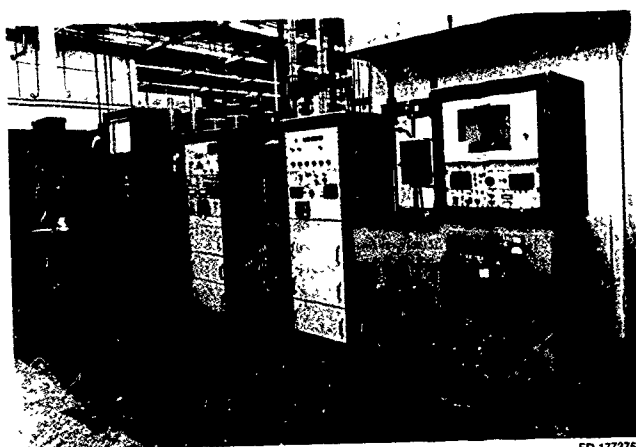
LABORATORY APPARATUS

Initial studies consisted of acoustic emission (AE) characterization of material (IN100) fatigue behavior during crack initiation and crack propagation studies. Low cycle fatigue (LCF) strain-controlled initiation testing was performed using the specimen configuration illustrated in Figure 2 by a servocontrolled, hydraulic test machine (Figure 3) developed at P&WA/GPD. Particular attention was focused on isolating the test load frame from extraneous vibration originating in the system hydraulics.



FD 177374

Figure 2. Constant Strain LCF Specimen



FD 177375

Figure 3. P&WA/GPD Component Life Analysis Group Test Area

AE laboratory apparatus used in the development of material characterizations was supplied by Dunegan/Endevco Corp., San Juan Capistrano, CA. The AE monitoring system and its configuration are illustrated schematically in Figure 4. The capability to monitor an AE event with three separate distribution analyzers was initially developed for P&WA by Dunegan/Endevco (Figure 5).

Modified compact specimens (Figure 6) were used for AE characterization of crack propagation in a simple specimen geometry. From the fracture mechanics tests, da/dN relationships were established at several temperature ranges.

Phase II studies of IN100 complex geometry LCF specimens for inspection technique assessment were conducted on two specimen geometries. Bolthole simulation and dovetail groove simulation LCF specimens are illustrated in Figures 7 and 8, respectively.

The eddy current (EC) bolthole inspections were conducted periodically using an Institute Dr. Forster Circog. Model 6 230 rotating probe instrument. The inspection fixture shown in Figure 9 was developed by P&WA/GPN NDT Engineering.

The EC inspections of dovetail groove simulation specimens were conducted with an Institute Dr. Forster Defectometer Model 2.164 instrument. The fixture illustrated in Figure 10 was developed by P&WA/GPD to maintain contact of a nonrotational probe with the specimen surface to minimize liftoff effects. The probes, which were designed and produced by P&WA/GPD - Quality Engineering, have also been used effectively during several engine disk inspection programs for evaluation of fatigue damage in broached slot regions.

Phase III development of the disk residual life prediction procedure involved the use of fatigue-damaged F100 1st-stage HPT disk S/N BM 798, for refinement and evaluation of inspection procedures (Figure 11). The disk was mechanically stressed in the P&WA/GPD ferris wheel fixture (Figure 12) for AE source location studies and to produce fatigue damage for EC and fluorescent penetrant (FP) studies. Another 1st-stage turbine disk, S/N BAA 43, was fatigue-cycled to failure in the ferris wheel, and crack length measurements were made periodically for an experimental stress intensity determination in the fracture critical region. S/N BAA 43 was also the subject of an experimental stress analysis program.

Centrifugal loads on engine disks can be conveniently simulated using the ferris wheel fixture. Radial loads are applied by means of pressurized hydraulic cylinders operating from a manifold and connected to drawbars simulating the blade/disk attachment configuration. Loads may be applied either in a steady-state condition, cyclic loading, or cycle loading with timed dwell at load. Elevated temperatures were achieved using resistance-heating ovens which sandwiched the test disk faces. Uniform temperatures in excess of 1200°F were accomplished by slowly rotating the entire fixture.

During Phase II, an EC probe was developed for inspection of the 1st-stage turbine disk blade attachment (firtree) regions. The fixture, shown in Figure 13, was designed to operate from the Defectometer Model 2.164 or, with installation of a balancing coil, the NDT Instruments Vector 111. The probe is capable of inspecting both the upper and lower disk broach slots on either side of the firtree.

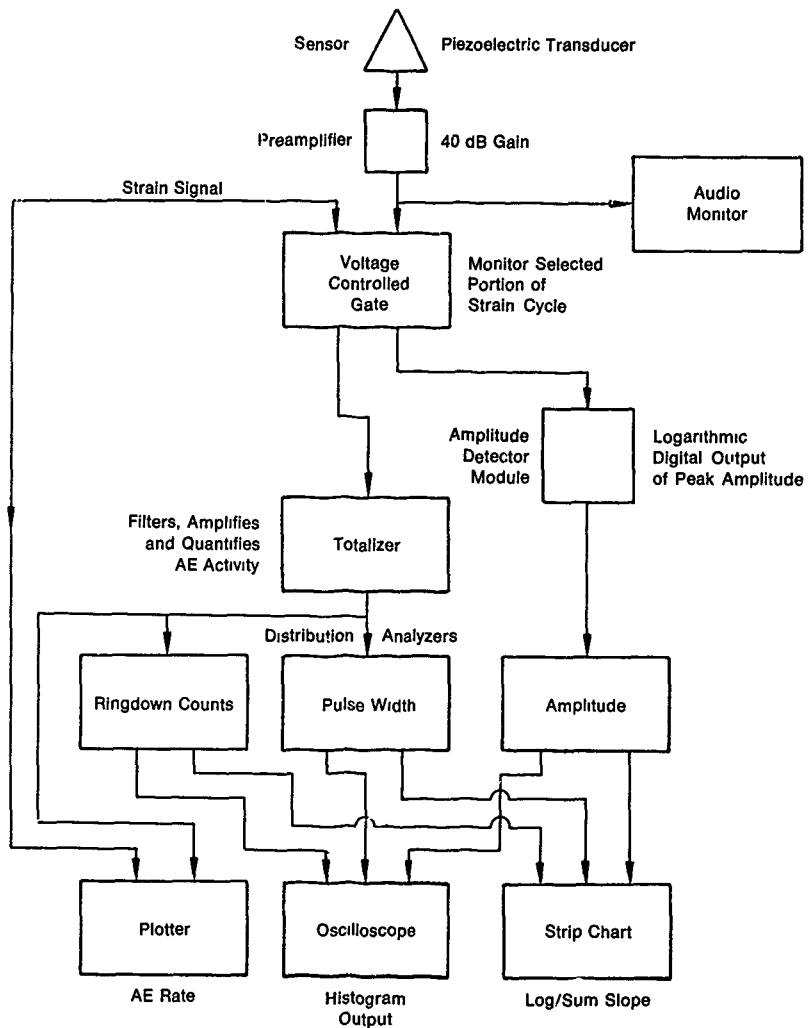
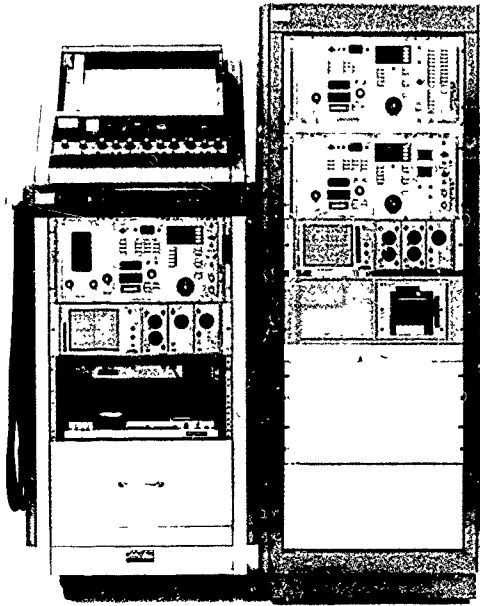


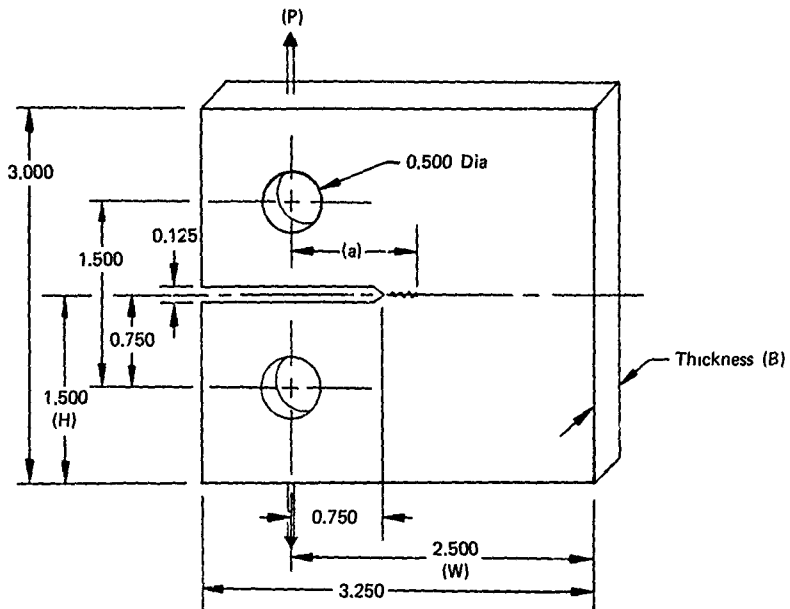
Figure 4. AE Monitoring Configuration for LCF Strain Control Testing of GATORIZED® IN100 (PWA 1073)

FD 164826



FAB 150354

Figure 5. AE Laboratory Apparatus Used for Continuous Inspections During Fatigue Testing



ΔK Calibration:

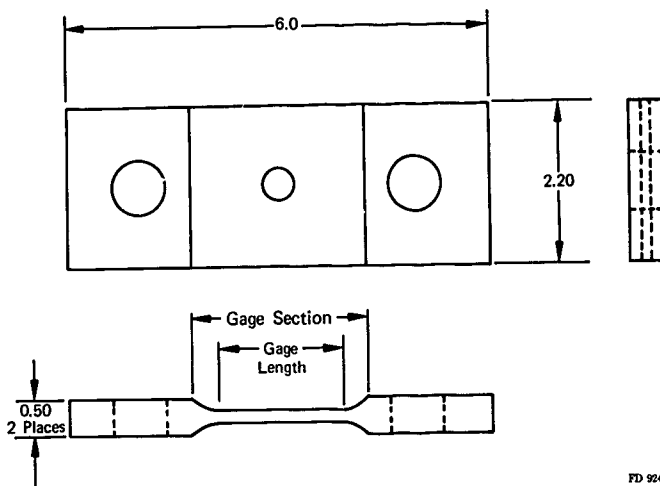
$$\Delta K = \frac{\Delta P}{B \sqrt{W}} \left[\frac{2+\alpha}{(1+\alpha)^{3/2}} (0.886 + 4.64\alpha - 13.32\alpha^2 + 14.72\alpha^3 - 5.6\alpha^4) \right]$$

where,

$\alpha = a/W$ (expression valid for $a/W \geq 0.2$)

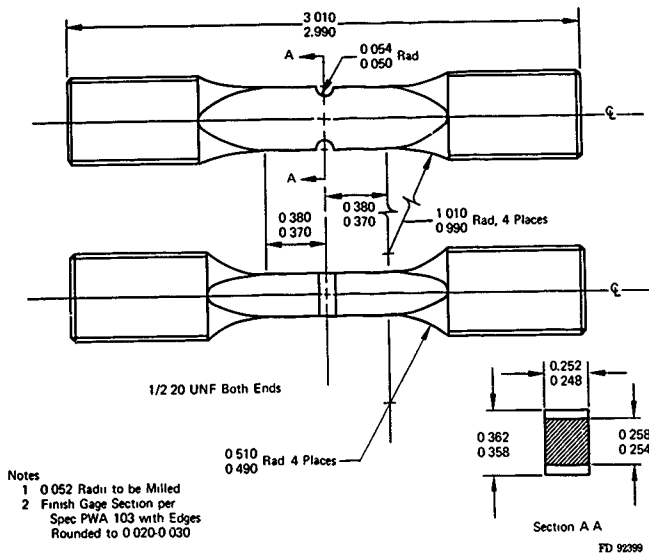
FD 8283A

Figure 6 Modified Compact Tension Specimen



FD 92414

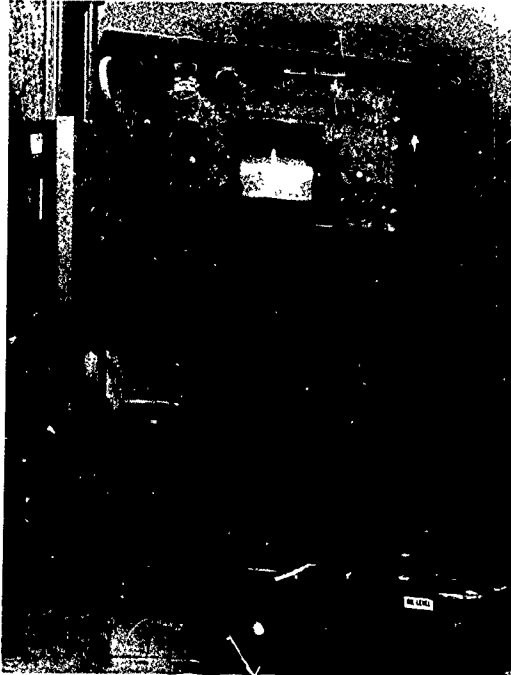
Figure 7. Bolthole LCF Specimen FML 96308A



- Notes
- 1 0.052 Radii to be Milled
 - 2 Finish Gage Section per Spec PWA 103 with Edges Rounded to 0.020-0.030

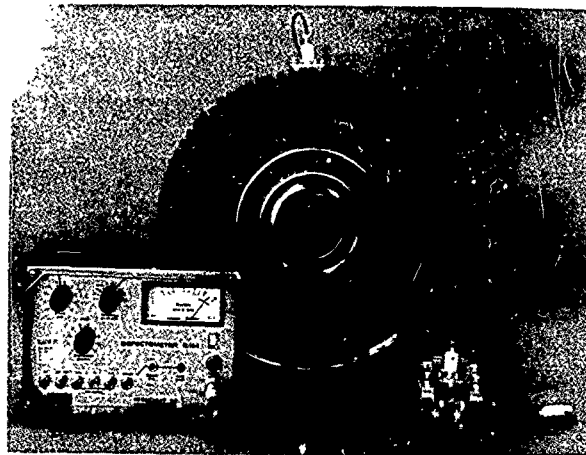
FD 92399

Figure 8. Dovetail Groove LCF Specimen PWA 1073 $K_1 = 2.0$



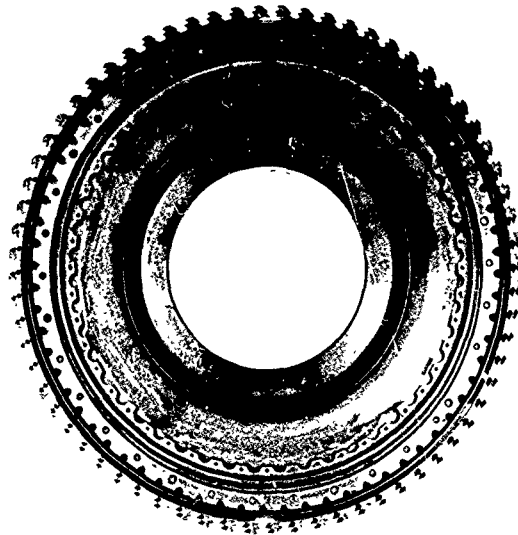
FAB 164650

Figure 9 *Circograph Model 6.230 Rotating Probe EC Inspection Instrument*



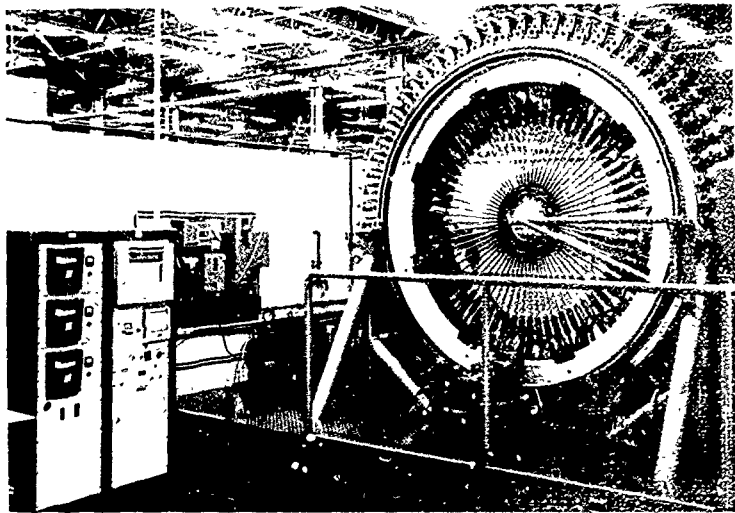
FAB 164649

Figure 10. Defectometer Model 2.164 EC Inspection Instrument With Fixtures and Probes



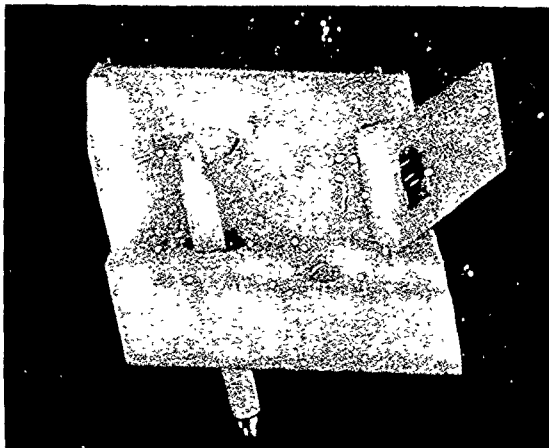
FD 150357

Figure 11. F100 1st-Stage High-Pressure Turbine Disk, Made of GATORIZED® P/M IN100



FD 112843

Figure 12. Structural Test Laboratory "Ferris Wheel" Facility



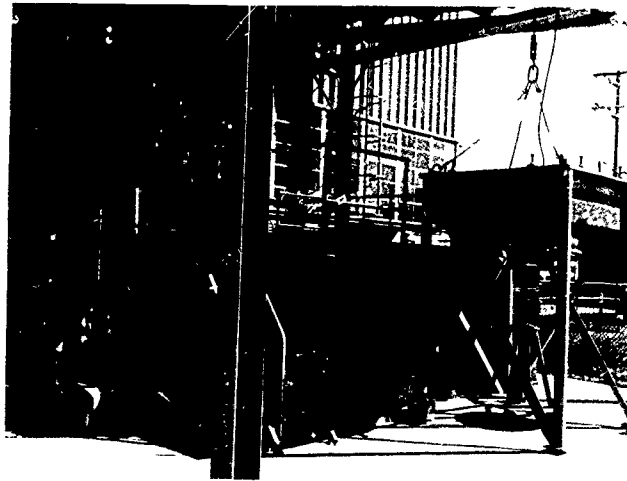
FD 136594

Figure 13. EC Probe for Firtree Inspection of F100 1st-Stage Turbine Disk

Phase III AE spin studies were performed at the P&WA/GPD Spin Rig Facility (Figures 14 and 15). The facility is used for centrifugal loading of complete engine disk assemblies for test purposes (including blades, as required). Test piece rotation is accomplished by means of an air-drive turbine (Barbour-Stockwell, Model 4146HD) which has a speed capability of 25,000 rpm when the test piece is contained in a rough vacuum in the range of approximately 300 to 100 μ . Drive and brake air can be alternately applied to the drive turbine under automatic control from a Hewlett-Packard dual-present controller/counter (Model 5332B) defining maximum and minimum speed limits when conducting speed cycle fatigue tests. Speed count is obtained from a magnetic pickup located in close proximity to a 60-tooth gear rotating on the drive turbine shaft and emitting voltage pulses that are counted over a period of time gated by the Hewlett-Packard counter.

Unique features not commonly found in most spin facilities include: (1) the use of scrap computer cards and/or paper as an energy-absorbing medium in the event of part burst, thus providing slow particle deceleration, minimum particle damage, and clean fracture faces for subsequent failure analysis, (2) vacuum enclosure only of the spinning part, making a higher vacuum possible for high-speed work and making possible the use of inexpensive scrap paper outside the workpiece vacuum can enclosure, and (3) still photography of the part burst condition, capturing the initial moment of particle separation, providing failure mode information.

A computerized AE system, Dunegan/Endevco Model 1032, was used during the spin studies to provide an automatic source determination of the simulated AE produced by a pulsing transducer. The system, shown in Figure 16, uses a four-sensor array for AE source determination (by time-difference calculations) and noise discrimination. The system is capable of simultaneously accepting input from eight different transducer arrays and displaying source information on a storage CRT and high-speed teleprinter. Gain is adjustable for each transducer from 40 to 99 dB. The system threshold is manually adjustable.



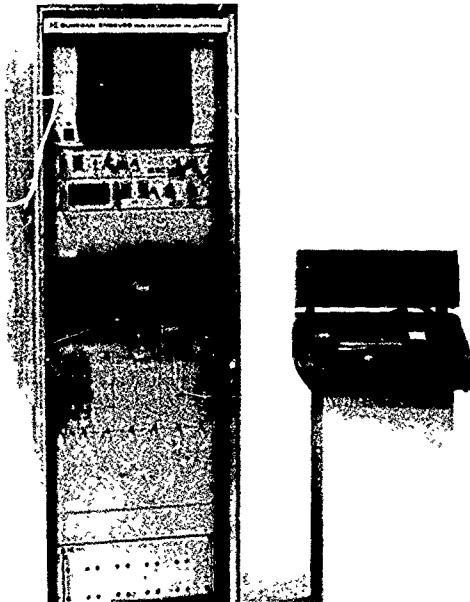
FC 23810

Figure 14. The MMT Spin Rig Showing Vacuum and Turbine Lubrication Pumps and Turbine Box



FC 23923

Figure 15. The MMT Spin Rig Basic Configuration Showing the Drive Schematic



FE 162735

Figure 16 The Dunegan/Endevco Model 1032 Computerized AE System

Phase IV inspections of F100 1st-stage turbine disks were conducted periodically using a Group VI FP system and the Circograph 6.230 for periodic inspections. The Dunegan/Endevco 3000 series AE instrumentation was used for continuous real-time inspection during fatigue testing.

TEST PROCEDURES

LCF strain controlled testing of IN100 was conducted at temperatures and strain levels which simulated localized operating conditions at the fracture critical location in an advanced gas turbine disk

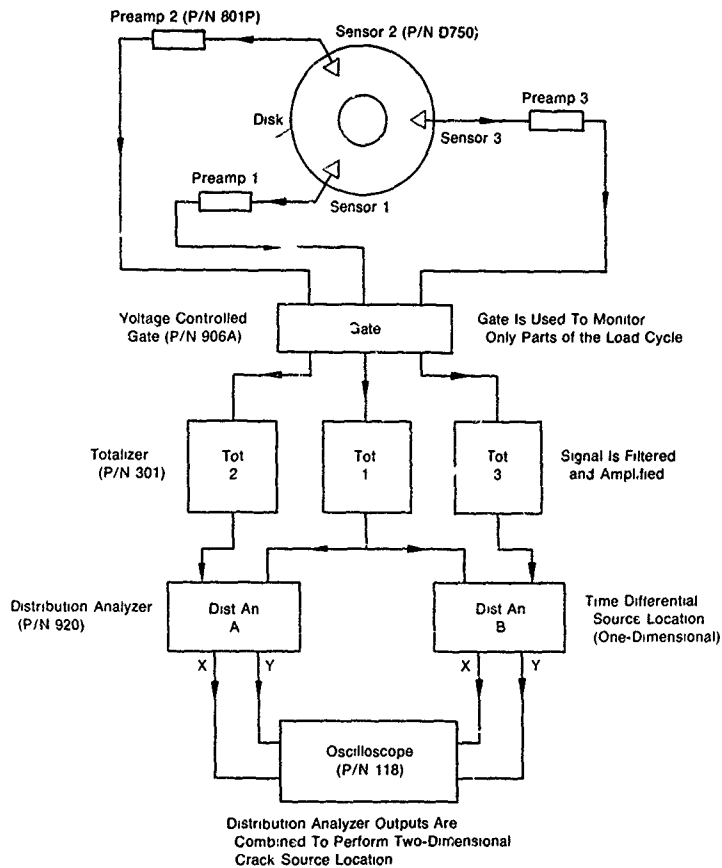
During initial AE monitoring, adjustments were made to the sampling parameters, including system gain, amplitude threshold and voltage controlled gate (operating from the strain signal) to establish the optimum balance between system sensitivity and rejection of extraneous mechanical and electrical noise. Adjustments were also made to distribution analyzer processing parameters (multiplier and signal envelope) to establish operating ranges which best characterize the AE signals associated with nickel alloy fatigue cracks. The AE sensor attachment was made directly to the load rod below the test specimen.

Strain-control LCF testing is accomplished through the use of a special specimen configuration (Figure 2) with integral collars for attachment of an extensometer. Electronic proximity probes are operated from the extensometer.

Phase II dovetail groove simulation specimens were tested at temperatures ranging from 800 to 1200°F and net stresses to 133 ksi ($R = 0.05$, producing strain ranges up to 1.07%). The AE inspection was performed continuously, with the transducer mounted directly to the load train, while periodic EC and FP inspections were conducted at intervals from 2000 to 4000 fatigue cycles (depending upon specimen fatigue life predictions). Several specimens were tested to failure while others were left intact as calibration standards.

Fatigue damage was produced in bolthole simulation specimens by cycling at net stresses up to 144 ksi ($R = 0.05$). Test temperatures ranged from room temperature to 1200°F. AE time-domain inspection was performed continuously, with the waveguide-mounted transducer attached outside the specimen gage section.

F100 1st-stage turbine disk S/N BM 798 was subjected to fatigue damage in experimental engine S/N P050 and in the ferris wheel fixture for Phase III nondestructive evaluation (NDE) studies. Fatigue macrocracks were detected at several rim locations using EC and FP techniques. Phase III AE studies were conducted at elevated temperature (1200°F) with three sensors mounted 120-deg apart on 6-in. waveguides. Waveguides were attached at small (No 4-40) drilled and tapped holes in the ends of disk firtrees. The AE apparatus used for two-dimensional source location studies is illustrated schematically in Figure 17.



FD 106760

Figure 17. Two-Dimensional Crack Source Location System for Engine Disks

Phase IV residual life predictions were conducted on three engine-cycled 1st-stage turbine disks. All three disks were bore-modified to produce a local stress distribution in the ferris wheel similar to that experienced in the engine. Bore modification was necessary to produce a realistic stress distribution at the fracture critical locations (radial cooling holes), but the procedure was not required for AE inspection of the disk rim regions in the ferris wheel. Pertinent operational data are listed in Table 1.

TABLE 1
TUREINE DISKS FOR PHASE IV STUDIES

Disk S/N	Heat Code	Experience Engine	Engine LCF Cycles		
			Type I	Type II	Type III
BAA 43	BADH	FX 217	259	—	1052
OZ 7463	ZWXW	PO 37	1001	—	—
BDB 257	BADV	FX 221	3425	25	5867

ACOUSTIC EMISSION INSPECTION PROCEDURES

AE Rate Analysis

Typically, an AE event from the receiving transducer may be represented as a damped sinusoid (Figure 18). The AE "counts" are measured as the system threshold is exceeded in the positive direction. An AE rate analysis indicates the number of times the preset threshold has been crossed during one test cycle, regardless of the absolute number of AE events, or wave packets, that may have been received.

AE rate is the most commonly used form of AE inspection to determine variations in mechanical stress wave activity from a specimen or component which is experiencing cyclic loading.

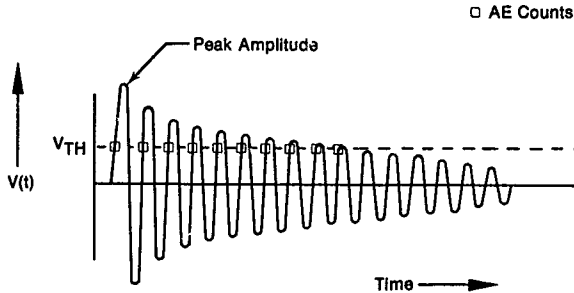


Figure 18 Classical Representation of an AE Event

FD 148902

Amplitude Distribution

Amplitude distribution analysis is an important mode of AE signal processing and probably the most widely accepted form of distribution analysis. The Dunegan/Endevco analyzer displays a transduced signal peak amplitude. A linear AE signal is converted to logarithmic form thereby creating a wide dynamic range. The log-amplified signal is peak detected and an analog-to-digital converter then outputs a series of 0 to 100 pulses that represent peak amplitude in decibels, with 1 dB resolution.

The summed peak amplitude distribution function, $E(V_o)$, is the number of events with amplitudes exceeding a given voltage value, V_o . It is of the form:

$$E(V_o) = KV_o^{-b} \quad (1)$$

where, K and b are constants for a given increment of loading on a structure. The exponent, b , is sensitive to changing distribution patterns and has therefore been used as an indicator of general structural integrity in monotonic loading situations.

In the logic of the distribution analyzer, each pulse represents the ratio of the input signal to $100\mu V$ (in decibels) through the relation:

$$\text{Pulse} = 20 \log \left(\frac{V_o}{100\mu V} \right)$$

Pulse Width Distribution

The pulse width distribution analyzer counts the time (10 μ sec resolution) that an envelope processor is energized, i.e., pulse width per event. An event is defined when the processor is energized at the first pulse of a burst. It remains energized during the burst and stays energized for a fixed envelope time after the last pulse of the burst above threshold. The end of the envelope time is defined as the end of an event. Total time the processor is energized is the burst pulse width.

Ringdown Counts Per Event

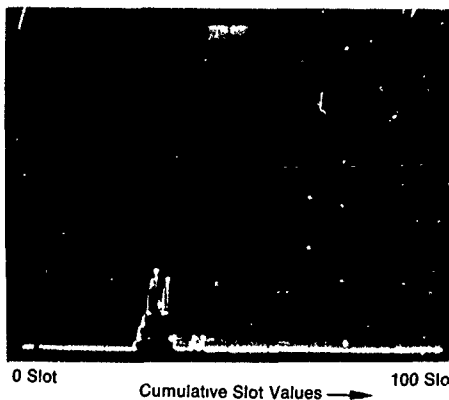
The ringdown counts distribution analyzer monitors the number of threshold crossings in each AE event. For a perfectly resonant transducer with a narrow frequency band, ringdown counts per event, pulse width, and peak amplitude would all be directly related when monitoring rapidly-decaying burst-type AE. The transducers used during this program were uniformly sensitive (within 5dB) over a 300 kHz bandwidth, having a resonant frequency near 650 kHz. Though the burst-type AE monitored during LCF testing displayed exponential decay in many cases, the three distributions functioned somewhat independently with amplitude being the most autonomous.

Source Location and Analyzer Operation

The Dunegan/Endevco Model 920 Distribution Analyzer sorts AE events (bursts) according to time-domain signal characteristics (pulse width, peak amplitude, ringdown counts, or one-dimensional source location). Each processed event is assigned a "slot" value from 0 to 100 according to the selected time-domain analysis, full-scale selection, and signal value. Analyzer output is then displayed in histogram form with slot values displayed along the X-axis and number of events assigned to each slot displayed along the Y-axis.

Figure 19 is an oscilloscope representation of a typical analyzer output. For example, if the analyzer had been operating in a one-dimensional source-locate mode, the X-axis would represent the distance (divided into 100 increments) between a transducer located at "0" and a second transducer located at "100". The Y-axis output would display the number of AE events whose source locations correspond to each of the 100 distance increments. Events whose sources are outside the boundaries determined by the two transducers are automatically assigned to either slot value 0 or 100.

Y Axis.
Number of Events at
Each Slot Value



Y Axis May Be Selected
as a Logarithmic Scale

Y Axis: Slot Values

FD 118578A

Figure 19 Distribution Analyzer Histogram, Normal Output

As an example of one-dimensional source location, suppose transducers 0 and 100 were located 100-in. apart on a length of pipe which is being proof tested. Each slot value (X-axis) would correspond to a 1-in. increment of pipe. If, as the test progressed, the distribution analyzer output appeared as in Figure 19, the test engineer would suspect structural damage in a region located roughly one third of the distance between the transducers. The bulk of acoustic activity occurs between slot locations 28 and 44, with highest registry occurring at slot 32.

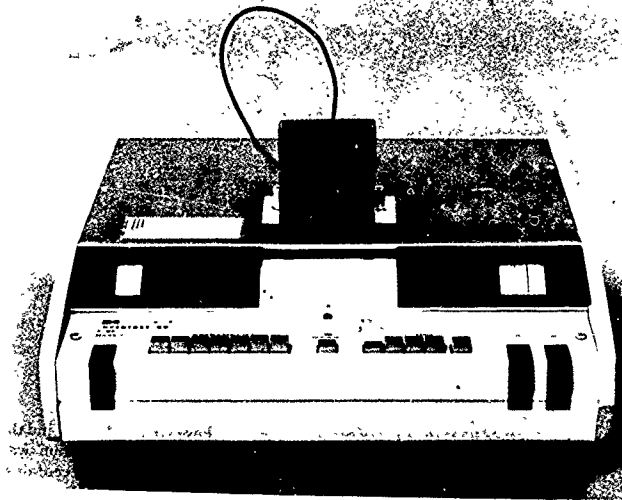
To conduct two-dimensional source location on a disk configuration, one more transducer and an additional distribution analyzer are required. Transducers are placed 120-deg apart near the disk outside diameter, different pairs of transducers are assigned to each of the two analyzers, and the surface is mapped using a transmitting transducer. Response from each analyzer is recorded as the transmitter (simulated AE) is placed at various locations on the disk. Finally, curved lines of constant analyzer readings are mapped along the disk for each distribution analyzer and the two-dimensional source location of an event is determined by the intersection of two of these lines. Two-dimensional source location analysis may be performed on many other surface configurations using similar methods, while the introduction of a third distribution analyzer permits three-dimensional analysis in specialized cases. See the Appendix to this report for a more detailed discussion of the principles of acoustic emission analysis.

EDDY CURRENT INSPECTION PROCEDURES

All EC probes used in this program were designed and manufactured by P&WA/GPD to maintain a characteristic inductance of $60 \pm 0.1 \mu\text{H}$. This rigid standard is economically upheld through the inspection of all ferrite toroids by a Q-meter type inspection system shown in Figure 20 (also developed at P&WA/GPD) before coils are wound and probes actually fabricated. Many supposedly high-sensitivity ferrites are rejected due to insufficient initial permeability. Typically, the toroids range in size from 0.100 to 0.150-in. diameter. Probe designs used for bolthole, cooling hole, and groove inspections are illustrated in Figure 21.

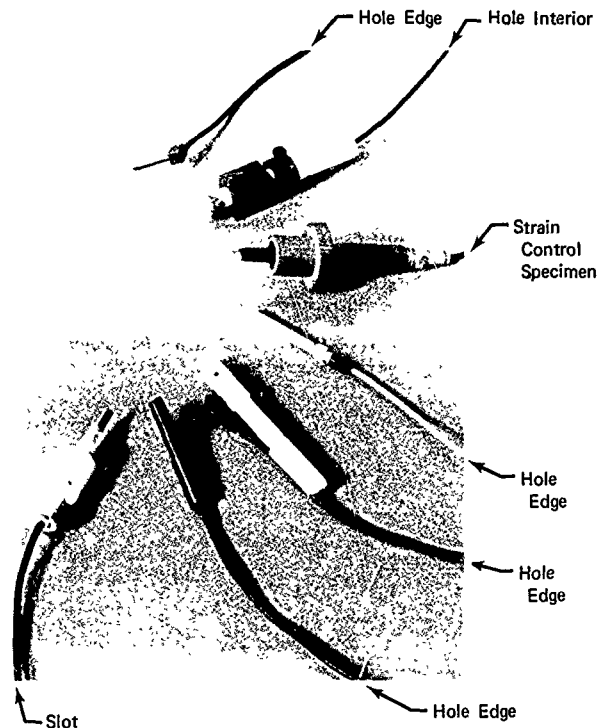
Circograph-type inspection of a disk radial cooling hole or bolthole simulation specimen is performed while a rotating probe (differentially wound) is lowered into the bolthole, never actually making contact with the specimen. Any defect inside the bolthole will disturb the passing EC field and a processed signal from the defect will appear on the Circograph storage oscilloscope. This is made possible by synchronous action of the rotating shaft and the scope, producing a 360-deg sweep of the bolthole with each sweep of the scope.

Photographs were taken of many Circograph indications for quantitative assessments of crack indications as the specimens were subjected to more fatigue cycles.



FE 164651

Figure 20. Q-Meter Inspection System for Ferrite Toroids

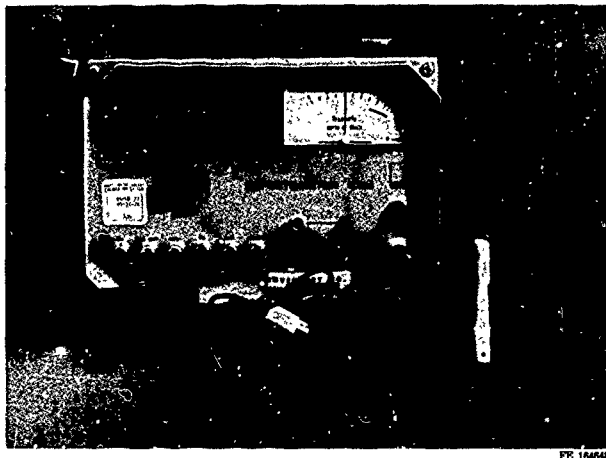


FD 131173

Figure 21. EC Probe Designs Used for Bolthole, Cooling Hole and Groove Inspections

Defectometer-type inspections were conducted on the Phase III disk firtrees and the bolthole and dovetail groove simulation specimens. The Circograph bolthole inspection was complemented by a bolthole edge-sensitive inspection performed with a probe which contains a partial horseshoe-shaped coil capable of bridging the edge of a hole. This complementary inspection, performed by the system shown in Figure 22, is especially important when fatigue cracks are introduced by stress concentrators at bolthole edges, and liftoff effects mask any edge indications produced by the Circograph.

As seen previously in the lower right corner of Figure 10, IN100 dovetail groove simulation specimens were held securely in a plexiglass fixture. Crack indications were produced by passing a probe back and forth along a slot in the fixture which allowed chatter-free contact of the probe with the specimen surface. The probe was typically passed to each end of the specimen slot until edge effects precluded any further inspection



FE 104648

Figure 22. Defectometer Model 2.164 EC Inspection Instrument With a Bolt-hole Edge-Sensitive Probe

Initially, preinspection surface preparation was conducted by applying a mild abrasive (crocus cloth) to the specimen. This procedure was later replaced by a stronger abrasive to remove residual oxidation layers.

FLUORESCENT PENETRANT INSPECTION (FPI) PROCEDURES

Static FPI was conducted by (1) applying Zyglo ZL 30 oil-base fluid, (2) allowing a 15-minute soak period, (3) wiping the suspect regions with cleaner on a cotton swab, (4) applying developer, and (5) inspecting the specimen in a darkroom with a black light, often using a magnifying lens

Static FPI was augmented by wink FPI while phase II specimens were installed in the fatigue test machine. This form of inspection proved to be much more sensitive to small fatigue cracks than static FPI. Wink FPI was performed by loading a specimen in the fatigue test machine to the maximum cyclic load, applying ZL 30 fluid, wiping with cleaner, unloading the specimen, applying developer, and inspecting with a black light. This procedure was later revised for compression disk inspections.

SECTION III
TEST RESULTS-F100 1ST STAGE TURBINE DISK

STRAIN-CONTROLLED LCF

The fatigue process at a typical engine disk fracture critical location, such as a bolt or cooling hole, has been proven during several programs at P&WA/GPD to be strain controlled. Strain-controlled LCF tests were conducted during Phase I to simulate AE output from IN100 turbine disk fracture critical locations during LCF

Twenty-two LCF strain control specimens from five different heats of IN100 were tested while monitoring with AE multiparameter distributions. Multiparameter time domain distributions included AE amplitude, pulse width, and counts-per-event analyses. Specimen test conditions, cycles to failure, and other pertinent data are listed in Table 2.

TABLE 2 LCF STRAIN CONTROL TESTING OF IN100

Specimen Number	Material Source	Engine LCF Cycles	Test Strain Level* (%)	Test Temp (°F)	Test Cycles	Remarks
217-1	Disk FX 217**	1,761	10	1000	9,984	Macrocracked
217-2	Disk FX 217	1,761	10	1000	4,559	Fractured.
217-3	Disk FX 217	1,761	10	1000	310	Specimen overstrained Test discontinued
217-4	Disk FX 217	1,761	10	1000	4,200	Test stopped for microcrack inspection
SC-1	Disk BDB 257**	1,123	10	1000	2,279	Macrocracked
SC-3	Disk BDB 257	1,123	10	1000	3,356	Fractured.
036-1	Disk PO36**	1,001	10	1000	3,811	Test stopped for microcrack inspection.
036-2	Disk PO36	1,001	10	1000	9,974	Fractured
036-3	Disk PO36	1,001	10	1000	2,225	Fractured
036-4	Disk PO36	1,001	10	1000	1,670	Macrocracked
V-7	Virgin Forging	None	10	1000	3,482	Fractured
V-8	Virgin Forging	None	12	1000	1,967	Fractured
V-9	Virgin Forging	None	10	1000	3,837	Macrocracked
V-10	Virgin Forging	None	10	1000	6,027	Fractured
V-11	Virgin Forging	None	10	1000	9,574	Fractured
V-12	Virgin Forging	None	10	1200	2,647	Fractured
V-13	Virgin Forging	None	10	1000	5,310	Fractured.
V-14	Virgin Forging	None	10	1000	2,700	Fractured.
V-15	Virgin Forging	None	10	1000	5,460	Fractured.
V-17	Virgin Forging	None	0.8	1200	8,845	Test stopped for microcrack inspection.
V-21	Virgin Forging	None	10	1000	3,325	Fractured
V-22	Virgin Forging	None	10	1000	8,487	Fractured

*Mean Strain = 1/2 Maximum Strain

**Engine cycled material

Typically, acoustic and distribution analyses during the course of a strain-controlled IN100 LCF test may be modeled as:

1. A period of initial shakedown. The AE rate registry is high. Pulse width, ringdown counts per event, and amplitude distributions reflect AE bursts with greatly varying characteristics.
2. A stable period. The AE rate decreases and the AE distributions indicate bursts with relatively short pulse widths, few ringdown counts per event, and low peak amplitudes.
3. Maximum AE signal pulse widths and maximum ringdown counts per event suddenly increase (possibly several times during this portion of the test), but AE signal peak amplitudes change relatively little. The AE rate may slightly increase.
4. Another stable period. AE distributions again indicate bursts with relatively short pulse widths, fewer ringdown counts per event and unchanged signal peak amplitudes. The AE rate is low.
5. A general increase in AE activity to specimen failure. The AE rate may increase two or more orders of magnitude. The AE distributions indicate burst registries with longer pulse widths, increased ringdown counts per event and higher peak amplitudes.

The above phenomena are represented graphically in Figure 23.

Testing of three specimens (036-1, V-17, and 217-4) was discontinued during period "3" for surface and internal inspections of the gage sections. External inspections were performed using EC and FP techniques, while the internal inspection procedure included sectioning each specimen axially and polishing through the inspection surface while microscopically scanning at 100X to 1600X. Thin-foil microscopy and replication at 20,000X were also performed on specimen V-17.

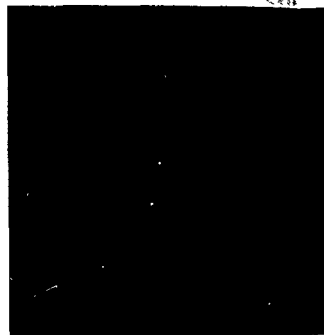
The EC (Defectometer) and FP inspections of the specimen 036-1 gage section surface produced no fatigue crack indications. However, upon sectioning the specimen axially and subjecting it to microscopic fractographic examination, multiple microcracks (on the order of 1/4 mil) were discovered internal to the specimen gage section, initiating primarily from microporosity. Further examination outside the most highly strained region of the gage section revealed no microcracking in the porous areas, discounting the possibility that the material was microcracked prior to testing.

Testing of specimen 217-4 was also discontinued after the period "3" of increased AE signal maximum pulse widths and ringdown counts per event (Figure 24). Even though 217-4 was machined from a different heat of material than 036-1, post-test external and internal inspections produced similar results. Gage section internal inspection again revealed microcracking from microporous areas at the center of the gage section, while no microcracking was noted outside the most highly strained region of the specimen.



Mag 20,000X

During Nucleation, Dislocations Stack Up At Obstacles Like Grain Boundaries



Mag: 20,000X

During Microcrack Initiation, Stacked Dislocations Release To Free Surfaces In Regions of Highest Stress Concentrations

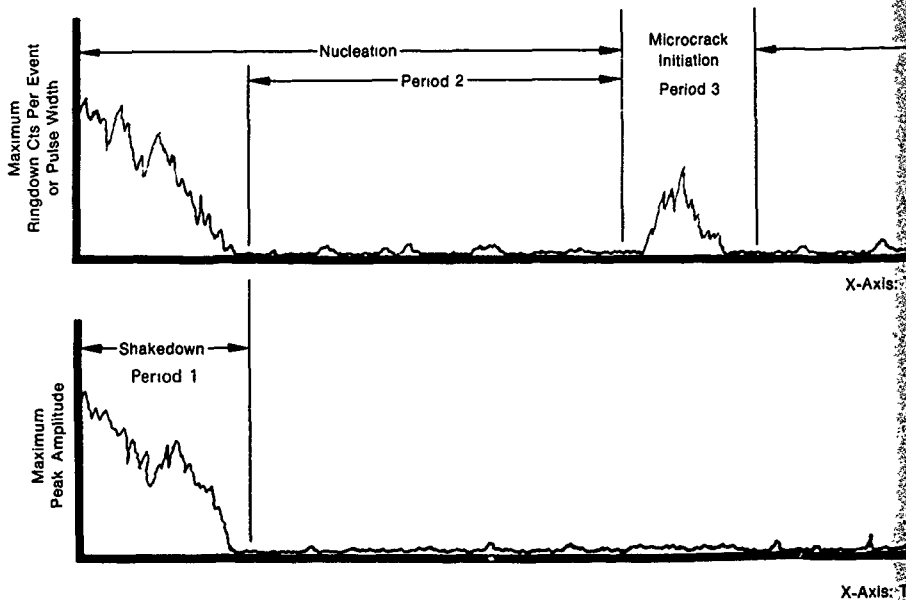


Figure 23. AE Multiparameter Distribution Model for



Mag: 1000X

During Transition, Dislocations Move Individually To Free Surfaces Like These Microcracks As They Occur



Mag: 40X

During Macrocrack Propagation, Relatively Large Incremental Advances In The Fatigue Crack Occur

Microcrack-To-Macrocrack Transition
Period 4

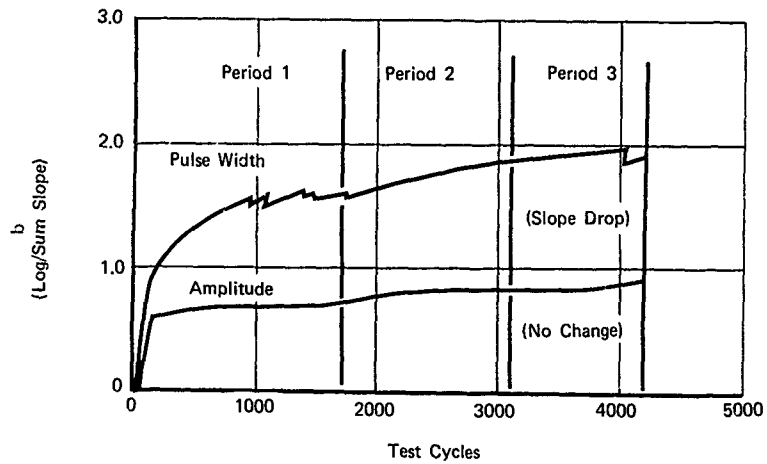
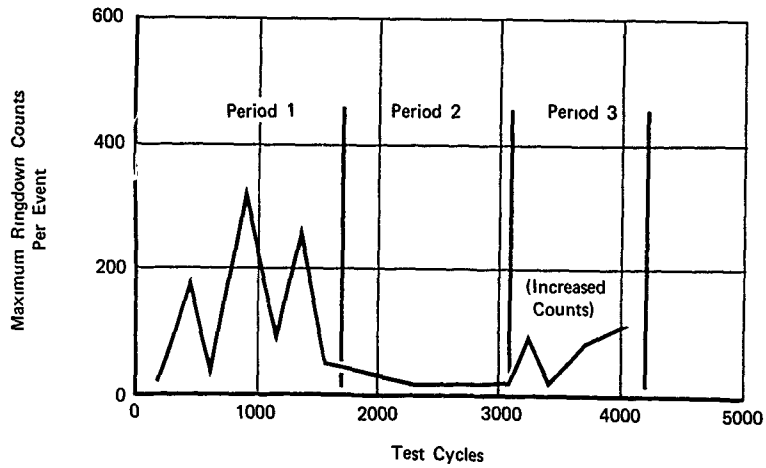
Macrocrack Propagation
Period 5

X-Axis Test Cycles

X-Axis Test Cycles

FD 1488-1A

Model for Fatigue Damage in Elevated Temperature IN100



Decreasing 'b' means a higher percentage of larger value pulse widths or amplitudes.

FD 118580

Figure 24. LCF Specimen 217-4

Replicas from the V-17 gage section showed multiple microcracks adjacent to the primary gamma prime (γ') particles. Thin-foil microscopy revealed numerous stacked dislocations at particle boundaries, as well as dislocation slipbands throughout the highly strained material.

Four tests (217-1, SC-1, 036-4, and V-9) were discontinued near the beginning of AE period "5" (general increase in AE activity). EC inspection disclosed macrocracks in all specimen gage sections. The distribution records of maximum pulse width, ringdown counts per event, and peak amplitude for the 217-1 test are presented in Figure 25, illustrating periods "1" through "5."

Tests which did not exhibit the above AE phenomena (periods "1" through "5") encountered long periods wherein AE registry was completely masked by extraneous noise, or multiple macrocracks were obvious on the specimen fracture surfaces, indicating a combination of mechanisms operating simultaneously (Figure 26)

FRACTURE MECHANICS TESTING

During AE inspection of an IN100 turbine disk, fatigue macrocrack propagation is the process which is expected to be most pronounced in fatigue-damaged locations. Fracture mechanics tests were conducted on modified compact specimens at several temperatures to produce da/dN vs AE rate relationships for application to Phase III and Phase IV disk studies. Test conditions are summarized in Table 3.

The da/dN vs stress intensity (ΔK) plots for specimens VTC-1, VTC-2, VTC-3 are illustrated as Figures 27, 28 and 29, respectively. The plots reflect anticipated results. Crack growth rate is higher at elevated temperature. The graphs also provide an explanation for the large difference in AE threshold (ΔK_{AE} thresh.) between room temperature crack propagation and elevated temperature propagation in IN100. The AE threshold appears to be dependent upon da/dN and occurs near a crack growth rate of 10^{-6} in./cycle in all cases.

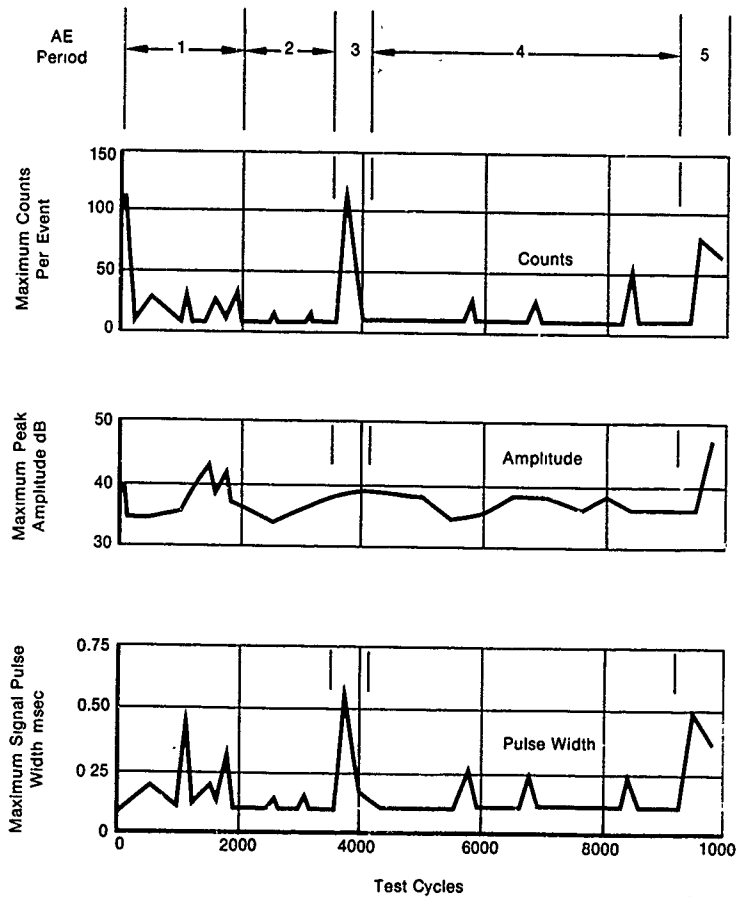
Figure 30 illustrates the difference between the AE rate vs ΔK relationship recorded from a room temperature test and the same relationship recorded from elevated temperature tests. Although the AE threshold is higher at room temperature, the average AE rate recorded above threshold from the room temperature test was higher than the AE rate levels recorded from elevated temperature testing over the stress intensity range of 16 ksi $\sqrt{\text{in.}}$ < 26 ksi $\sqrt{\text{in.}}$

The relationship may be affected by specimen thickness, the room temperature specimen being twice as thick as the elevated temperature specimens. Harris (Reference 12) has shown that energy released during crack propagation can be related to relevant material constants and fracture mechanics parameters. The energy release parameter may be represented as:

$$\frac{B}{E} \left(\frac{da}{dN} \right)^{1/2} \left(\frac{\Delta K}{1-R} \right) \quad (3)$$

where,

- B = specimen thickness
- E = Young's Modulus
- R = $\sigma_{min}/\sigma_{max}$



FD 11861

Figure 25. LCF Specimen 217-1



FD 114843A

Figure 26. LCF Specimen Fractured After Multiple Macrocrack Indications

TABLE 3
PHASE I CRACK PROPAGATION TESTING OF VIRGIN IN100

Specimen Serial Number	Specimen Type	Thickness (in.)	Test Temp (°F)	R	ν (cpm)	ΔK_{AE} Thresh (ksi $\sqrt{\text{in.}}$)
VTC-1	Compact Tension	0.125	1000	0.1	10	90
VTC2	Compact Tension	0.125	1200	0.1	10	90
VTC2	Compact Tension	0.250	R.T.	0.1	10	160

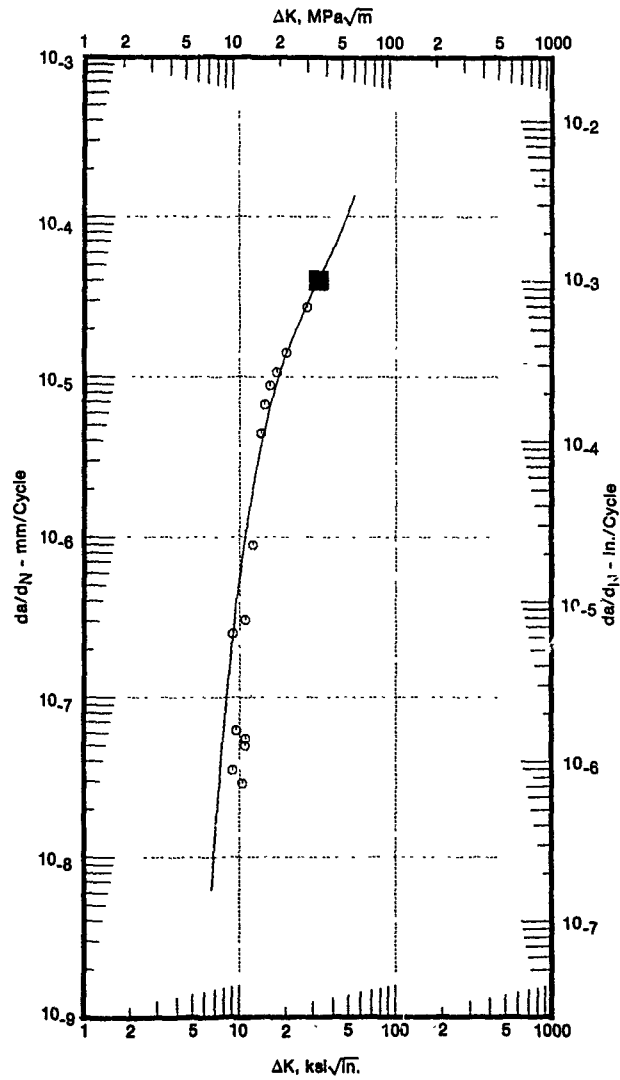
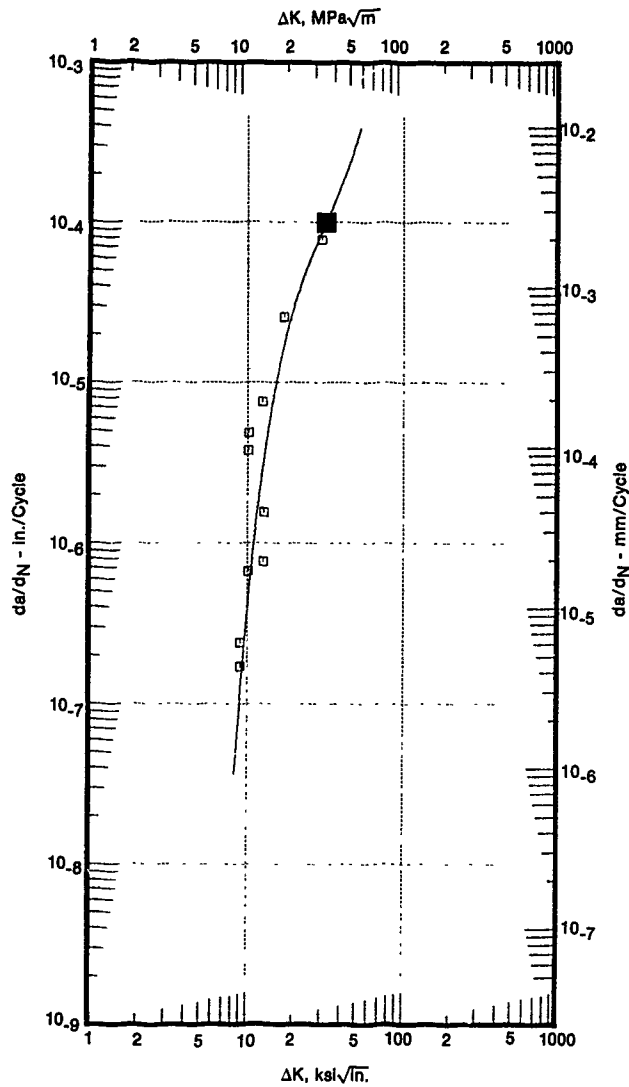
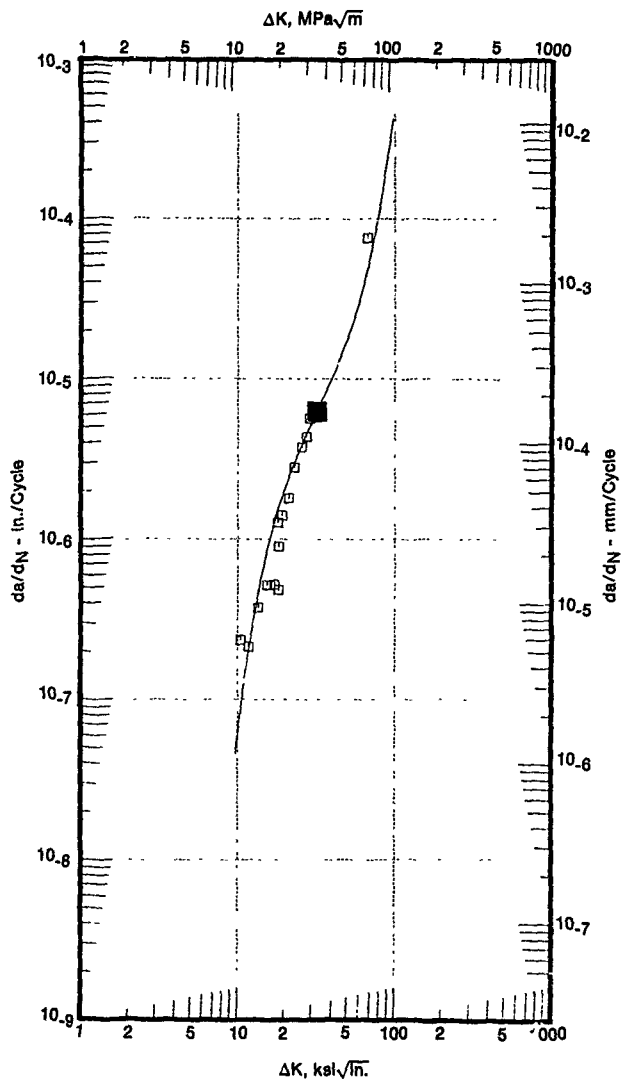


Figure 27. Crack Growth Characteristics of IN10 at 1000°F, $R = 0.1$, 10 cpm

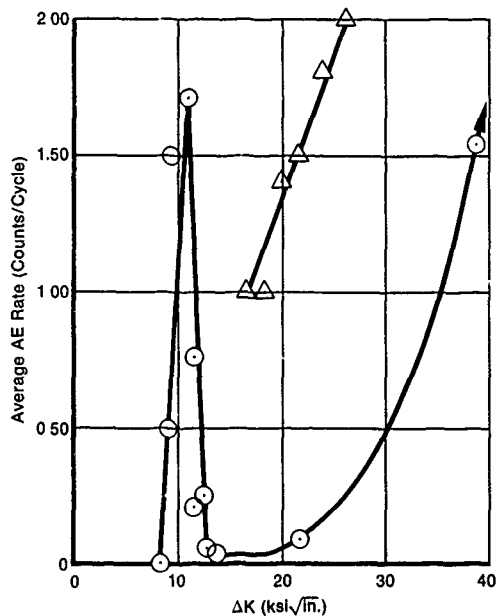
FD 148603





FD 148905

Figure 29. Crack Growth Characteristics of IN100 at Room Temperature, $R = 0.1$, 10 cpm



○ S/N VTC-2, Temperature = 1200°F, Thickness = 0.125 in.
 △ S/N VTC-3, Room Temperature, Thickness = 0.250 in.

FD 148906

Figure 30 Stress Intensity vs Average AE Rate for IN100 MCT Specimens

A^F has also been related to total energy release during da/dN testing (Reference 13 and 14), thereby establishing a relationship between AE output and specimen thickness, B. Although a similar waveguide was used for all three crack growth tests, several factors such as waveguide oxidation and damping of AE along the waveguide by insulating materials also influenced the perceived AE rate levels during elevated temperature testing.

DOVETAIL SPECIMENS

During Phase II (determination of optimum inspection procedures for complex IN100 LCF specimen geometries) dovetail LCF specimens were tested to simulate local fatigue damage at the blade attachment regions in a turbine disk. Dovetail specimens were fatigue cycled at conditions listed in Table 4. Periodic EC Defectometer and FP inspections and continuous AE inspection were performed during each test. Continuous AE inspection included AE rate (counts per cycle) at 90 dB gain, pulse width distributions, amplitude distributions, and counts per event distributions. Linear spatial filtering of the load train was used during several tests for noise discrimination.

TABLE 4
IN100 DOVETAIL GROOVE SIMULATION LCF SPECIMENS FATIGUE
TEST INSPECTION RECORD

Specimen S/N	Inspection Cycle	FP Indication				Remarks
		AE Indication	EC Indication	Wink	Static	
D-1						Test Temperature = 1200°F, $\sigma_{net} = 117$ ksi
D-1	Pretest	—	No	No	No	Notches polished
D-1	2,000	No	No	No	No	
D-1	4,000	No	No	No	No	
D-1	6,000	No	No	No	No	
D-1	8,000	No	No	No	No	
D-1	10,000	No	No	No	No	
D-1	12,000	No	Yes	Yes	No	2c = 0.060 in (FP)
D-1	*12,250	Yes	—	—	—	AE rate
D-1	13,000	Yes	Yes	Yes	Yes	2C = 0.250 in (FP)
D-2						Test Temperature = 800°F, $\sigma_{net} = 133$ ksi
D-2	Pretest	—	No	No	No	Notches polished
D-2	4,000	No	No	No	No	
D-2	8,000	No	No	No	No	
D-2	12,000	No	No	No	No	
D-2	16,000	No	Yes	No	No	EC Indication not a macrocrack, but located at region which eventually cracked.
D-2	18,000	No	Yes	No	No	EC Indication not a macrocrack, but located at region which eventually cracked.
D-2	20,000	No	Yes	No	No	EC Indication not a macrocrack, but located at region which eventually cracked
D-2	22,000	No	Yes	No	No	EC Indication not a macrocrack, but located at region which eventually cracked
D-2	*25,000	Yes	—	—	—	AE Rate
D-2	26,000	Yes	Yes	Yes	No	2c = 0.010 in. (FP)
D-2	30,000	Yes	Yes	Yes	Yes	2c = 0.090 in. (FP)
D-3						Test Temperature = 1000°F, $\sigma_{net} = 133$ ksi
D-3	Pretest	—	No	No	No	Notches polished
D-3	2,000	No	No	No	No	
D-3	4,000	No	No	No	No	
D-3	6,000	No	No	No	No	
D-3	8,000	No	No	No	No	
D-3	10,000	No	No	No	No	
D-3	12,000	No	No	No	No	
D-3	14,000	No	No	No	No	
D-3	16,000	No	No	No	No	
D-3	18,000	No	No	No	No	
D-3	19,500	No	No	No	No	
D-3	22,200	No	Yes	No	No	EC Two indications, one is false
D-3	24,200	No	Yes	No	No	EC One indication
D-3	26,200	No	Yes	Yes	No	WFP: Indicates same region as EC at 24,200 cycles. 2c = 0.008 in. (FP)
D-3	*26,500	Yes	—	—	—	AE Rate and distributions
D-3	28,200	Yes	Yes	Yes	No	2c = 0.030 in. (FP)
D-3	29,920	Yes	Yes	Yes	No	Failure

TABLE 4
IN100 DOVETAIL GROOVE SIMULATION LCF SPECIMENS FATIGUE
TEST INSPECTION RECORD

Specimen S/N	Inspection Cycle	AE Indication	EC Indication	FP Indication		Remarks
				Wink	Static	
D-4						Test Temperature = 1000°F, σ_{net} = 133 ksi
D-4	Pretest	—	No	No	No	Notches polished
D-4	2,000	No	Yes	No	No	EC indicates a scratch, polished out
D-4	4,000	No	No	No	No	
D-4	6,000	No	No	No	No	
D-4	8,200	No	No	No	No	
D-4	10,200	No	No	No	No	
D-4	12,200	No	No	No	No	
D-4	14,140	No	No	No	No	
D-4	17,000	No	No	No	No	
D-4	19,000	No	No	No	No	
D-4	21,500	No	No	No	No	Testing discontinued to use D-4 as an EC baseline standard for no crack
D-5						Test Temperature = 1200°F, σ_{net} = 117 ksi
D-5	Pretest	—	No	No	No	Notches polished
D-5	2,000	No	No	No	No	
D-5	* 7,100	Yes	—	—	—	AE rate
D-5	8,029					Failure

*Real time inspection during fatigue test.

Inspection results for dovetail groove simulation specimens (S/N D-1 through S/N D-6) are summarized in numerical order for each test in Table 4. Specific specimen test results follow

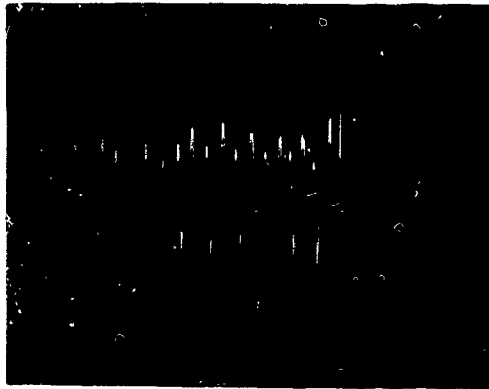
Specimen S/N D-1 (fatigue cycled at 1200°F, σ_{net} = 117 ksi) received a Defectometer crack indication at the 12,000-cycle inspection (Figure 31) The AE record and standard FPI revealed nothing. However, wink FPI performed in the test machine showed a 60 mil fatigue macrocrack. The flaw was then documented with replication.

Upon restart of the fatigue cycling, AE rate indications on the order of 50 to 400 counts per cycle against a quiet background began to occur near test cycle 12,250 and continued to the 13,000-cycle periodic inspection. The AE amplitude distribution from cycle 12,500 to 13,000 displayed an increase in peak amplitude from approximately 40 to over 50 dB (Figure 32).

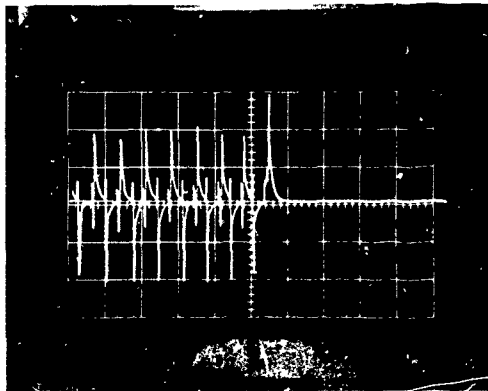
At 13,000 cycles the crack length was approximately 0.25 in. However, due to the high concentration of surface stresses in this specimen design, the depth was approximately 20 mils, or less.

Specimen S/N D-2 (fatigue cycled at 800°F, σ_{net} = 133 ksi) received Defectometer indications as early as the 16,000-cycle periodic inspection. No fatigue crack was confirmed until 26,000 cycles, when wink FPI indicated a 10 mil flaw. Even though the Defectometer and FPI agreed as to the flaw location, a fracture mechanics analysis of the notch resulted in less than 5,000 cycles of predicted macrocrack propagation, connoting that earlier Defectometer indications were not macrocracks. Continuous AE rate inspection indicated macrocracking from 25,000 cycles, and at 30,000 cycles wink FPI confirmed a flaw of 90-mils length.

Specimen S/N D-3 (fatigue cycled at 1000°F, σ_{net} = 133 ksi) was tested to 22,200 cycles when the Defectometer produced crack indications in both notches. At 24,200 cycles one indication disappeared while the other remained unchanged.



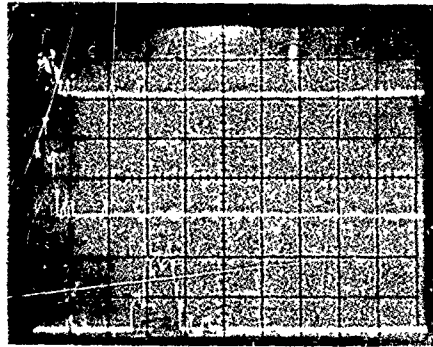
Uncracked Notch: Peaks Are Edge Lift-Off Effect as Probe Is Passed Back and Forth Many Times



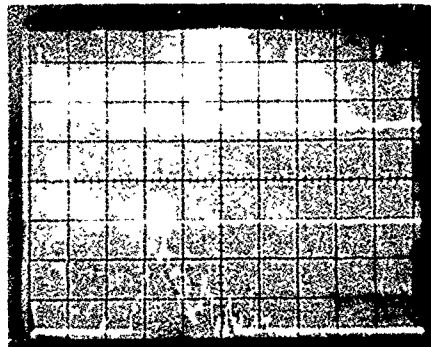
Cracked Notch Short Spikes Between Edge Lift-Off Effects Are the Macrocrack Indications

FD 128993

Figure 31 Dovetail Groove LCF Specimen S/N D-1 EC Defectometer Records



No Fatigue Macrocrack Indications



Macrocracking Indicated: Increase in All Three Maximum Parameters

FD 128995

Figure 32. Dovetail Groove LCF Specimen S/N D-1 AE Distribution Histogram Records

At the 26,200-cycle periodic inspection, wink FPI indicated an 8 mil crack. As testing continued, AE rate and distribution analyses began to produce fatigue macrocrack indications which continued to the 28,200-cycle inspection. The wink FPI and replication techniques then confirmed the crack at 30-mils length.

Specimen S/N D-4 (fatigue cycled at 1000°F, $\sigma_{\text{net}} = 133$ ksi) was tested to 21,500 cycles with no crack indications. Fatigue cycling was then discontinued and S/N D-4 was used as a baseline standard for remaining EC Defectometer inspections (after cleaning) as a no-crack specimen.

Specimen S/N D-5 (fatigue cycled at 1200°F, $\sigma_{net} = 117$ ksi) was the subject of an AE spatial filtering experiment. Periodic EC and FP inspections were not conducted close enough to specimen failure to detect macrocracking. However, AE rate indicated macrocrack initiation near test cycle 7120.

One-dimensional spatial filtering of the load train to perform subsequent time-domain distributions was not successful in sorting macrocrack propagation indications to the proper distribution slot locations. Spatial filtering is performed by attaching AE sensors at opposite ends of the load train and conducting one-dimensional AE source location characterization of the region of interest (the specimen gage section). The Dunegan/Endevco Model 920 Distribution Analyzer may then be programmed to accept only those signals whose source is determined to be the region of interest for further processing in external memory modules. However, should one sensor be located far enough away from a relatively low amplitude source that the signal level is below threshold at that single sensor, the signal will register as extraneous noise in either the 0 to 100 slot (depending upon which sensor receives the signal) of the distribution analyzer. This was the unfortunate case during the test period near cycle 7120 for specimen S/N D-5. The distribution analyzer record for test cycles 7000 to 7500 is shown in Figure 33. The top histogram is a record of the spatial filter for this test period, with slots 40 to 50 corresponding to the specimen gage section. It is obvious that the macrocrack initiation indications did not register in the proper region and, since the primary sensor from which the rate plot was taken corresponded to slot location 0, it must be assumed that all of the macrocrack indications registered in slot 0 (i.e., the signals were above the threshold detection level of the primary sensor, but not above the threshold level of the reference sensor).

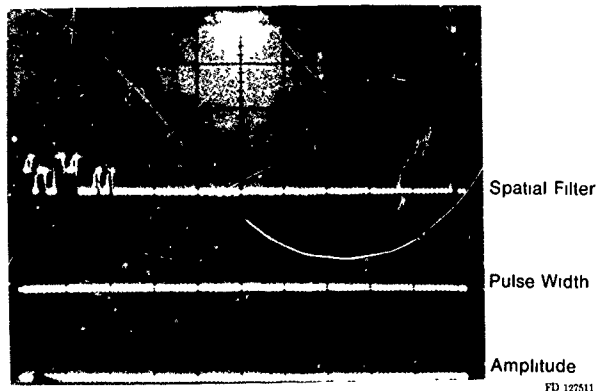


Figure 33 Dovoetail Groove LCF Specimen S/N D-5 AE Distribution Histogram Records

The fact that AE indications diminished during later portions of the fatigue test is significant. It may be possible for a specimen of the dovetail configuration to contain a relatively large fatigue macrocrack without AE verification.

BOLTHOLE SPECIMENS

During Phase II, bolthole LCF specimens were tested to simulate local fatigue damage at bolt and cooling holes in an IN-100 turbine disk. Bolthole specimens were fatigue cycled at conditions listed in Table 5. Periodic EC Circograph and Defectometer, FP, and continuous AE inspections were performed during each test. Continuous AE inspection included AE rate (counts per cycle) at 90 dB gain, pulse width distributions, amplitude distributions, and counts per event distributions.

TABLE 5
IN100 LCF BOLTHOLE SPECIMENS FATIGUE TEST INSPECTION RECORDS

Specimen S/N	Inspection Cycle	AE Indication	EC Indication	FP Indication		Remarks
				Wink	Static	
BR-1						Room Temperature, $\sigma_{net} = 114$ ksi
BR-1	Pretest	—	No	No	No	Hole honed and polished
BR-1	5,000	No	No	No	No	
BR-1	10,025	No	Yes	No	No	EC Indication not a macrocrack, but located at region which eventually cracked
BR-1	15,050	No	Yes	Yes	No	
BR-1	* 15,120	Yes	—	—	—	AE rate and distributions
BR-1	15,400	Yes	Yes	Yes	Yes	2c = 0.125 in. (FP) Failure
BR-2						Test Temperature = 800°F, $\sigma_{net} = 94$ ksi
BR-2	Pretest	—	No	No	No	Hole honed and polished
BR-2	5,000	No	No	No	No	
BR-2	10,000	No	No	No	No	
BR-2	15,000	No	Yes	No	No	EC: Not a macrocrack
BR-2	20,000	No	Yes	No	No	EC: Not a macrocrack
BR-2	25,000	No	Yes	No	No	EC: Not a macrocrack
BR-2	30,000	No	Yes	No	No	EC: Not a macrocrack
BR-2	35,000	No	Yes	No	No	EC: Not a macrocrack
BR-2	40,000	No	Yes	No	No	EC: Indication shifted, not a macrocrack
BR-2	45,000	No	*Yes	No	No	EC: Indication shifted, not a macrocrack
BR-2	50,000	No	Yes	No	No	EC: Indication shifted, not a macrocrack
BR-2	55,000	No	Yes	No	No	EC: Indication shifted, not a macrocrack
BR-2	60,000	No	Yes	No	No	EC: Indication shifted, not a macrocrack
BR-2	65,000	No	Yes	No	No	EC: Indication shifted, not a macrocrack
BR-2	70,000	No	Yes	No	No	EC: Indication shifted, not a macrocrack
BR-2	* 70,100	Yes	—	—	—	AE rate and distributions
BR-2	* 71,700					Failure at thermocouple tack weld. Fractography: no cracks in bolthole
BR-3						Test Temperature, = 1000°F, $\sigma_{net} = 90$ ksi
BR-3	Pretest	—	No	No	No	Hole honed and polished
BR-3	5,000	No	Yes	No	No	EC Not a macrocrack
BR-3	10,000	No	Yes	No	No	EC Not a macrocrack
BR-3	15,000	Yes	Yes	No	No	AE Clevis pin failure
BR-3	20,350	No	Yes	No	No	EC Not a macrocrack
BR-3	* 20,400	Yes	—	—	—	EC Not a macrocrack
BR-3	21,300					AE rate and distributions Failure at thermocouple tack weld. Fractography: no cracks in bolthole

TABLE 5
IN100 LCF BOLTHOLE SPECIMENS FATIGUE TEST INSPECTION RECORDS
(Continued)

Specimen S/N	Inspection Cycle	AE Indication	EC Indication	FP Indication		Remarks
				Wink	Static	
BR-4						Test Temperature = 1200°F, $\sigma_{net} = 82$ ksi
BR-4	Pretest	—	No	No	No	Hole honed and polished
BR-4	5,000	No	No	No	No	
BR-4	10,000	No	No	No	No	
BR-4	15,000	No	Yes	No	No	EC Indication not a macrocrack, but located at region which eventually cracked
BR-4	20,000	No	Yes	No	No	EC Indication not a macrocrack, but located at region which eventually cracked
BR-4	* 24,700	Yes	—	—	—	AE rate indications
BR-4	25,000	Yes	Yes	No	No	Rectograph 2c = 0.040 in
BR-5						Test Temperature = 1000°F, $\sigma_{net} = 90$ ksi
BR-5	Pretest	—	No	No	No	Hole honed and polished
BR-5	5,000	No	No	No	No	
BR-5	10,000	No	No	No	No	
BR-5	15,000	No	Yes	No	No	EC: Not a macrocrack
BR-5	20,000	No	Yes	No	No	
BR-5	25,000	No	Yes	No	No	
BR-5	30,000	No	Yes	No	No	
BR-5	35,000	Yes	Yes	No	No	No
						AE May be false or resulting from initiation at internal defect
BR-5	40,000	Yes	Yes	No	No	EC Not a macrocrack
BR-5	45,000	No	Yes	No	No	EC Not a macrocrack
BR-5	50,000	No	Yes	No	No	EC Not a macrocrack
BR-5	55,000	No	Yes	No	No	EC Not a macrocrack
BR-5	60,000	No	Yes	No	No	EC Not a macrocrack
BR-5	65,000	No	Yes	No	No	EC Not a macrocrack
BR-5	70,000	No	No	No	No	EC Revised preinspection hole preparation
BR-5	75,000	No	No	No	No	
BR-5	80,000	No	No	No	No	
BR-5	85,000	No	No	No	No	
BR-5	90,100	No	No	No	No	σ_{net} raised to 99 ksi
BR-5	95,150	No	No	No	No	
						No additional periodic inspections
BR-5	*109,200	Yes	—	—	—	AE distributions
BR-5	109,730					Failure from internal defect inside bolt-hole
BR-6						Test Temperature = 1200°F, $\sigma_{net} = 82$ ksi
BR-6	Pretest	—	No	No	No	Hole honed and polished
BR-6	5,000	No	No	No	No	
BR-6	10,000	No	No	No	No	
BR-6	15,000	No	No	No	No	
BR-6	20,000	No	No	No	No	
BR-6	25,000	No	No	No	No	
BR-6	30,000	No	Yes	No	No	EC Two indications, not macrocracks
BR-6	35,000	No	Yes	No	No	EC One indication repeated, not a macrocrack

TABLE 5
IN100 LCF BOLTHOLE SPECIMENS FATIGUE TEST INSPECTION RECORDS
(Continued)

Specimen S/N	Inspection Cycle	AE Indication	EC Indication	FP Indication		Remarks	
				Wink	Static		
BR-6	40,000	No	Yes	No	No	EC Not a macrocrack	
BR-6	45,000	No	Yes	No	No		
BR-6	50,000	No	Yes	No	No		
BR-6	55,000	No	Yes	No	No		
BR-6	60,000	No	No	No	No		
BR-6	65,000	No	No	No	No	EC Revised preinspection hole preparation σ_{net} raised to 9 ksi	
BR-6	70,000	No	No	No	No		
BR-6	75,000	No	No	No	No		
BR-6	80,000	No	No	No	No		
BR-6	85,000	No	No	No	No		
BR-6	90,100	No	No	No	No		
BR-6	95,150	No	No	No	No		
BR-6	100,000	No	No	No	No		
BR-6	105,000	No	No	No	No		
BR-6	110,000	No	No	No	No		
BR-6							Test discontinued
BC-1							Test Temperature = 1000°F, σ_{net} = 120 ksi
BC-1	Pretest	—	No	No	No		Hole honed and polished
BC-1	* 4,500	Yes	—	—	—	AE distributions	
BC-1	5,000	Yes	Yes	No	No	Failure at thermocouple track weld. Fractography; 0.030 in crack at region indicated by EC	
BC-1	5,570						
BC-2						Test Temperature = 1200°F, σ_{net} = 110 ksi	
BC-2	Pretest	—	No	No	No	Hole honed and polished	
BC-2	* 3,150	Yes	—	—	—	AE rate	
BC-2	3,450					Failure before periodic inspections	
BC-3						Room Temperature σ_{net} = 144 ksi	
BC-3	Pretest	—	No	No	No	Hole honed and polished	
BC-3	5,000	No	No	No	No		
BC-3	10,000	No	No	No	No		
BC-3	15,000	No	Yes	No	No		
BC-3	17,500	No	Yes	Yes	No	2c = 0.010 in. (FP and replica) Used as EC standard	
BQ-1						Test Temperature = 1000°F, σ_{net} = 100 ksi	
BQ-1	Pretest	—	No	No	No	Hole honed and polished	
BQ-1	* 5,800	Yes	—	—	—	AE rate	
BQ-1	6,000	Yes	Yes	Yes	Yes	2c = 0.125	
BS-1						Test Temperature = 1000°F, σ_{net} = 113 ksi	
BS-1						Skewed bolthole (25-deg angle)	
BS-1	Pretest	—	No	No	No	Hole honed and polished	
BS-1	2,000	No	No	No	No	EC Revised preinspection hole preparation	
BS-1	7,000	No	No	No	No		
BS-1	12,000	No	No	No	No		
BS-1	17,000	No	No	No	No		
BS-1	22,000	No	No	No	No		
BS-1	27,000	No	No	No	No		

TABLE 5
IN100 LCF BOLTHOLE SPECIMENS FATIGUE TEST INSPECTION RECORDS
(Continued)

Specimen S/N	Inspection Cycle	AE Indication	EC Indication	FP Indication		Remarks
				Wink	Static	
BS-1	32,000	No	No	No	No	
BS-1	35,000	No	No	No	No	
BS-1	*36,300	Yes	—	—	—	AE rate and amplitude dist
BS-1	37,300					Failure
BS-2						Test Temperature = 1000°F, $\sigma_{net} = 113$ ksi
						Skewed bolthole (25-deg angle)
BS-2	Pretest	—	No	No	No	Hole honed and polished
BS-2	4,560	No	No	No	No	EC Revised preinspection hole prep- aration
BS-2	9,560	No	No	No	No	
BS-2	12,560	No	No	No	No	
BS-2	16,560	No	No	No	No	
BS-2	21,560	No	No	No	No	
BS-2	*23,300	Yes	—	—	—	
BS-2	23,500					Failure

*Real Time Inspection during fatigue test

Inspection results for bolthole simulation specimens (S/N BR-1 through S/N BR-6, S/N BQ-1, BS-1, BS-2, and S/N BC-1 through S/N BC-3) are listed in chronological order for each test in Table 5

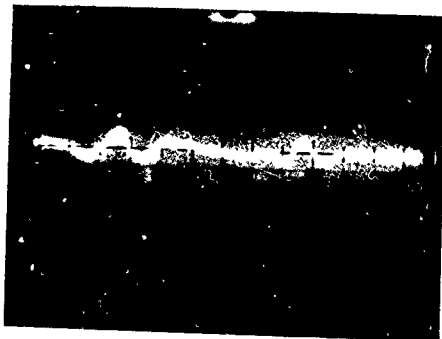
Specific specimen test results follow:

Specimen S/N BR-1 (fatigue cycled at room temperature, $\sigma_{net} = 144$ ksi) received crack indications by both EC inspection methods at the 15,050-cycle periodic inspection. Figure 34 is the Circograph record from this inspection, indicating cracks at 90 (primary initiation site) and 270-deg (secondary initiation site). Slight FPI indications were recorded from both sides of the bolthole

Upon restart of fatigue cycling, AE rate and distribution analyses began to indicate fatigue macrocrack propagation near cycle 15,120. Count rate increased by more than an order of magnitude and maximum peak amplitudes of the incoming AE bursts increased from 50 to over 80 dB. By fatigue cycle 15,400 the primary fatigue crack was over 1/8 in. long, and at 15,850 cycles the specimen fractured. Figure 35 clearly illustrates the subcritical crack propagation regions.

Specimen S/N BR-2 (fatigue cycled at 800°F, $\sigma_{net} = 93.7$ ksi) received Circograph indications as early as the 15,000-cycle periodic inspection. A fracture mechanics analysis of the specimen disclosed that, while these indications occurred at high-stress regions, macrocrack propagation life of this specimen ($a_1 = 0.003$ in.) was on the order of several thousand cycles; and, therefore, the indications were not originating from fatigue macrocracks.

Although EC and FPI produced no indications of impending failure (fracture occurred at a thermocouple tack weld site on the gage section), AE rate and distribution records indicated macrocrack activity commencing 1,500 cycles before final fracture at 71,700 cycles. Fractographic analysis of the bolthole revealed no fatigue macrocracks.

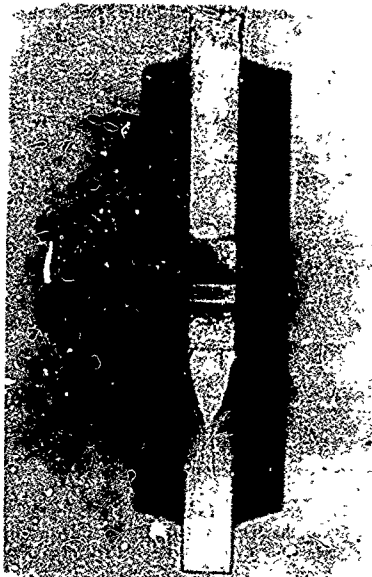


Cracks Are Indicated at 90° (Primary Initiation Site) and 270° (Secondary Site)

FD 131174

Figure 34 LCF Bolthole Specimen BR-1, 15,000-cycle Circograph EC Inspection Records

TEST CONDITIONS: $\sigma_{Max} = 144$ ksi,
ROOM TEMP, $N_f = 15,950$ CYCLES



FD 131175

Figure 35 LCF Bolthole Specimen BR-1 Fracture Surface

Specimen S/N BR-3 (fatigue cycled at 1000°F, $\sigma_{net} = 90$ ksi) received AE indications near cycle 15,000. At the periodic inspection, these indications were determined to be initiating from a cracked clevis pin in the load train.

Although EC and FPI could not detect fatigue damage at the unexpected initiation site (thermocouple weld), AE rate and distribution analyses indicated over 1,000 cycles of macrocrack propagation before specimen failure. Fractography revealed no cracks in the boltholes.

Fractographic analysis was performed on specimen S/N BR-4 (fatigue cycled at 1200°F, $\sigma_{net} = 82$ ksi) after the 25,000-cycle periodic EC and FPI. Circograph inspection at 15,000, 20,000 and 25,000 cycles had produced indications at the same region of the bolthole (Figure 36); and, near 25,000 fatigue cycles, continuous AE rate inspection indicated macrocrack activity. FPI and Defectometer inspections with the edge-sensitive probe produced no positive results.

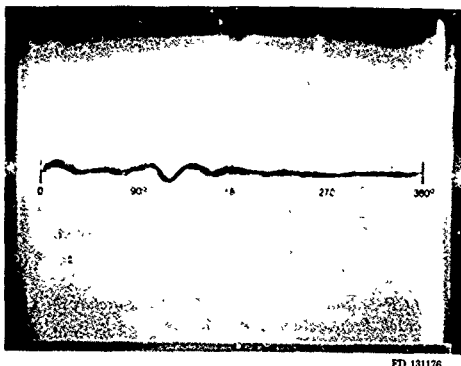
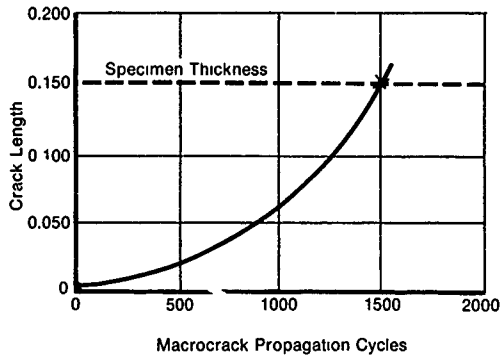


Figure 36. LCF Specimen BR-4, 15,000-cycle Circograph EC Inspection Records

Fractographic analysis revealed a fatigue crack in the bolthole near a corner (indicated near 90 deg in Figure 35), with dimensions of approximately 40-mils length by 60-mils depth. A smaller crack (less than 10-mils length) had initiated from the far side of the bolthole.

Specimen S/N BR-5 (fatigue cycled at 1000°F, $\sigma_{net} = 90$ ksi for 85,000 cycles, raised to 99 ksi for the final 24,700 cycles) was the focus of surface preparation refinements for EC inspections. Circograph inspection had produced large indications in the high-stress regions of the bolthole as early as 30,000-cycle inspection. Although a mild abrasive was being used to prepare the specimen for inspection, it became apparent after several inspections that Type II errors were present. Studies performed at P&WA/GPD predicted less than 2,000 cycles of macrocrack propagation for this test (Figure 37). As a result, the mild abrasive procedure was replaced by a stronger plastic wool (Scotch Brite) attached to a drill motor fixture. Figure 38 shows that the large Circograph indication recorded at 270 deg during the 65,000-cycle inspection was removed before the 70,000-cycle inspection. A question still remains regarding selectivity of this oxidation problem to high-stress regions of the bolthole.

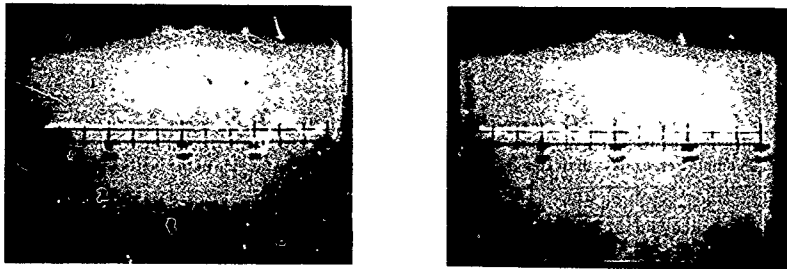


Test Conditions
 $\sigma_{Net} = 99 \text{ ksi}$
 Temperature = 1000°F

- Assumptions:
- 1 Initial Flaw Length = 6 mils
 - 2 Surface Initiation
 - 3 Specimen Fails When Crack Grows Through Thickness

FD 131177

Figure 37. LCF Bolthole Specimen S/N BR-5 Fracture Mechanics Macro crack Propagation Life Analysis



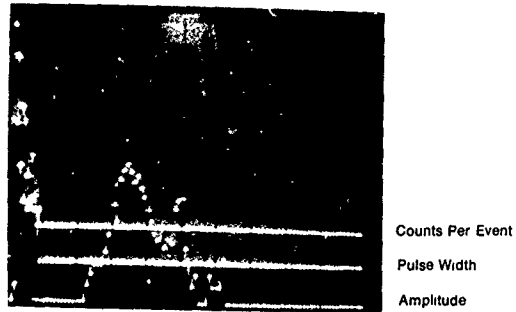
65,000-Cycle Circograph Eddy Current Indication at Hole Interior

70,000-Cycle Circograph Eddy Current Record After Cleaning

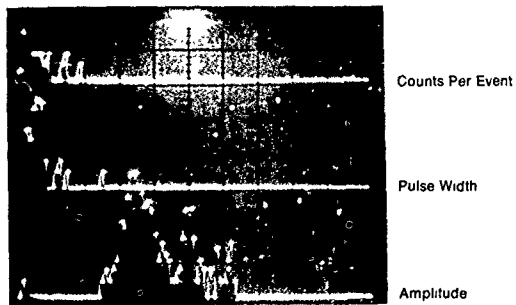
FD 131178

Figure 38. LCF Bolthole Specimen BR-5 Circograph Records

After the 95,000-cycle inspection of specimen S/N BR-5 it was decided, in the interest of expediting the test, that periodic inspections would be discontinued until continuous AE inspection indicated macrocrack activity. AE indications occurred only within the final 500 cycles of the test. The most pronounced indications of impending failure came from AE pulse width and counts per event distributions which revealed a 50% increase in maximum parametric values during the final period of the test (Figure 39).



Cycles 108,000 to 109,090



Cycles 109,091 to 109,730 (Failure)

FD 124897

Figure 39 LCF Bolthole Specimen BR-5 Distribution Analyzer Histogram Records

Fractographic analysis of S/N BR-5 resulted in the observation that macrocrack initiation occurred at an aluminum rich, one-mil diameter inclusion located several mils from the bolthole edge (Figure 40). It is likely that the lack of a pronounced AE macrocrack indication until the final stage of the test was due to the anoxic state of fatigue crack growth from an internal defect during the initial stage



Bolthole
Edge

Mag: 500X

FD 12498

Figure 40 LCF Bolthole Specimen BR-5 Fracture Surface

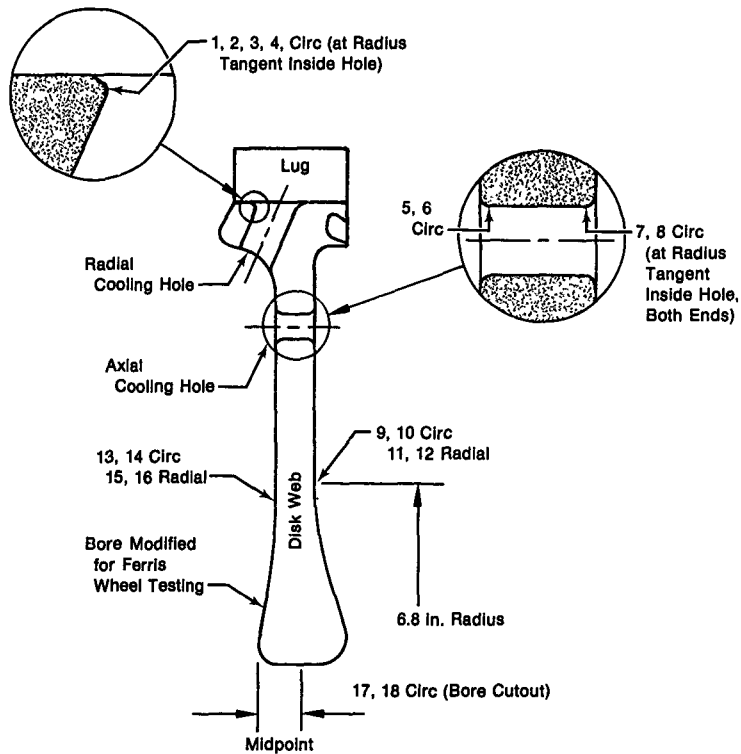
Specimen S/N BR-6 (fatigue cycled at 1200°F, $\sigma_{\text{net}} = 82$ ksi for 65,000 cycles, raised to 90 ksi for an additional 45,000 cycles) was the continued focus of preinspection cleaning procedure experiments. Circograph indications apparently resulting from selective oxidation at high-stress regions of the bolthole also appeared near the 30,000-cycle mark of this test. At the 60,000-cycle inspection, the highly abrasive cleaning procedure was initiated. The next ten periodic inspections produced no false indications. Fatigue cycling of S/N BR-6 was discontinued at 110,000 cycles to expedite the program.

DISK INSPECTIONS (PHASE III)

An experimental stress analysis of F100 1st-stage turbine disk S/N BDB 257 was conducted for Phase IV ferris wheel residual life studies. As mentioned previously, Phase IV subject disks were bore-modified to produce engine-simulating rim stress during ferris wheel testing. Maximum strain (0.81%) was recorded at a radial cooling hole acute corner. Room temperature strain survey results are listed in Table 6, with strain gage locations illustrated in Figure 41.

TABLE 6
 F100 1st-STAGE HPT DISK S/N BDB 257
 ROOM TEMPERATURE STRAIN SURVEY
 (See Figure 47 for Strain Gage Locations)

Gage No	Run No	Strain (Micro in / in.) For Radial Load (lb) of.										
		2000	4000	6000	8000	10000	11080	10000	8000	6000	4000	2000
1	1	1400	2780	4240	5720	7280	8110	6950	5660	4570	3130	1410
	2	1420	2780	4250	5730	7270	8110	6920	5630	4530	3040	1380
2	1	1340	2660	4030	5380	6810	7590	6540	5390	4340	2950	1370
	2	1360	2660	4050	5400	6820	7590	6530	5380	4310	2860	1350
3	1	1330	2700	4160	5610	7120	7930	6940	5870	4640	3060	1310
	2	1350	2710	4190	5660	7140	7940	6940	5850	4610	2990	1360
4	1	1320	2610	3970	5320	6370	7490	6380	5240	4180	2820	1380
	2	1340	2600	3960	5330	6730	7480	6380	5240	4170	2760	1370
5	1	1010	2030	3070	4080	5120	5670	4850	3910	3110	2090	950
	2	1020	2030	3080	4110	5150	5680	4860	3920	3100	2040	950
6	1	1020	2050	3110	4160	5210	5770	4980	4050	3180	2100	960
	2	1020	2050	3120	4170	5230	5780	4990	4060	3170	2050	960
7	1	1190	2350	3450	4460	5430	5900	4880	3780	2900	1820	690
	2	1220	2360	3450	4460	5430	5930	5910	3830	2940	1790	650
8	1	1150	2330	3540	4720	5940	6570	5710	4660	3650	2420	1100
	2	1160	2330	3550	4740	5950	6580	5720	4660	3650	2360	1110
9	1	480	960	1430	1900	2380	2630	2340	1800	1470	1000	500
	2	460	940	1430	1900	2370	2620	2330	1860	1450	950	480
10	1	470	930	1400	1860	2340	2580	2310	1840	1430	960	450
	2	460	920	1400	1870	2340	2580	2300	1840	1420	930	450
11	1	-10	-10	-10	-10	0	0	10	0	-10	-10	-10
	2	-10	-10	-10	-20	-20	-10	0	-10	-20	-20	-20
12	1	0	0	0	0	0	0	0	0	-10	0	10
	2	0	0	0	0	0	0	0	-10	-10	-10	10
13	1	470	930	1380	1840	2310	2540	2260	1800	1400	940	450
	2	450	910	1380	1840	2300	2540	2250	1800	1390	910	450
14	1	450	900	1360	1800	2270	2510	2240	1780	1380	920	440
	2	430	890	1350	1810	2260	2500	2230	1770	1370	890	430
15	1	60	110	150	190	230	250	230	190	150	100	50
	2	60	100	140	180	220	250	230	180	130	90	50
16	1	50	100	150	190	230	260	230	190	150	110	60
	2	50	100	140	190	230	250	230	180	140	100	60
17	1	620	1260	1880	2500	3110	3420	3170	2480	1860	1220	600
	2	620	1260	1890	2500	3110	3420	3180	2480	1860	1200	600
18	1	640	1270	1880	2500	3120	3440	3170	2420	1840	1230	600
	2	630	1260	1880	2490	3110	3430	3160	2420	1830	1180	590



FD 148907

Figure 41. F100 1st-Stage Turbine Disk S/N BDB 257 Strain Gage Locations for Experimental Stress Analysis

1st-stage turbine disk S/N BM 798 was engine-cycled in experimental engine P050, receiving 330 Type I LCF cycles, 45 Type II LCF cycles, and 2157 Type III LCF cycles (a total of 774 7 hr). The importance of using an engine-cycled disk for Phase III studies is primarily in the realm of EC inspection. The preinspection preparation procedure was further refined during Phase III to eliminate Type II EC inspection errors arising from oxidation effects. The disk was not bore modified before being subjected to 5310 Type I LCF cycles in the ferris wheel at 1200°F and 11,700 lb maximum drawbar load to produce fatigue cracking in radial cooling holes (primary fracture critical) and blade slots.

Prior to AE inspection of disk S/N BM 798 in the ferris wheel, the disk was characterized using a pulsing transducer to simulate AE to determine source location readings along the entire disk rim adjacent to the radial cooling hole acute corners (see "AE Inspection Procedures" for explanation of characterization procedure). This one-dimensional characterization for each of two distribution analyzers is presented as Figure 42. The distribution analyzer output for each disk location corresponded to a "slot" value between "0" and "100." The characterization was performed using three Dunegan/Endevco D750 transducers mounted on 6-in. waveguides, spaced 120 deg apart along the disk rim. The characterization was checked at total gain settings of 80 and 90 dB.

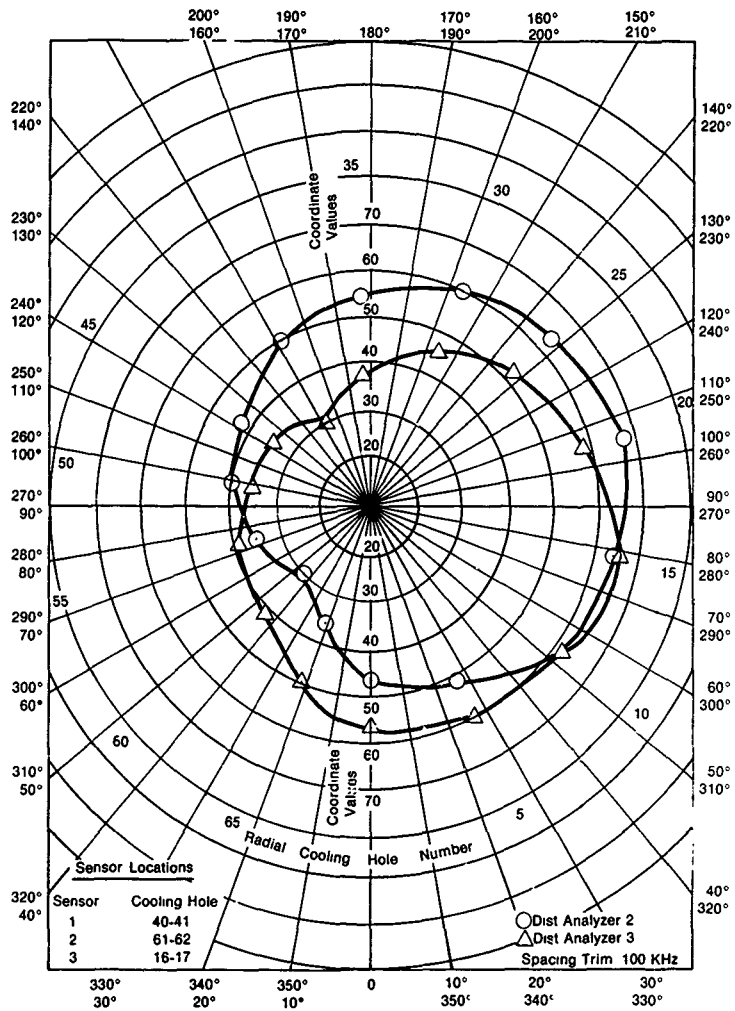
Distribution analyzer output during 100 ferris wheel fatigue cycles indicated the disk regions listed in Table 7. Since the disk radial cooling holes were the only regions to be AE-characterized, indications from the blade attachment regions appeared in terms of the closest radial cooling holes.

Two FP inspections were conducted on the blade attachment regions of disk S/N BM 798 after ferris wheel initiation of fatigue cracks and AE inspection. The first FP was conducted as a standard production inspection, while the second was performed under carefully controlled laboratory conditions. Results of both inspections are listed in Table 8.

The EC Circograph inspections were also performed in the disk radial cooling holes according to the procedure outlined in Section II. Abrasive preinspection surface preparation procedures were used to eliminate oxidation layer effects. Originally, Scotch-brite plastic wool was used before Circograph inspection. Then the radial cooling holes and disk lugs were vapor blasted before a second inspection run. Subtle changes in several indications occurred as a result of the vapor blast and will be discussed in Section IV. The Circograph inspection record is listed in Table 8.

The EC Defectometer-type inspections were conducted in the disk lug regions using an NDT Instruments Vector 111 system and the fixture shown in Figure 13. With the addition of a balancing coil to the probe designed for Defectometer use, the Vector 111 is designed to simplify adjustment for lift-off effects. The probe performed satisfactorily for Phase III disk inspections, but the fixture itself proved to be unsatisfactory. Although several changes were made to the fixture, it still allowed the probe to drift as it was moved along a broach slot. The fixture was finally made workable for laboratory use, but a design similar to that shown in Figure 43 is recommended for future studies. The Defectometer inspection record is listed in Table 8.

Fractography was then conducted on selected disk radial cooling holes and blade attachment regions in an attempt to produce flaw confirmations. Results are also listed in Table 8.



FD 148808

Figure 42 Source Locate Characterization F100 1st-Stage HPT Disk Radial Cooling Holes

TABLE 7
ACOUSTIC EMISSION SOURCE LOCATION INSPECTION
F100 1st-STAGE HPT DISK S/N BM 798

<i>Analyzer 1 Reading</i>	<i>Analyzer 2 Reading</i>	<i>Indicated Radial Cooling Hole</i>
48	58	1
63	51	26
56	40	34
61	48	28 (crack located in lug between holes 28 and 29).
56	40	34 (crack located in lug between holes 34 and 35).
35	40	55 (no crack confirmed)
37	51	65 (crack located in lug between holes 65 and 66).

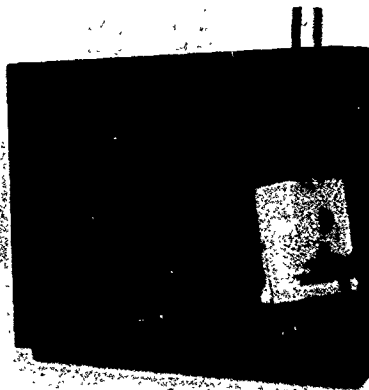
TABLE 8
PHASE III DISK INSPECTION RECORD F100 1st-STAGE HPT DISK
S/N BM 798

<i>Radial Cooling Hole No</i>	<i>AE Indication</i>	<i>Circograph Indication</i>	<i>Production FP Indication</i>	<i>Fractography (in. Length X in. Depth)</i>
1	Yes	Large	Yes	0.045 X 0.022
9	No	Small	No	--
12	No	Small	No	--
13	No	Small	No	--
14	No	Small	No	--
15	No	Small	No	Uncracked
19	No	Small	No	--
20	No	Small	No	--
21	No	Small	No	--
22	No	Small	No	--
23	No	Small	No	--
24	No	Medium	No	0.010 X 0.005
25	No	Small	No	--
26	Yes	Large	Yes	0.160 X 0.100
27	No	Small	No	Uncracked
29	No	Small	No	--
30	No	Small	No	--
31	No	Small	No	--
32	No	Small	No	--
33	No	Small	No	--
34	Yes	Large	Yes	0.200 X 0.145
35	No	No	No	Uncracked
42	No	Small	No	--
44	No	Small	No	--
45	No	Small	No	Uncracked
46	No	Small	No	--
54	No	Small	No	--
55	Yes	No	No	--
58	No	Small	No	--
66	No	Small	No	--

TABLE 8
 PHASE III DISK INSPECTION RECORD F100 1st-STAGE HPT DISK S/N BM 798
 (Continued)

Disk Lug Location	AE Indication	Vector III Indication	FP Indication		Fractography (in. Length × in. Depth)
			Production	Laboratory	
1-2	No	Yes	No	Yes	Yes, see note.
2-3	No	Yes	No	Yes	Yes, see note
3-4	No	Yes	No	No	—
4-5	No	No	No	Yes	—
5-6	No	Yes	No	Yes	—
6-7	No	No	No	Yes	—
9-10	No	No	No	Yes	—
10-11	No	Yes	No	No	—
11-12	No	Yes	No	No	Uncracked
18-19	No	Yes	No	Yes	—
19-20	No	Yes	No	Yes	Yes, see note
20-21	No	Yes	No	No	—
21-22	No	No	No	Yes	—
23-24	No	Yes	No	No	—
24-25	No	Yes	No	No	—
27-28	No	Yes	Yes	Yes	0.35 × 0.12
28-29	Yes	Yes	Yes	Yes	0.36 × 0.12
34-35	Yes	Yes	Yes	Yes	0.40 × 0.12
40-41	No	Yes	No	No	—
44-45	No	Yes	Yes	Yes	(Crack Gaping Open)
46-47	No	No	No	Yes	—
56-57	No	Yes	No	No	—
65-66	No	Yes	Yes	Yes	0.43 × 0.19

NOTE. Lug broken open adjacent to visible crack



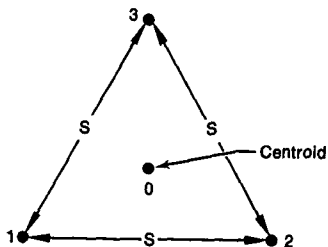
FAB 16399

Figure 43. Recommended EC Probe Fixture for Disk Lug Inspections

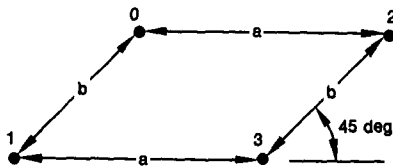
SPIN STUDY (PHASE III)

Five miniature AE transducers, Dunegan/Endevco P/N S1000 BM, were obtained for AE evaluations during spin testing of an F100 1st-stage HPT disk. The single-ended transducers are 5/16-in. in diameter and mounted conveniently inside the disk snapping, where centrifugal loading acted to increase transducer coupling. Centrifugal loading from each transducer was calculated to be less than 200 lb at 10,000 rpm.

The standard 1032 AE inspection system computer program, whose transducer arrangement is shown in Figure 44(a) was determined to be unsuitable for AE disk inspections due to a requirement for a center transducer or three parallel transducers in place of the center transducer. Instead, an alternate computer program whose normal sensor arrangement is illustrated in Figure 44(b) was modified to accommodate evaluation of a disk surface. Since transducer arrangement in the snapping could not be conducted to the required 45 deg parallelogram and AE signal paths around the disk bore produced large errors in computer calculation of rectangular coordinates for emission sources, characterization of the disk surface with simulated AE was required to enable correlation of calculated (x,y) coordinates with actual locations on the disk surface. Such a correlation for the disk snapping region is illustrated as Figure 45. With proper software alternations the existing packaged computer program could be rendered more suitable to the disk geometry, but the above mapping process would still be required. Dunegan/Endevco is currently developing a "random array" package which will eliminate the necessity of mapping complex test surfaces. During spin studies, simulated AE from a pulsing S1000 BM transducer was used to various rpm ranges to demonstrate feasibility of real time AE inspection during spin testing.



a. Standard "Quad" Array (Transducer "O" May Be Replaced by Three Parallel Transducers for Disk Inspections)



b. Alternate Array

FD 148000

Figure 44. Dunegan/Endevco Model 1032 Computerized AE System Transducer Arrays

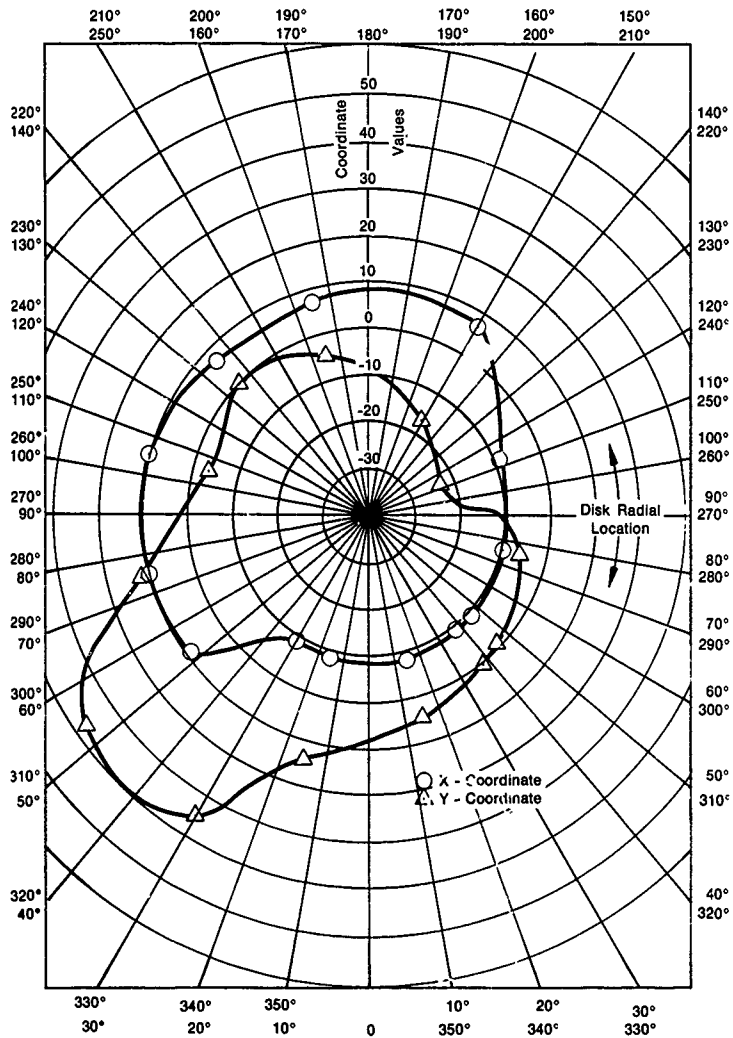


Figure 45 AE Characterization of F100 Balance Weight Snap Ring

FD 148910

Before the spin program began, system electrical noise studies were conducted to determine the effects of passing the AE signal along standard (not coaxial) conductors on the disk surface and through the slipring assembly. Various sections of the system were assessed independently by determining the maximum total gain setting which was attainable without inundating the system with electrical noise. Results are summarized in Table 9. Obviously, the first slipring to be used with the AE system contributed greatly to the ambient noise level.

TABLE 9
ELECTRICAL NOISE ASSESSMENT FROM
SPIN CONFIGURATION

Condition	Description	Maximum Gain (dB)
A	Baseline	99*
B	Spin Configuration	58
C	Slipring Omitted	75
D	Disk Omitted	66
D'	Improved Slipring	99*

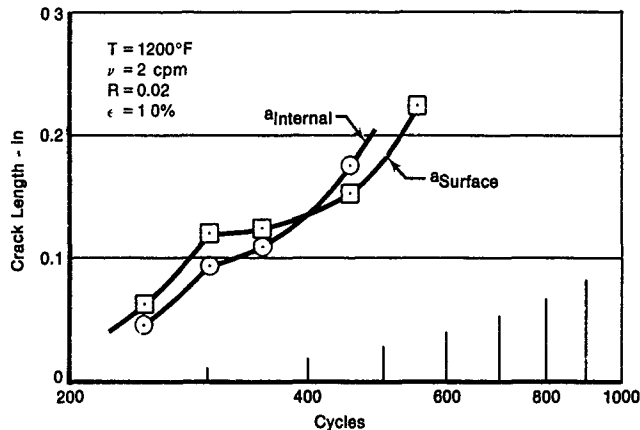
A baseline (condition A) was first established by attaching a standard coax cable to a reference sensor on location at the spin rig. At a maximum total gain of 99 dB, the system was functional. The system was then connected in the spin configuration, passing signals from the turbine disk through a Tilton slipring assembly (condition B). Maximum total gain attainable was only 58 dB before spurious electrical noise inundated the system. In order to determine the primary noise source, the AE system was then connected, bypassing the slipring, directly to the disk (condition C). Maximum total gain was then 75 dB. The system was then assessed by passing signals through the slipring from an external reference sensor (disk omitted from the configuration, condition D). Maximum gain in this condition was only 66 dB. It was apparent that the slipring was the primary noise source.

The pulsing transducer (simulated AE source) was fixed at a location corresponding to approximately 45 deg in Figure 45. Functionality of the system was checked continuously using the pulser from a static condition to a spin condition of 7300 rpm. Ambient extraneous noise level did not change appreciably from the static condition, even at the maximum spin condition. In fact, there was a noticeable decrease in ambient noise as the disk assembly went from a static to a spin condition, again indicating a problem with signal transmission through the Tilton slipring. While the system did remain functional, with the pulsing transducer being received and source located throughout the spin program, the serious electrical noise problem would prevent the use of total system gain at the required level to receive AE from actual propagating cracks. A possible solution, using an improved slipring, is presented in Section IV.

RESIDUAL LIFE STUDIES (PHASE IV)

Disk S/N BAA 43 received 743 operational hours in experimental F100 engine S/N FX 217. The disk was then subjected to 11,140 room-temperature, Type I LCF cycles in the ferris wheel fixture in an attempt to precrack the disk for fracture mechanics analysis. Maximum measured strain was 0.97% at the acute corner of a radial cooling hole at 14,640-lb drawbar load. An AE inspection during the room temperature cycles and periodic inspection using the conventional NDE techniques produced no flaw indications. Fracture mechanics minimum residual life analysis for further ferris wheel testing at elevated temperature was therefore initiated from an initial flaw size of 10-mils (see Section IV for residual life calculations).

Ferris wheel testing was then continued at 1200°F, $\epsilon_{max} = 1.0\%$, 2 cpm, with AE real time inspection being performed to detect initiation. Near 100 cycles, AE inspection began to indicate crack activity. At 250 cycles, the disk received an inspection using conventional NDE techniques, revealing fatigue cracks in three radial cooling holes. Periodic measurements were then made of the largest crack until the disk failed at 550 elevated-temperature cycles. Crack length measurements along the outside of the radial cooling hole and into the hole are presented as Figure 46.



FD 148911

Figure 46 1st-Stage Turbine Disk Fatigue Crack Measurements, Radial Cooling Hole

First-stage turbine disk S/N OZ 7463 received 1001 Type I LCF cycles in F100 engine S/N P036. The disk was subjected to an additional 909 elevated-temperature Type I cycles in the ferris wheel before room temperature AE inspection was performed by loading the disk to a maximum drawbar load of 12,300 lb for 41 cycles. An AE inspection and subsequent conventional NDE assessments produced no flaw indications. Fracture mechanics minimum life predictions (Section IV) were then made from an initial flaw size of 10-mils

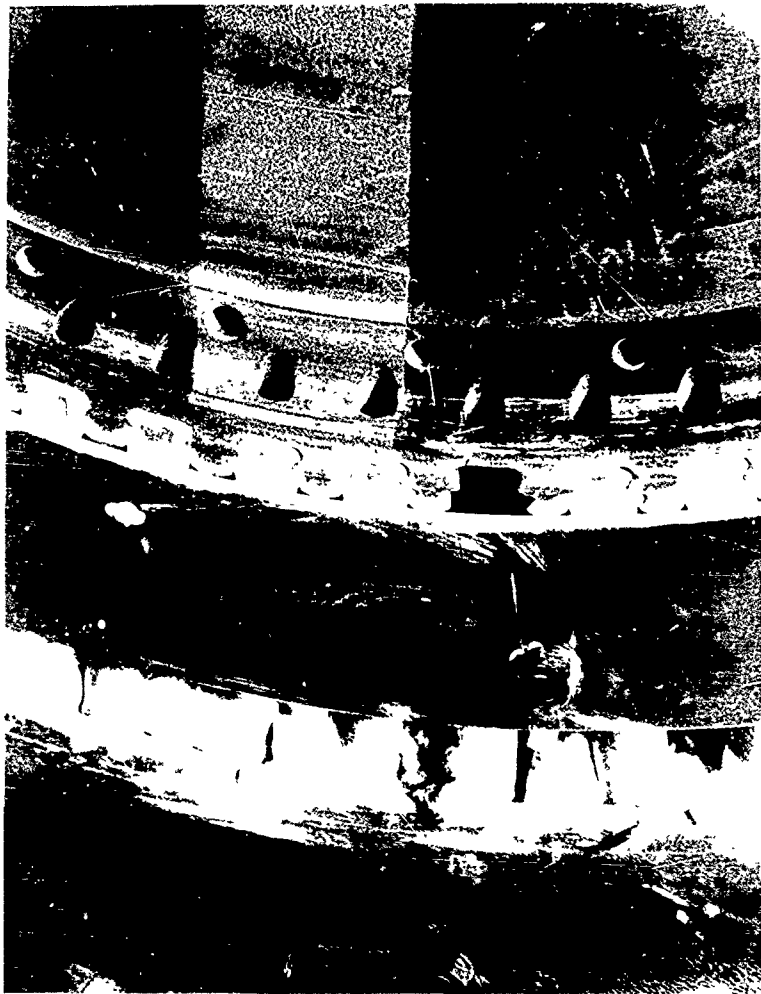
Elevated-temperature fatigue cycling was then resumed at 975°F, $\epsilon_{max} = 0.92\%$, 2 cpm, with AE real time inspection being performed to detect initiation. AE inspection indicated fatigue crack extension from cycle 1550, and conventional NDE performed after cycle 2500 confirmed the presence of two cracked radial cooling holes. One of the cracks propagated 100% through the disk at 3400 total elevated temperature ferris wheel cycles

In summary, crack initiation life for disk S/N OZ 7463 was between 1910 and 2551 cycles (including 1001 engine cycles) and propagation life was bounded by 1850 to 2491 cycles.

First-stage turbine disk S/N BDB 257 was engine-cycled in experimental engine FX 221 to a total of 1121 Type I, 25 Type II, and 755 Type III LCF cycles. The disk was then subjected to room temperature AE inspection in the ferris wheel, as well as conventional NDE, before being reinstalled in FX 221. The inspection procedure was repeated periodically (before engine rebuilds) a total of four times before the disk was finally retired, still receiving no NDE indications. Disk S/N BDB 257 accumulated a total of 3425 Type I, 25 Type II, and 5867 Type III LCF cycles in FX 221. Fracture mechanics minimum life predictions for the subsequent ferris wheel test were then based upon an initial flaw size of 10-mils.

After bore modification, the disk was subjected to Type I LCF cycles at 1050°F, $\epsilon_{max} = 0.95\%$, 2 cpm in the laboratory. Continuous AE inspection and periodic inspections using FP and the Circograph were conducted throughout the ferris wheel program. Fatigue cracking was first indicated by AE inspection near ferris wheel cycle 11,000, and the following periodic inspection at 11,500 cycles produced EC indications from two radial cooling holes. All of the radial cooling holes, axial boltholes, and one axial cooling hole received Circograph indications before the disk finally failed at 14,062 ferris wheel cycles. Since the likelihood was low that all of the radial cooling holes and axial boltholes in BDB 257 were cracked, the preinspection preparation procedure was modified to include vapor blasting for oxide layer removal. Subsequently, all Circograph indications, except one in a radial cooling hole, disappeared. Fractographic analysis of the disk confirmed only that single crack.

Failure of BDB 257 was nonstandard. A furnace element shorted against the disk at the edge of an axial cooling hole (not the fracture critical location), causing a weak recast layer which initiated the fatal fatigue crack (Figure 47). However, the confirmed radial cooling hole crack would have caused disk failure in less than 100 cycles. The inspection record from the BDB 257 ferris program is listed in Table 10.



FD 11156

Figure 47 Front View Showing Crack from Axial Cooling Hole at "Failure" Condition

TABLE 10
1st-STAGE TURBINE DISK S/N BDB 257
FERRIS WHEEL PROGRAM INSPECTION RECORD

<i>Cycle</i>	<i>AE Indication</i>	<i>Circograph Indication</i>	<i>FP Indication</i>
6,500	No	No	No
7,550	No	No	Yes (scratches)
8,550	No	No	No
9,550	No	No	No
10,253	No	No	No
11,000	*Yes	—	—
11,500	Yes	Two Radial Holes	No
12,500	Yes	Six Radial Holes One Axial Cooling Hole	One Axial Cooling Hole
13,592	Yes	66 Radial Holes All Axial Boltholes One Axial Cooling Hole	One Axial Cooling Hole
14,062 (Failure)	Yes	68 Radial Holes All Axial Boltholes Failure at Axial Cooling Hole	Bore (initiation at a second recast area)
Vapor Blast Radial Holes	—	One Radial Hole (Confirmed by Fractography)	—

*Real time inspection during fatigue test.

SECTION IV
DISCUSSION — F100 1st STAGE TURBINE DISK

PHASE I (ACOUSTIC EMISSION FATIGUE CHARACTERIZATION)

Crack propagation studies revealed the AE threshold (stress intensity above which crack propagation AE is detectable) to be lower for elevated temperatures (1000°F and 1200°F) than room temperature. However, the AE threshold appeared to be associated with a similar crack growth rate (da/dN) in all cases, indicating that an AE rate vs da/dN relationship may be more universally applicable than an AE rate vs ΔK relationship.

It is apparent from the strain-control LCF test results that at least four different stages of fatigue damage in elevated temperature IN100 may be characterized using time-domain AE multiparameter distributions (MPD). The respective AE characteristics are illustrated in Figure 23. The four fatigue stages are:

Stage I — Nucleation

MPD Phenomenon

- All three time-domain distributions (ringdown counts per event, pulse width, and peak amplitude) fluctuate during the initial "shakedown" portion of a typical test, followed by relatively small consistent parametric values.

Mechanism

- "Shakedown" is a combination of extraneous noise from the test load train and acoustic output from initial plasticity at the specimen gage section.
- During nucleation, dislocations stack up at obstacles such as microporosity and grain boundaries.

Stage II — Microcrack Initiation

MPD Phenomena

- Increased maximum ringdown counts per event
- Longer signal pulse widths
- Little variation in peak amplitudes

Mechanism

- Microcracks begin to form in regions of highest stress concentrations both internally and externally. These events occur individually over longer periods of time than stackup (producing longer AE signal pulse widths and greater ringdown counts per event), but energy release is not great enough to appreciably affect AE amplitude distributions.

Stage III — Transition

MPD Phenomena

- Maximum ringdown counts per event and maximum signal pulse widths decrease to levels occurring previously during the nucleation stage.
- Amplitude distributions still display little change.

Mechanism

- Dislocations are moving to free surfaces (microcracks) as they occur. Lack of stacking before dislocations are released produces shorter lived individual acoustic bursts (i.e., shorter pulse widths and fewer ringdown counts per event than during microcrack initiation).

Stage IV — Macrocrack Propagation

MPD Phenomenon

- All three time-domain distributions display increases in maximum parametric values.

Mechanism

- Large incremental advances in the fatigue crack(s) occur, producing relatively large acoustic energy release with each advance. Internal crack propagation reaches the specimen surface and oxidation layer cracking (as well as the large acoustic energy release) contributes to higher acoustic peak amplitudes. Each event occurs over a longer period of time than those occurring during nucleation or transition phases, thus producing longer signal pulse widths and more ringdown counts per event.

Detection of fatigue macrocracking may be performed solely on the basis of AE peak amplitude distribution analysis. The results support the theory (Reference 15) that larger deformation events produce more AE energy, and, therefore, larger AE peak amplitudes.

PHASE II (NONDESTRUCTIVE EVALUATION OF COMPLEX GEOMETRY SPECIMENS)

It was apparent that the AE MPD phenomena associated with microfatigue damage in the IN100 strain control LCF specimens was not readily detectable from the complex geometry LCF specimens. These subtle AE characteristics were not useful to classify fatigue damage in the Phase II specimens because: (1) the highest strain volume of the complex geometry dovetail and bolthole specimens was relatively small compared to that of a strain control specimen, and the AE phenomena recorded during the microcrack initiation stage of Phase I tests resulted from many microdeformations or fractures rather than single events, (2) extraneous AE signals (from load trains, etc.), resulting from higher loads required to fatigue Phase II specimens, masked most subtle changes in the AE distributions as testing progressed.

Because EC inspection may be capable of detecting local material perturbations due to early fatigue damage in the IN100 LCF specimens, it is difficult to distinguish between false indications and real defects (a Type II error). Although fracture mechanics analyses from a 3 mil initial flaw size would disclaim the possibility that macrocracks existed at the first EC indications during several tests, these early indications were not considered false if they registered at surface locations which eventually developed into fatigue macrocracks.

The edge-sensitive EC probe developed at P&WA/GPD was evaluated during bolthole simulation inspections with the Defectometer system. However, even though the design revision was useful for edge cracks, the probe was virtually ineffective because of bolthole interior crack initiations during each test. The probe was not capable of inspecting cracked regions.

Type II errors were a major obstacle during Phase II EC inspections. A revised preinspection preparation procedure using an abrasive plastic wool (Scotch Brite) proved to be effective in removing most of the oxidation effects which were a primary cause of the Type II errors, and during Phase III and IV vapor blasting was introduced to streamline the procedure.

The AE Type II errors were substantially reduced through (1) use of a relatively high resonant frequency (approximately 750 kHz) transducer, (2) use of spatial filtering, and (3) development of antrub coatings for load mechanisms.

Bolthole simulation specimen BC-3 was tested at room temperature to a fatigue crack length of approximately 10-mils at the bolthole. Continuous AE inspection failed to produce any distinct macrocrack indications before EC, wink FPI, and replication confirmed the flaw. This result is in agreement with previous crack propagation testing performed to relate AE threshold levels to stress intensity. It was determined that the stress intensity at the tip of a 10-mil flaw subjected to a 144 ksi net stress field was less than the room temperature AE threshold stress intensity ($16 \text{ ksi} \sqrt{\text{in}}$) for the inspection parameters (sensor, gain, system threshold, etc) employed.

Heat treatments at 1200°F in air were conducted on BC-3 to determine the effect of oxidation layers on acoustic activity from the small (10-mil) fatigue crack. Room temperature cycles were then conducted while monitoring with one-dimensional AE source location to distinguish between AE from the fatigue crack and extraneous noise from the load train. Test cycles were conducted using the 750 kHz resonant Dunegan/Endevco D750A transducer.

The specimen was again heat treated and subjected to similar room temperature cycles while monitoring with a 140 kHz resonant sensor. It was determined that introduction of an oxidation layer in the fatigue crack did cause it to emit at detectable levels even at the relatively low stress intensity of approximately $13 \text{ ksi} \sqrt{\text{in}}$, and AE output was more readily detected with the 140 kHz resonant piezoelectric crystal.

An important point was demonstrated through the failure of bolthole specimens at locations other than primary regions of interest. The AE inspection was able to produce indications of impending failure even when the origins were unknown, the entire specimen gage section was being inspected in each case. It would have been impossible to inspect the regions under tack-welded thermocouples with EC or FPI and, in most cases, it is impractical to use EC inspection in regions other than primary fracture critical zones.

Fracture mechanics life predictions were made for Phase II bolthole and dovetail groove simulation specimens to permit estimates of flaw size detectability by AE and EC inspection techniques. Calculations were made using the GPD \bar{K} computer program (developed by T. Cruse and P. Besuner) which is capable of analyzing a crack located in a stress gradient, such as the region adjacent to a bolthole or groove. The technique utilizes an influence function requiring only the uncracked stress field to determine a stress intensity solution. Table 11 lists calculated macrocrack propagation lives (NDE) for most of the Phase II specimens and propagation cycles confirmed by NDE.

**TABLE 11
CALCULATED MACROCRACK PROPAGATION LIVES
FOR PHASE II SPECIMENS***

Specimen S/N	Net Stress (ksi)	Test Temperature (°F)	Crack Type	Predicted Propagation Life Cycles	Actual Propagation Life Cycles
Dovetail					
D 1	117	1,200	Surface	2,000	>1,000
D-2	133	800	Surface	>3,000 (from 1000°F data)	5,000
D-3	133	1,000	Surface	3,000	>3,720
D-4	133	1,000	Surface	3,000	—
D-5	117	1,200	Surface	2,000	> 929
Bolthole					
BR-1	144	RT	Corner	2,300	> 800
BR-4	82	1,200	Corner	1,700	—
	82	1,200	Surface	1,350	> 300
BR-5	99	1,000	Corner	1,700	—
	99	1,000	Surface	1,500	> 530
BR-6	82	1,200	Corner	1,700	—
	82	1,200	Surface	1,350	—
BC-2	110	1,200	Corner	800	> 300
BC-3	144	RT	Corner	2,300	> 200

*Initial flaw size = 3 mils

The fracture mechanics analyses, along with actual observed crack sizes, entered into the creation of surface flaw detectability estimates for dovetail groove and bolthole simulation specimens. Estimates of flaw detectability and probability of Type II errors are also based on communications with inspection personnel and inferences from actual data. The relative ratings of the various techniques, where possible, have been confirmed experimentally.

Fracture surface analysis/striation spacing of dovetail specimen D-3 resulted in an estimate of over 2300 macrocrack propagation cycles.

Phase II NDE comparisons indicated no inherently superior technique as the optimum inspection procedure for the F100 1st-stage high pressure turbine (HPT) disk. However, a listing of the relative advantages and disadvantages of each technique was produced, along with suggestions for complementary inspections. The listing is presented in Section IV.

PHASE III (NDE OF THE TURBINE DISK)

Fractography results from disk S/N BM 798 indicate that EC inspection produced Type II errors during both cooling hole and lug inspections. It is possible that all of the cooling hole "small" indications shown in Table 8 were Type II errors, although confirming fractography of all the radial cooling holes was prohibited by cost and time restraints.

Inspection results from disk S/N BM 798 also confirm Phase II results showing inspection to be the most sensitive of the three techniques evaluated (see cooling hole No. 24)

Initially, an abrasive plastic wool was used to prepare the disk radial cooling holes prior to EC Circograph inspection. Results shown in Table 8 reflect this preinspection preparation. However, the radial cooling holes were later mildly vapor blasted to remove any residual oxidation effects, and subtle changes occurred in the subsequent EC indications. In general all indications, as well as baseline flutter, were reduced in size. However, indications from several holes, including hole No. 24 (containing a 0.010×0.005 in. crack), were actually sharpened and more easily resolved. This phenomenon can be explained as either elimination of residual oxidation effects or rearrangement of residual stresses in the cooling holes. Further investigation is currently underway at GPD. Preliminary impetus for the use of vapor blast to prepare EC inspection surfaces, instead of manual preparation using abrasive plastic wool, is reduction in manhours required to perform the procedure. However, these results indicate that greater crack resolution may also be obtainable using vapor blast as preparation.

Phase III laboratory vs production FP results indicate production inspection may miss disk lug cracks which are detectable under more carefully controlled laboratory conditions.

Spin study results using the computerized AE system were encouraging from the standpoint that the system did remain functional as an automatic AE source locator through the full range of spin conditions. But due to the low gain levels required to prevent reception of spurious electrical noise, the system is currently incapable of actual fatigue crack inspection. The system has recently been rechecked in the laboratory in Condition D of Table 9 using a slipring manufactured by Lebow Associates, Inc. Maximum gain achievable using the new slipring was 99+ dB, as good as the baseline condition. This means that the system could be run at gain settings which are practical for the detection of fatigue crack propagation in IN100 with adaptation of the Lebow slipring. The associated cost of fixturing and spin modifications cannot be considered within the scope of this program, but future spin studies will incorporate the new slipring design. An IR&D program, whose goal is to detect an actual propagating crack in a spinning disk, is scheduled for late 1979.

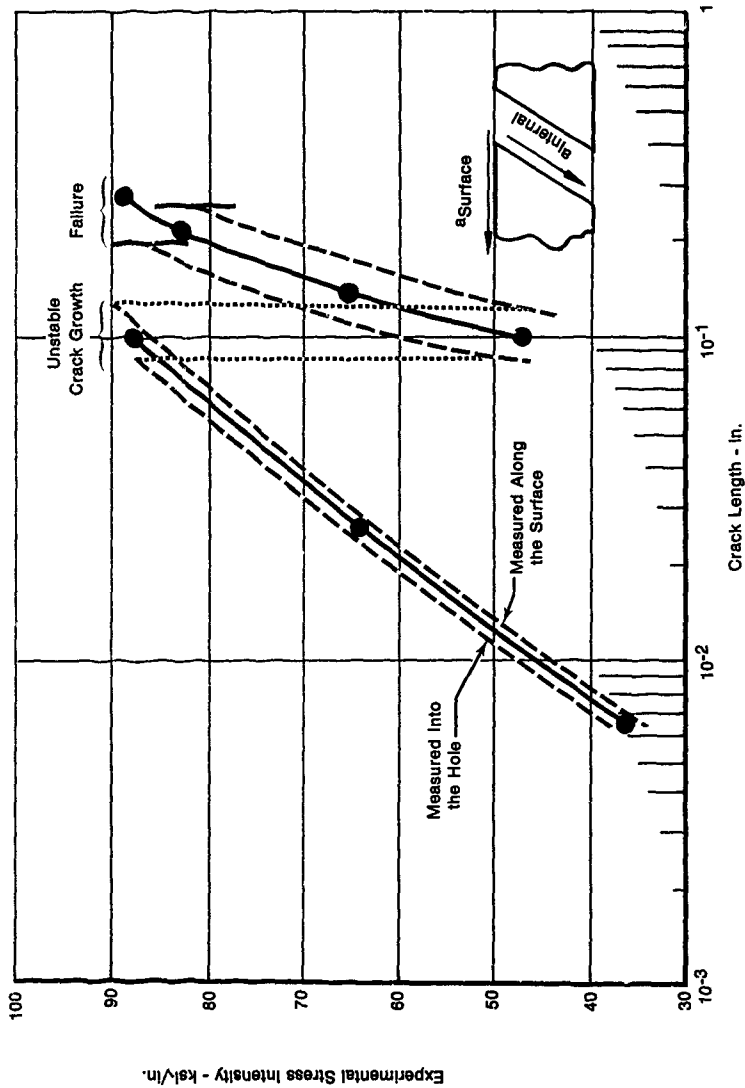
PHASE IV (DISK RESIDUAL LIFE STUDIES)

Life predictions for ferns wheel LCF testing of three 1st-stage turbine disks were based on an interpolative empirical fracture mechanics model based on the hyperbolic sine Model development was performed by GPD personnel for AFML Contract F33615-75-C-5097. Development and primary applications of the hyperbolic sine model are thoroughly discussed in References 5, 6 and 7. The interactive effects of stress, temperature, time and environment are described with the model.

$$\text{Log}(da/dN) = C_1 + \sinh(C_2 + (\log(\Delta K) + C_3)) + C_4 \quad (4)$$

The stress intensity solution for Phase IV disk life predictions was developed from empirical data generated during crack propagation testing of turbine disk S/N BAA 43. Crack growth (a vs N) data developed from the disk test (Figure 46) were correlated with da/dN vs ΔK data from compact tension specimen tests at the same temperature, stress ratio, and frequency, to produce a normalized K vs a relationship (Reference 16). The model is presented as Figure 48.

The K/ϵ vs a plot reflects an abrupt change in crack growth rate the first time $90 \text{ ksi}/\sqrt{\text{in}}$ was attained. Ultimate failure of the disk occurred when $90 \text{ ksi}/\sqrt{\text{in}}$ was again reached. This value corresponds approximately to the maximum value observed during crack growth rate testing. Whereas exceeding this maximum stress intensity results in failure during laboratory da/dN testing, it is felt that the bulk of the disk surrounding the cooling hole prevented catastrophic failure when this critical value was first exceeded; failure of the material surrounding the hole occurred when this was exceeded a second time.



FD 148812

Figure 48. K/ϵ vs a Relationship for F100 1st-Stage Turbine Disk Radial Cooling Hole

Disk S/N BAA 43 was LCF tested in the ferris wheel at 1200°F, 2 cpm, R = 0.02. Since no fracture mechanics data were available at those conditions, the hyperbolic sine model for existing 1200°F, 10 cpm, R = 0.1 data was stress ratio and frequency adjusted to produce an interpolative da/dN vs ΔK relationship for the disk test. The da/dN data from which the frequency model was derived are illustrated in Figure 49. From Figure 50, "Effect of Frequency on SINH Model Coefficients C₂ and C₄," the coefficients C₂ and C₄ for the 2 cpm model were calculated as 3.68 and -4.20, respectively. From the C₃ vs C₄ relationship in Figure 49, C₃ was determined to be -1.422. For IN100, C₁ has a fixed value of 0.500. The model for 1200°F, 2 cpm, R = 0.1 takes the form

$$\text{Log}(da/dN) = 0.5 \sinh(3.68(\log(\Delta K) - 1.42)) - 4.20 \quad (5)$$

From the stress ratio model, colnearity of the sinh curve inflection points (Figure 51) may be described by.

$$C_4 = -M_3 C_3 + B_3 \quad (6)$$

Assuming linear change of M₃ with frequency change, M₃ = 0.92. C₃ and C₄ are already known; therefore:

$$C_4 = -0.92 C_3 - 5.51. \quad (7)$$

From Figure 52, "Effect of Stress Ratio, R, on sinh Model Coefficient, C₃":

$$C_3 = M_4 \log(1-R) + B_4 \quad (8)$$

Assuming linear change of M₄ with frequency change,

$$B_4 = 0.542 \log(1-0.1) - 1.42 = -1.45 \quad (9)$$

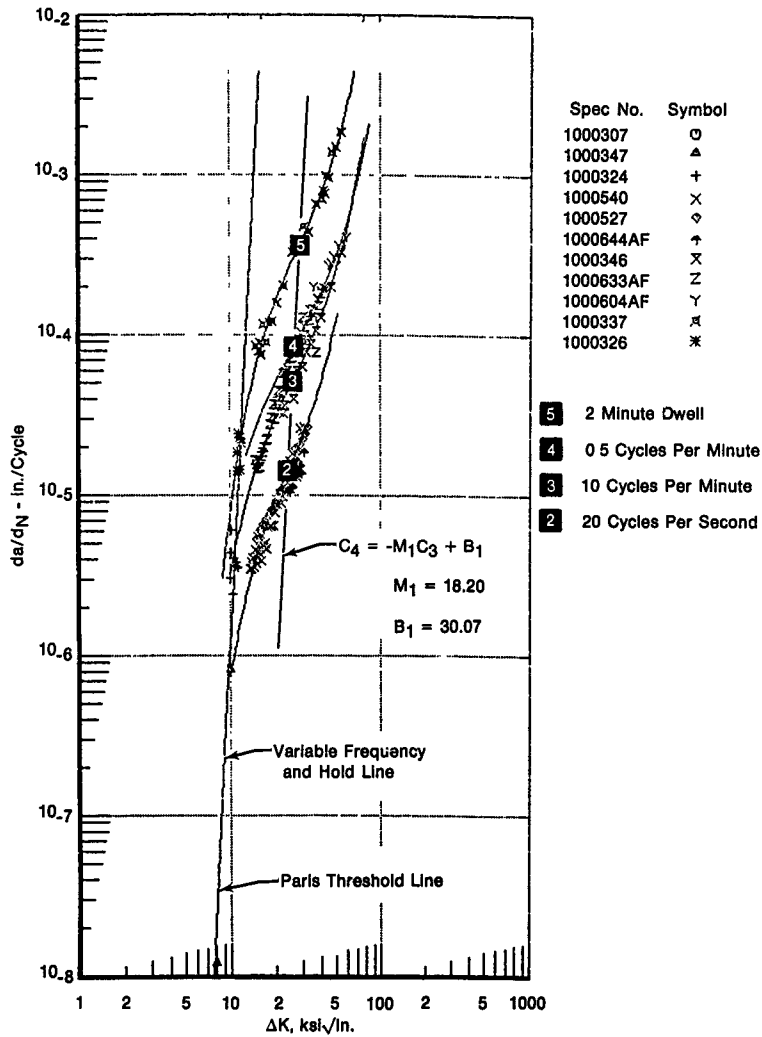
$$C_3 = -0.542 \log(1-R) - 1.45. \quad (10)$$

Using equation (10) for the new stress ratio, R = 0.02, C₃ = -1.442. From equation (7), C₄ = -4.18. Prior experience has shown that C₂ varies little with minor changes in stress ratio, so the interpolative crack growth model for disk S/N BAA 43 test conditions (1200°F, 2 cpm, R = 0.02) is

$$\text{Log}(da/dN) = 0.5 \sinh(3.68(\log(\Delta K) - 1.44)) - 4.18 \quad (11)$$

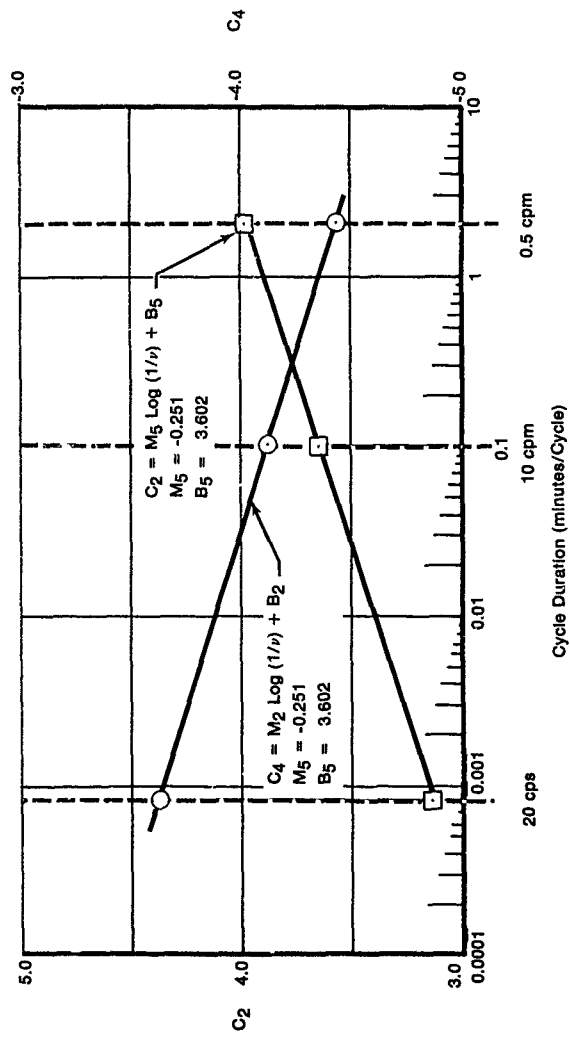
The above crack growth rate model is presented in Figure 53 as curve No. 1. Upon development of the experimental stress intensity model, the GPD life analysis computer program was checked for functionality (correlating actual vs calculated life cycles). The comparison is shown as Figure 54.

The 1st-stage turbine disk S/N OZ 7463 (retired from experimental F100 engine P036) was ferris wheel LCF tested at 975°F, R = 0.02, with a 2-min dwell at maximum load. Crack growth data did not exist for the above conditions, so the available 1200°F, R = 0.1, 2-min dwell curve was adjusted for temperature and stress ratio to produce an interpolative hyperbolic sine da/dN model for the disk test.



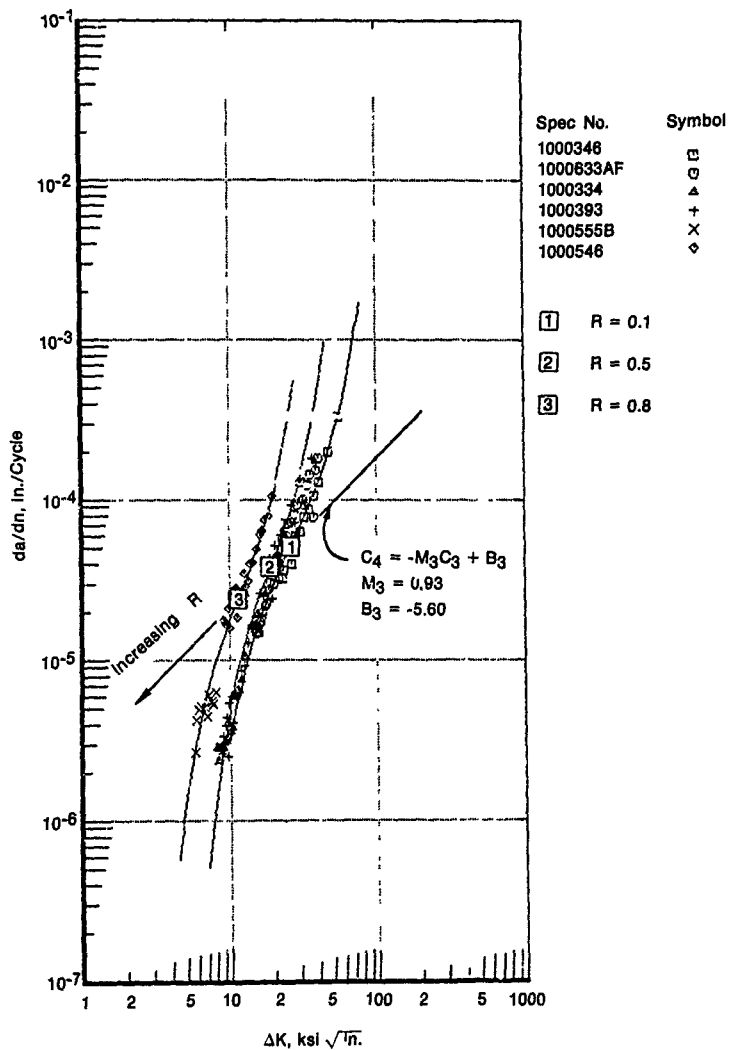
FD 14811

Figure 49. The Effect of Frequency on Crack Growth Rate at 1200°F, R = 0.1



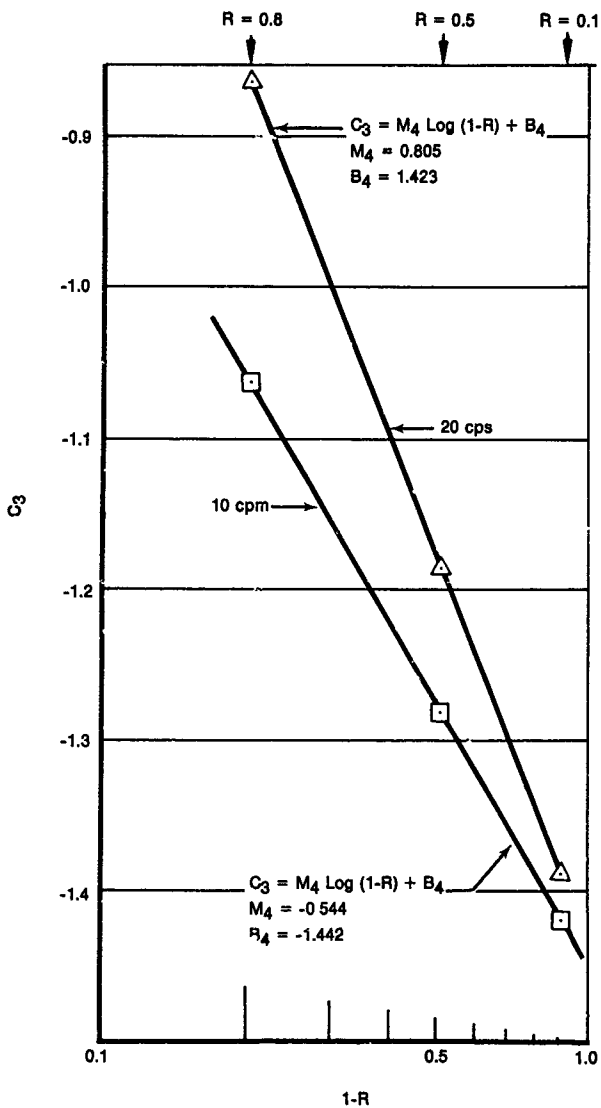
FD 14894

Figure 50. Effect of Frequency on Sinh Model Coefficients C_2 and C_4 at $1200^\circ F$, $R = 0.1$



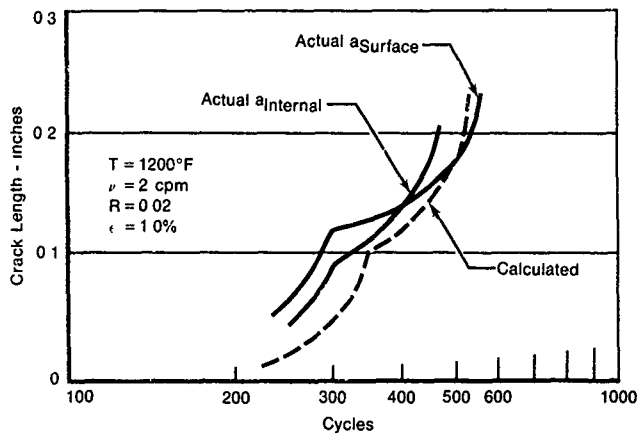
FD 148915

Figure 51. Effect of Stress Ratio on Crack Growth Rate at 1200°F, 10 cpm



FD 148916

Figure 52. Effect of Stress Ratio, R , on Sinh Model Coefficient, C_3 , at $1200^\circ F$



FD 164827

Figure 54. 1st-Stage Turbine Disk S/N BAA 43, Actual vs Calculated Crack Length, Radial Cooling Hole

The SINH model for 1200°F, R = 0.1, 2-minute dwell is:

$$\text{Log}(da/dN) = 0.5 \sinh(4.20(\log(\Delta K) - 1.45)) - 3.50. \quad (12)$$

Using equation (6) again and assuming linear change of M_3 with frequency change (2-min dwell = 0.5 cpm for frequency adjustments), $M_3 = 0.92$. C_3 and C_4 are known from equation (12), so $B_3 = -4.83$ and,

$$C_4 = -0.92 C_3 - 4.83. \quad (13)$$

Using equation (8) again, and assuming a linear change of M_4 with frequency change, $B_4 = -1.48$ and,

$$C_3 = -0.542 \log(1 - 0.02) - 1.48 = -1.47. \quad (14)$$

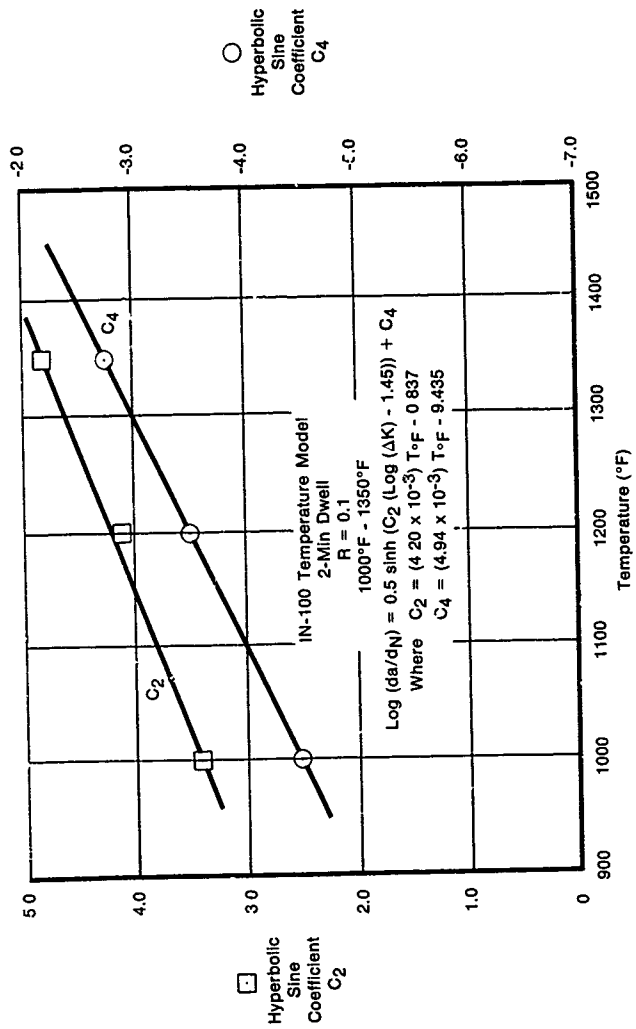
From equation (13), $C_4 = -3.48$. So the interpolative crack growth model for 1200°F, R = 0.02, 2-min dwell, is

$$\text{Log}(da/dN) = 0.5 \sinh(4.20(\log(\Delta K) - 1.47)) - 3.48. \quad (15)$$

The effect of temperature on 2-min dwell testing of IN100 may be illustrated as in Figure 55. Using the relationships,

$$\Delta C_2 = (4.20 \times 10^3) \Delta T_p, \text{ and} \quad (16)$$

$$\Delta C_4 = (4.94 \times 10^3) \Delta T_p. \quad (17)$$



FD 148918

Figure 55 Effect of Temperature on Sinh Coefficients, 1000-1350°F, $\nu = 2$ Minute Dwell, $R = 0.1$

C_2 and C_4 are calculated as 3.26 and -4.59, respectively. The interpolative crack growth model for disk S/N OZ 7463 ferris wheel test conditions is,

$$\text{Log}(da/dN) = 0.5 \sinh(3.26(\log(\Delta K) - 1.47)) - 4.59. \quad (18)$$

The model is shown in Figure 53 as curve No. 2.

Using equation (18) and the experimental stress intensity model developed from the disk S/N BAA 43 program, a *minimum* residual life of 1750 cycles was computed from an initial detectable flaw size of 0.010 in. The initial flaw size was arbitrarily determined from Phase II and Phase III results as the minimum detectable flaw size in the disk radial cooling hole (remembering that before ferris wheel testing was initiated, no flaws were detected). This minimum residual life calculation compares favorably with the actual crack propagation life of 1850 to 2491 cycles. Actual and calculated a vs N are presented as Figure 56.

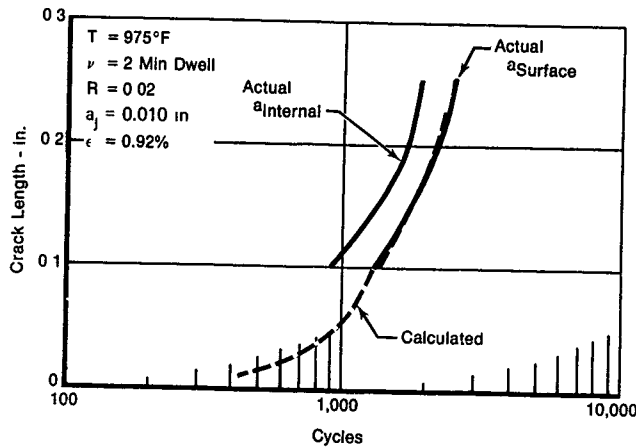
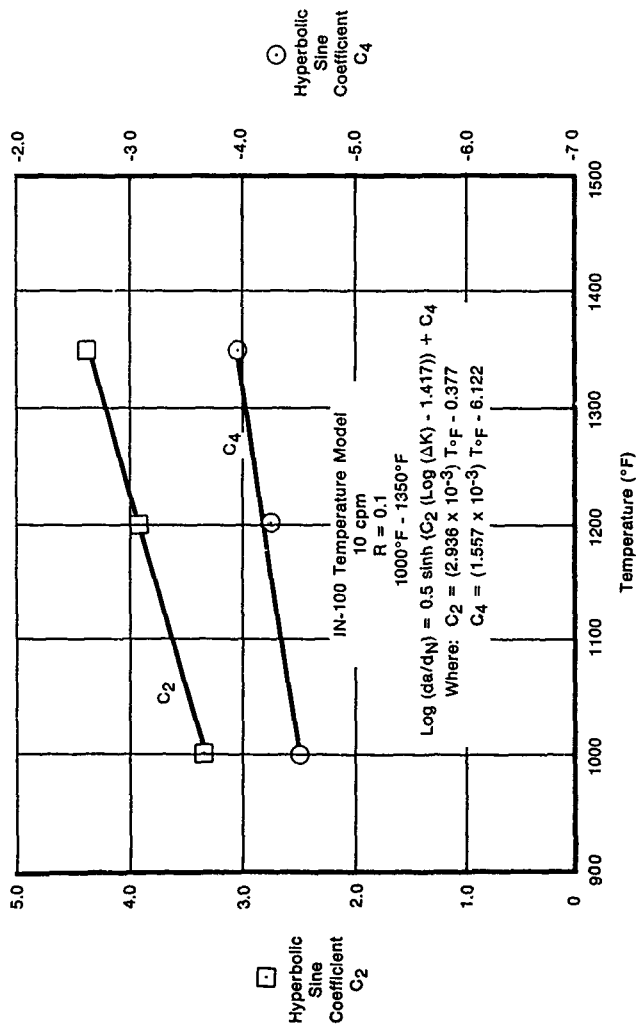


Figure 56. 1st-Stage Turbine Disk S/N OZ 7463 Radial Cooling Hole Residual Life Analysis

To produce an interpolative crack growth model for disk S/N BDB 257 ferris wheel test conditions, the model for disk S/N BAA 43 equation (11) was temperature adjusted from 1200°F to 1050°F. Assuming that the effect of temperature on sinh coefficients C_2 and C_4 is similar at a cyclic frequency of 2 cpm to that at 10 cpm, the relationships of Figure 57 were used to calculate $C_2 = 3.24$ and $C_4 = -4.42$. The crack growth model for disk S/N BDB 257 ferris wheel test conditions (1050°F, 2 cpm, $R = 0.02$) is represented as,

$$\text{Log}(da/dN) = 0.5 \sinh(3.24(\log(\Delta K) - 1.44)) - 4.42. \quad (19)$$

The da/dN model is shown in Figure 53 as curve No. 3.



FD 14820

Figure 57 Effect of Temperature on Sinh. Coefficients, 1000-1350°F, $\nu = 10$ cpm, $R = 0.1$

A fracture mechanics residual life analysis was again performed using equation (19) and the stress intensity solution of Figure 48. The resulting a vs N relationship (Figure 58) predicts a residual life of 959 cycles from a $a_0 = 0.010$ in. Therefore, periodic inspections were performed during the ferris wheel test program in increments of 1000 cycles or less to demonstrate flaw inspectability before disk failure (the basis of Retirement-for-Cause philosophy).

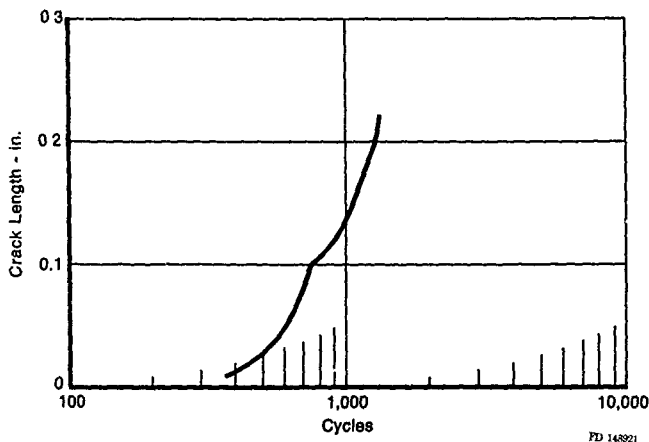


Figure 58 1st-Stage Turbine Disk S/N BDB 257 Radial Cooling Hole Residual Life Prediction

After the disk had exhausted a "safe" portion of its LCF life, periodic inspections began at cycle 6500. Real time AE rate inspection indicated fatigue cracking beginning near cycle 11,000, but EC inspection could not locate a defect in a radial cooling hole (primary fracture critical location). At 12,500 cycles, FP inspection located the crack in an axial cooling hole, so the EC inspection procedure was modified to evaluate all axial holes, as well as the radial cooling holes. The disk failed at 14,062 cycles from the axial cooling hole crack, which was caused by a weak recast layer at the hole edge. The importance of performing AE and FP inspections is illustrated in this case when fracture originated at a nonstandard location.

By the time BDB 257 failed, most of the radial and axial holes contained Circograph indications. As mentioned in Section III, the radial holes were vapor blasted after disk failure in an effort to remove any oxidation effects. The procedure worked well, since the only remaining Circograph indication after vapor blast was verified by fractography as a fatigue crack. The 0.050-in. crack was easily detected using the Circograph and would have taken approximately 700 additional cycles to cause disk failure.

It is apparent that an F100 1st-stage turbine disk tested at the conditions of S/N BDB 257 (1050°F, 2 cpm, $R = 0.02$, $\Delta\epsilon = 1.0\%$) will contain an inspectable defect using the inspection methodology developed during this program (complementary AE, FP and EC evaluations) and strategically spaced inspections. By a similar philosophy, a 1st-stage turbine disk could be periodically removed from an F100 engine and inspected until a quantifiable defect necessitates "Retirement-for-Cause." This would require stringent, laboratory-controlled inspection procedures not currently available at Air Force overhaul depots.

Both of the previous Phase IV disk tests support the residual life prediction philosophy in that actual residual ferris wheel fatigue lives correlated closely with predicted crack propagation lives from an a_c below the inspectability limit when a "no flaw" situation was indicated by NDE at the final inspection. Disk test results are summarized in Table 12.

TABLE 12
DEMONSTRATION OF RESIDUAL
LIFE PREDICTION PROCEDURE

<i>Disk S/N</i>	<i>BAA 43</i>	<i>OZ 7463</i>	<i>BDB 257</i>
F100 Engine	FX217	PO36	FX221
Engine LCF Cycles	1311	1001	9317
Baseline Inspection	*	*	*
F/M Minimum Life ($a_c = 0.010$ in)	303 Cycles	1750 Cycles	959 Cycles
First Flaw Indication From Acoustic Emission	100 Cycles	1550 Cycles	11,000 Cycles
Residual Life	550 Cycles	3400 Cycles	14,062**Cycles
Residual Life From First Indication***	450 Cycles	1850 Cycles	3,062 Cycles

*No indications from AE, FPI, or Eddy Current.

**Failure at nonstandard location

***Compare with "F/M Minimum Life ($a_c = 0.010$ in)"

SECTION V
CONCLUSIONS — F100 1st STAGE TURBINE DISKS

Development and evaluation of AE technology throughout this program has resulted in the following observations:

- AE inspection is *sensitive to unexpected defects in the entire component*, as well as those in primary fracture critical locations
- AE inspection is *not limited to surface or near-surface defects*,
- Application of AE techniques to real time component inspection of operating gas turbine engines is a possibility.

While AE inspection would not be successful as a periodic inspection to indicate *initiation* stages in an IN100 turbine disk (due to lengthy periods of low AE activity), it has been successful as an indicator of fatigue crack *propagation* damage and would suffice as a periodic inspection in that realm (Figure 59). There is no available NDE technique which will perform satisfactorily as a periodic inspection to assess fatigue initiation damage.

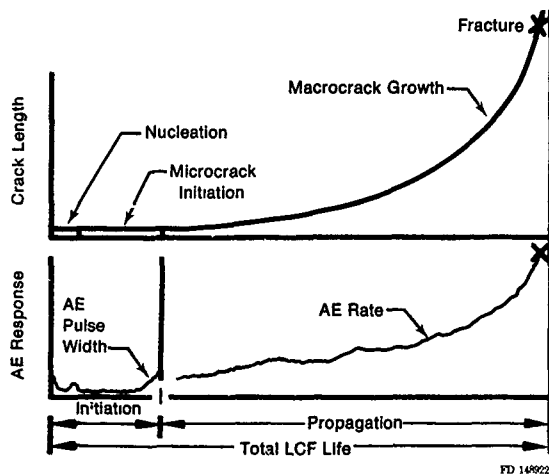


Figure 59 AE Response During Total Fatigue Life of Wrought GATORIZED[®] IN100

The results of Phase IV NDE and fracture mechanics studies indicate that, based on a fracture mechanics minimum residual life prediction, an F100 1st-stage HPT disk could be periodically inspected at realistic intervals, reinstalled in an engine, and retired only when a series of complementary inspections produces a flaw indication. The complementary inspections include specialized applications of AE, EC, and FP techniques. The resulting Retirement-for-Cause philosophy may be expanded to include many "fracture-limited" engine components through application of fracture mechanics life analysis and state-of-the-art laboratory NDE.

Phase III disk inspection and fractography results demonstrate the necessity of complementary and redundant inspections to diminish both Type I and Type II errors. For any particular inspection requirement the relative economics of inspection costs vs the impact of increasing Type I and Type II errors will have to be weighed to produce the optimum inspection method.

The basis for Phase II studies was a comparative analysis of state-of-the-art NDE techniques as applied to simulated turbine disk fracture critical locations. Rather than producing a "most sensitive" technique, a set of relative advantages and disadvantages was determined for each procedure, leading to intelligent application of each toward a complementary inspection methodology for the F100 1st-stage HPT disk.

ACOUSTIC EMISSION

Advantages

1. Inspection is sensitive to unexpected defects in the entire component, as well as those in primary fracture critical locations.
2. Inspection is not limited to surface or near-surface defects, e.g., AE was sensitive to internal defect in bolthole specimen.
3. Application of AE techniques to real time component inspection of operating gas turbine engines is a possibility.

Disadvantages

1. The specimen or component must be stressed to perform AE inspection.
2. Inspection sensitivity is dependent upon material characteristics.

For example, cast IN100 specimens stressed at elevated temperature produced AE rates two orders of magnitude higher than wrought IN100 specimens stressed at similar conditions upon initiation of fatigue cracking.

EDDY CURRENT

Advantages

1. A small flaw (crack length of approximately 20-mils or less) is more easily detected in a properly prepared surface using this technique.
2. Required inspection fixturing is relatively simple since no stressing of the specimen or component is required.

Disadvantages

1. Inspection is so sensitive to extraneous materials, such as oxidation layers, that only a rigorous and highly controlled preinspection surface preparation may prevent an intolerable number of rejections due to Type II errors. Of the inspection methods evaluated, EC produced the highest incidence of erroneous flaw indications.

2. The technique is viable only for inspection of consistent specimen or component geometries. Major setup changes are required to inspect varied surface configurations.
3. Inspection is limited to surface or near-surface (within 30-mils depth) imperfections.

WINK FLUORESCENT PENETRANT

Advantages

1. More sensitive to surface fatigue cracks than the standard static FPI or room temperature AE inspection of wrought IN100.
2. Laboratory FP inspection has a relatively low incidence of Type II errors when compared to EC or AE inspection.

Disadvantages

1. The specimen or component must be stressed to perform wink FPI.
2. Inspection procedures must be performed while the specimen or component is being stressed, making accessibility to the F100 1st-stage HPT disk (Phase III inspection objective) fracture critical locations difficult.
3. Preinspection surface preparation is required.
4. Inspection is limited to surface defects.

STATIC FLUORESCENT PENETRANT

Advantages

1. A relatively low cost, uncomplicated inspection technique.
2. Relatively low incidence of Type II errors (Laboratory FP)

Disadvantages

1. Inspection sensitivity is much lower than the sensitivity of any other technique evaluated, causing a higher incidence of Type I errors.
2. Preinspection surface preparation is required.
3. Inspection is limited to surface defects.

**REPLICATION — (TRANSFER OF INSPECTION SURFACE DETAILS TO ACETATE FILM;
MICROSCOPIC EXAMINATION OF ACETATE REPLICA)**

Advantages

1. Replicas taken while a specimen or component is being stressed may be as sensitive to small surface cracks as with FPI.
2. A replica acts as a permanent pictorial record of each inspection.

Disadvantages

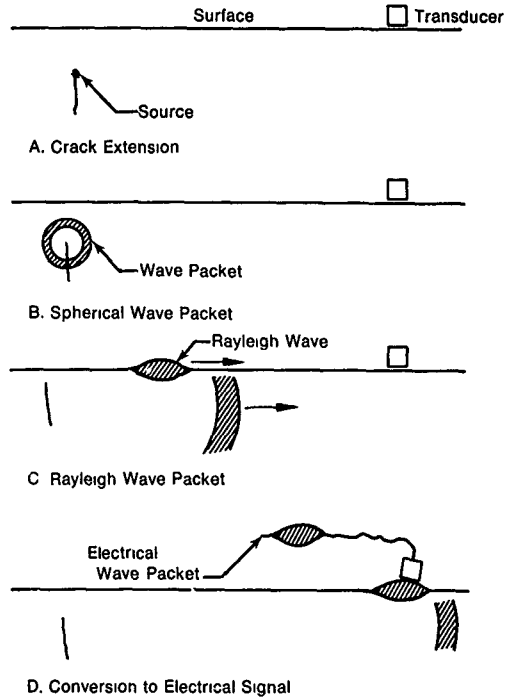
1. The inspection surface must be properly stressed to allow a high degree of sensitivity to small, normally closed fatigue cracks.
2. Tedious preinspection surface preparation is called for to prevent difficulty in visual interpretation of results.
3. Performance of replication inspection and data interpretation is relatively time-consuming.
4. Inspection is limited to surface defects.

**APPENDIX
ACOUSTIC EMISSION ANALYSIS**

NATURE OF AN ACOUSTIC EMISSION EVENT

Acoustic emissions (AE) are low intensity waves that can occur when a material is stressed. The mechanisms for AE range from basic dislocation motion to macroscopic crack growth (References 17 through 20.)

Figure 60 illustrates a simple AE event. Assume a material imperfection such as a crack in a deformable solid. When the material is stressed, it is possible that the crack advances a small amount. The energy input to create new crack surfaces is balanced in part by elastic energy dissipated in the form of a complex spherical wave. It is important to understand that this is a transient event. If this wave continued to propagate in an infinite body, it would lose energy at a rate proportional to R^2 , where R is the distance from the source.



FD 175144

Figure 60 A Simple Picture of an Acoustic Emission Event

In a real engineering structure, however, this complex wave packet soon confronts a boundary. When monitoring AE, a piezoelectric transducer is mounted on this boundary. Depending on the thickness of the structure, Rayleigh or Lamb surface waves are created. These surface waves are stronger than internal waves in that they decay as R^{-1} . In reality, these surface waves are generally composed of both longitudinal and shear components, and the transducer response to these components is a function of its design. The ideal transducer has good, flat response over a relatively broad frequency range.

ANALYSIS OF AE SIGNALS: TIME DOMAIN

An underlying motivation in AE research is to correlate the electrical signal output of the transducer to the integrity of the component being monitored. The characterization of the AE signals therefore requires a thorough understanding of AE signal analysis techniques, stress wave transmission properties of the material component, the transducer response, and of course the deformation and fracture processes in the material.

Cumulative Counts and Count Rate

The most common and simplest measure of AE is the threshold-crossing counts technique. Here, as the transducer resonates due to some input energy, the number of events that exceed a set threshold voltage value are counted, as shown in Figure 61. Total counts or count rates are usually obtained as a function of some secondary test parameter(s), e.g., load or time. This method is best suited for burst-type AE and is, of course, sensitive to amplitude. The "count" is only indirectly related to the damage event as experienced at the transducer.

Ringdown Counts Per Event

The number of ringdown counts per event (η) is related to the amplitude and pulse width of the signal. For burst-type emission, it has been assumed (Reference 14) that the signal is a damped sine wave of the form:

$$V_t = V_o e^{-t/\tau} \sin 2\pi ft \quad (20)$$

where,

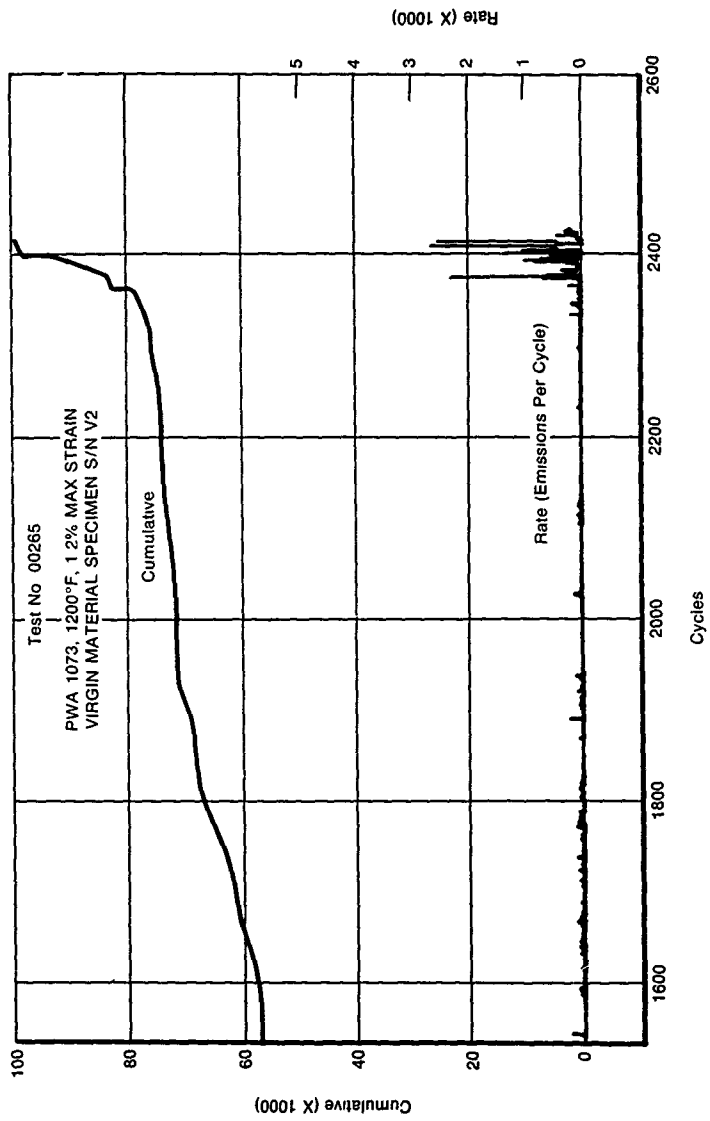
- V_t = AE signal at the transducer
- V_o = peak voltage
- f = transducer resonant frequency
- τ = damping factor
- t = time

If the ringdown time is large compared to the period of oscillation, then:

$$\begin{aligned} \eta &= fr \ln \frac{V_o}{V_t} \\ &= fr \ln \frac{CG}{V_t} \end{aligned} \quad (21)$$

where,

- η = ringdown counts per event
- G = total gain
- C = proportionality constant



FD 173145

Figure 61. Test No. 00265: Cumulative Emissions and Emissions Rate vs Cycles

The values of f and τ depend upon the geometry and acoustic transmission properties of the structure, the loading system, the resonant properties, and mounting of the transducer.

There are serious drawbacks to using counting techniques alone. Among these are sensitivity to the threshold voltage and unsuitability for monitoring continuous type emission

RMS Voltage

For the case of continuous emission, it can be assumed that if the signal is of constant amplitude V_0 and frequency f , the signal can be represented by:

$$V_1 = V_0 \sin 2\pi ft \quad (22)$$

The rms voltage, V_{rms} , is measured as a mean value over some averaging time. It is comparable to the count rate measurement and is ideally suited for measuring continuous emission. A problem arises if the background noise is more than half the intensity of the real signal. The true signal can then be corrected by the approximate expression (Reference 22).

$$V_{rms}(\text{corrected}) = [V_{rms}^2(\text{measured}) - V_{rms}^2(\text{noise})]^{1/2} \quad (23)$$

The energy rate, or power, of the AE signals can be approximated by the square of V_{rms} (Reference 21)

$$U = \int_0^1 V_1^2 dt = V_0^2 \int_0^1 \sin^2 2\pi ft dt \approx V_0^2 \approx V_{rms}^2 \quad (24)$$

The integration of V_{rms} is comparable to the total count measurement.

Energy

The energy in an AE signal is proportional to the square of the voltage. Figure 62 presents a schematic of the logic in the D/E Energy Processor. One advantage to this type of signal conditioning is the ability to differentiate an event. Using the damped sine AE signal model, Reference 21 develops a relationship between the energy for the event and counts:

$$u \sim \frac{\tau V_{in}^2}{4} \left(\frac{G_0}{G_n} \right)^2 e^{2\eta\tau/fr} \quad (25)$$

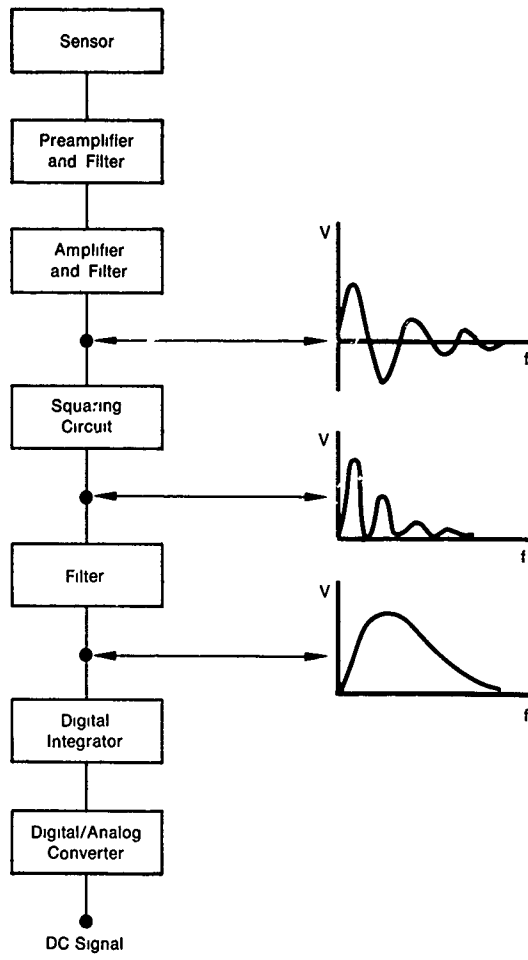
where,

V_{in} = counter threshold
 G_0, G_n = processor and counter gains, respectively
 η = counts per event

There are several ways to evaluate τ for use in the above models. If η for a given event is known at two different gain settings, then τ can be calculated. From equation 21:

$$\eta_1 - \eta_2 = fr \left[\ln \left(\frac{CG_1}{V_{in}} \right) - \ln \left(\frac{CG_2}{V_{in}} \right) \right] = fr \ln \left(\frac{G_1}{G_2} \right) \quad (26)$$

However, it is not possible to determine a single value of τ for all techniques used. Therefore, the general use of relationships such as equation 25 have limited value at this time



FD 175146

Figure 62. Schematic Representation of Components in Energy Measuring Device

Amplitude Distribution Analysis

The amplitude distribution analysis is an important mode of AE signal processing. The Dunegan/Endevco 920/921 Distribution Analyzer characterizes the transduced signal according to the peak amplitude of the signal. The linear AE signal is converted to a logarithmic signal, thereby creating a wide dynamic range. The log amplification characteristics of the system are given in Figure 63. The log amp output is peak-detected to derive a dc voltage proportional to the log of the peak amplitude of the signal. An analog to digital converter then outputs to the 920 Distribution Analyzer a series of 0 to 100 pulses that represents the peak amplitude in dB, with 1 dB resolution.

The peak amplitude distribution function $E(V_o)$ is the number of events with amplitudes exceeding a given voltage value V_o . It is of the form.

$$E(V_o) = kV_o^b \quad (27)$$

The terms k and b are constants for a given increment of loading on a structure. A decrease in b indicates higher amplitude events and therefore, impending failure. The term b might also be independent of the distance between source and transducer (Reference 23).

The logic of the Dunegan/Endevco 921 Amplitude Detector is that each pulse (count) represents the ratio of the input signal, in dB, referenced to $100 \mu V$. The input signal and output count are related by:

$$\text{count} = 20 \log \left(\frac{V_{in}}{100 \mu V} \right) \quad (28)$$

The conversion time in this system is 1 msec plus $20 \mu\text{sec}$ per dB.

Pulse Width

The pulse-width distribution analyzer counts the time that the envelope processor is energized, i.e., pulse width per event. The pulse width on the D/E 920 is defined as

$$PW_{AE} = (\text{Slot Number}) \times \text{Multiplier} \times 10 \mu\text{sec} \quad (29)$$

An event is defined as follows: the processor is energized at the first pulse of a burst. It remains energized during the burst and stays energized for the envelope time period selected after the last pulse of the burst above threshold. The end of the envelope time is defined as the end of an event. The total time that the processor is energized is the burst pulse width (see Figure 64). Four envelope times are available: $50 \mu\text{sec}$, $100 \mu\text{sec}$, 1 msec , and 10 msec .

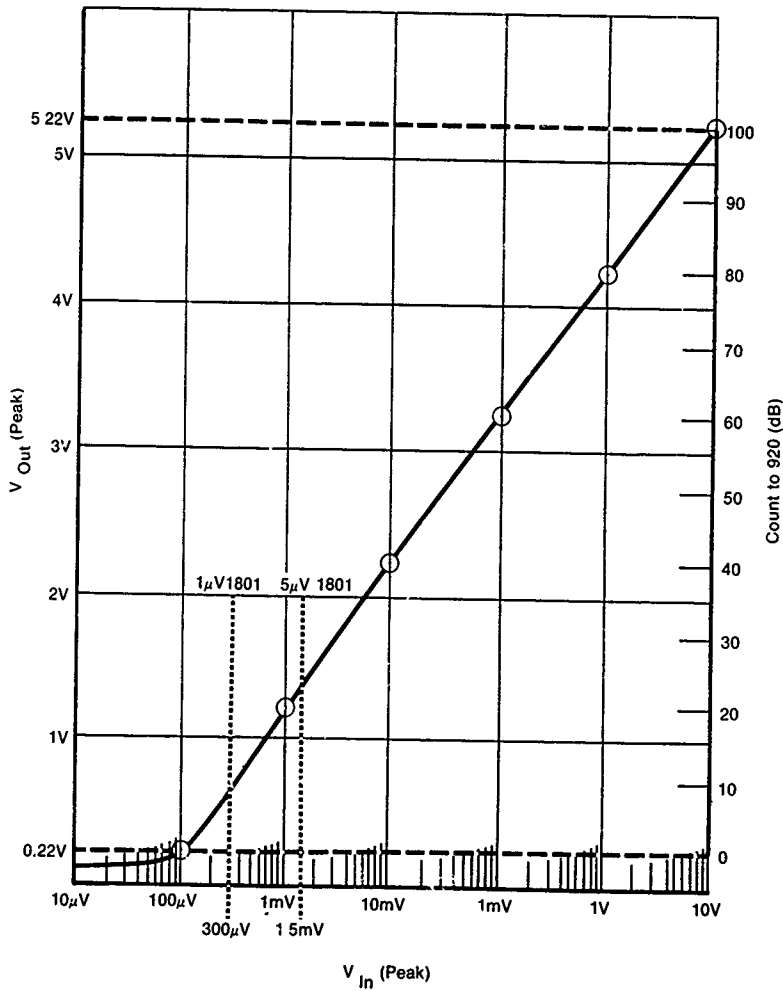
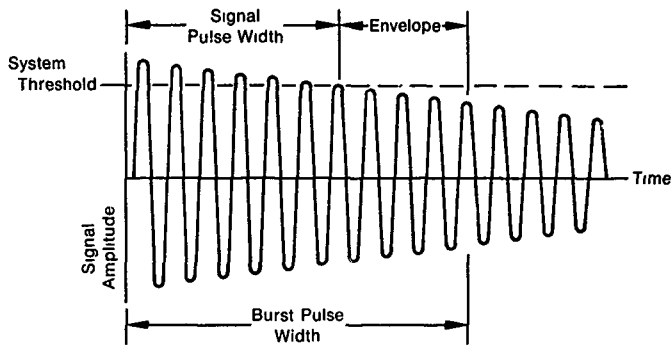


Figure 63. Log Amplification Characteristics of Dunegan/Endevco 920/921 Amplitude Distribution Analyzer

FD 175147



FD 175148

Figure 64 Burst Time Pulse Width Composed of Signal Pulse Width Plus Envelope Time (Manually Selected as 50 μ sec, 100 μ sec, 1 msec, 10 msec)

INSTRUMENTATION AND SIGNAL PROCESSING

The instrumentation used to monitor AE in Phase I of this contract is schematically illustrated in Figure 65

Acoustic Emission Sensor and Preamplifier

The primary transducer being used at the Materials Engineering and Technology Laboratory is the Dunegan/Endevco Model D750, with a 750 kHz peak resonant frequency. This transducer has been found to provide optimum sensitivity to fracture events in IN100.

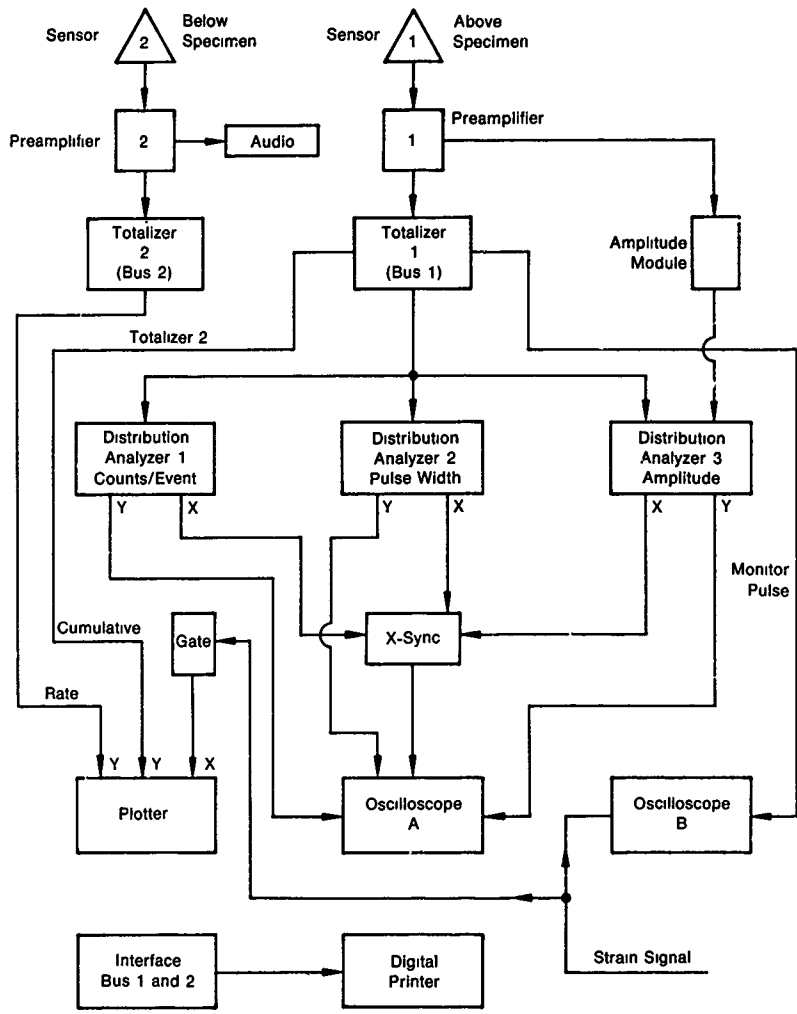
The D750 converts mechanical stress waves to electrical signals through a piezoelectric crystal. Frequency response is shown in Figure 66. Dunegan/Endevco's patented differential design, incorporated into the D750, helps isolate the sensor signal from electrical noise.

The sensor and a Dunegan/Endevco Model 801-P Preamplifier are connected with a short length (2 ft) of shielded cable. When used with a differential transducer, the 801-P provides 40 dB rejection of common-mode noise while supplying 40 dB gain to the processed signal. Internal noise is less than 6 μ volts.

Totalizer

An AE signal is further processed in the Totalizer (Dunegan/Endevco Model 301) through amplifications up to 60 dB and bandpass filtering.

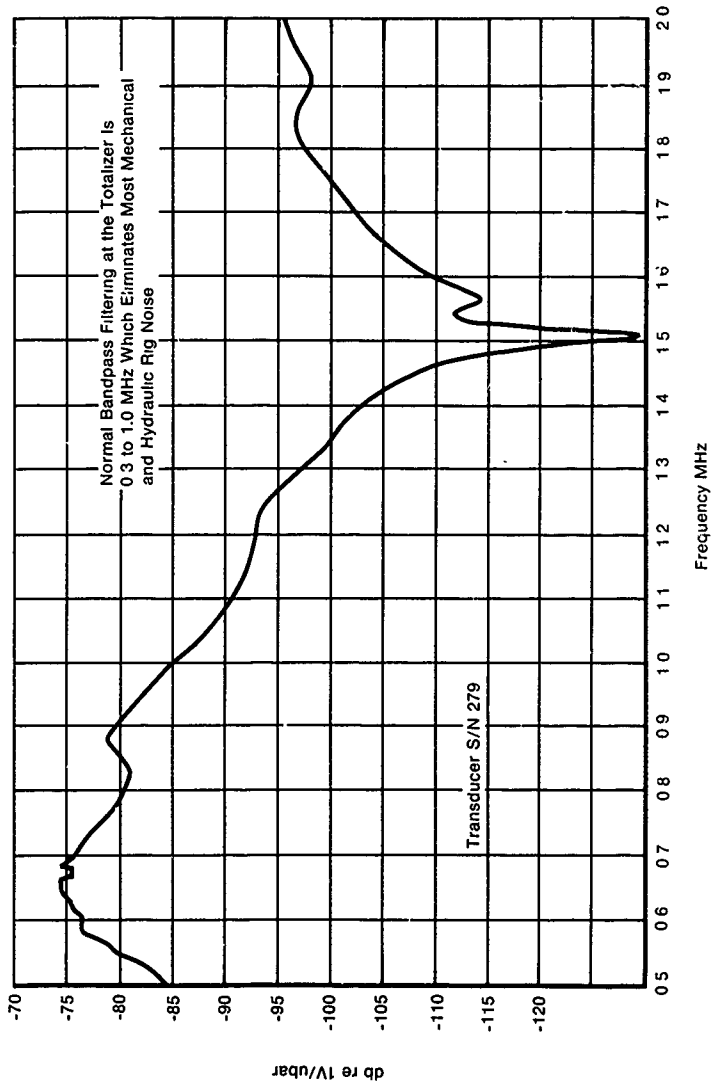
The Totalizer digitally displays the amount of processed AE in a cumulative or rate form (when the signal is gated). A dc output is also provided to drive an x-y recorder.



Power Supplies 1, 2 and 3 and Interconnect Cables Not Shown

FD 175149

Figure 65. Acoustic Emission Configuration to Monitor Strain Control Tests Phase I. Acoustic Emission Characterization of Fatigue Damage



FD 75150

Figure 66. Typical Frequency Response of a Dunegan/Endevco Model D750 Transducer

Distribution Analyzer Operation and Output

The FMDL has three Dunegan/Endevco Model 920 Distribution Analyzers, each capable of sorting AE events according to the number of ringdown counts, time duration, or peak amplitude of the event. The analyzers are also able to perform one-dimensional source location between two sensors by sorting the difference of arrival times of conditioned AE events.

Analyzer output is divided into 101 slots, with each of the slots 1 to 99 representing 1% of the full scale output and slot absolute values being additive from left to right as shown in Figure 67. Slots 0 and 100 are "catch-all" slots for event values which are less than 1% of full scale and greater than or equal to full scale, respectively. Slot values 0 to 100 are always presented along the x-axis of an output.

The number of events at each slot location are registered along the y-axis of the analyzer output, with a linear and logarithmic output capability. In addition, summation of events from right to left is also possible in the output.

Analyzer operation is optimized through use of a multiplier and variable signal envelope. The multiplier is capable of expanding the full X-range by three orders of magnitude. Signal envelope is the time duration after ringdown of a processed AE event before the system resets to receive another signal. Envelope times from 50 μ sec to 10 msec may be selected.

Figure 67 illustrates a typical registry for ringdown counts (top), pulse width (middle), and peak amplitude (bottom). Two events are registered in the ringdown counts number 0 slot (multiplier is 10). Therefore, the ringdown counts in each of these events were less than 10.

Pulse-width registry output incorporates emission pulse width plus envelope time to yield the total burst pulse width shown in Figure 64. Two events are registered in the burst pulse width 1.1 msec slot (multiplier is 10) in Figure 67. The envelope time was selected as one msec so the AE pulse width-to-ringdown below a predetermined amplitude threshold is between 0.1 and 0.2 msec.

Amplitude registry covers the range 0 to 100 dB peak amplitude (multiplier not applicable). Amplitude levels in Figure 67 span 22 to 43 dB. An amplitude threshold of 22 dB was chosen for this test.

The Model 920 Distribution Analyzer is also capable of spatial filtering within the slot locations 0 to 100. This function is especially important when a particular amplitude range, pulse width, etc., is characteristic of a phenomenon which the test engineer wants to observe.

The analyzer output may be displayed on an oscilloscope, as in Figure 67, or on an x-y plotter. The output may also be input to a computer for further processing.

REFERENCE — F100 1st STAGE TURBINE DISK

1. Hill, R. J., "Report with Recommendations on Turbine Engine Component Fatigue Life Prediction," Air Force Materials Laboratory, Wright-Patterson AFB, December 1974.
2. Buckley, M. J., "The Future Economic Role of NDE," IEEE Transactions on Sonics and Ultrasonics, Vol. SU-23, No. 5, September 1976.
3. Johnson, D. P., "Cost Risk Optimization of Nondestructive Inspection Level," Electric Power Research Institute Technical Report 5(217-1) September 1975.
4. Johnson, D. P., "Inspection Uncertainty: The Key Element in Nondestructive Inspection," Electric Power Research Institute Technical Report 1(117-1) May 1975.
5. Annis, C. G., R. M. Wallace, and D. L. Sims, "An Interpolative Model for Elevated Temperature Fatigue Crack Propagation," AFML-TR-76-176 part I, November 1976.
6. Annis, C. G., R. M. Wallace, and D. L. Sims, "An Interpolative Model for Elevated Temperature Fatigue Crack Propagation," AFML-TR-76-176, part II, November 1976.
7. Sims, D. L., C. G. Annis, and R. M. Wallace, "Cumulative Damage Fracture Mechanics at Elevated Temperatures," AFML-TR-76-176, part III, November 1976.
8. "Acoustic Emission Multiparameter Distribution Analyses of the Gas Turbine Alloy, IN100," submitted as 1st interim report for AFML Contract F33615-76-C5172, for period 1 April 1976 to 30 April 1977.
9. Wallace, R. M., M. C. VanWanderham, "Applications of Acoustic Emission During Jet Engine Development," Pratt & Whitney Aircraft, Florida Research and Development Center, October 1974.
10. McMasters, R. C., ed., *Nondestructive Testing Handbook*, Vols. I and II, Society for Nondestructive Testing, Roland Press, 1963.
11. "Evaluation of Acoustic Emission, Eddy Current and Fluorescent Penetrant Inspection of Fatigue Damage in the Gas Turbine Alloy, IN100," submitted as 2nd interim report for AFML Contract F33615-76-C5172, for period 1 May 1977 through 31 December 1977.
12. Harris, D. O. and H. L. Dunegan, "Continuous Monitoring of Fatigue Crack Growth by Acoustic Emission Techniques," Dunegan/Endevco TRDE-73-2, January 1973.
13. Radon, J., A. Pollock, "Acoustic Emissions and Energy Transfer During Crack Propagation," *Engineering Fracture Mechanics*, 1972, Vol. 4, pp. 295-310.
14. Harris, D., R. Bell, "The Measurement and Significance of Energy in Acoustic Emission Testing," Dunegan/Endevco TRDE-74-3A, September 1974.
15. Pollock, A. A., "Acoustic Emission Amplitudes" pp. 264-269, *Nondestructive Testing*, October 1973.
16. James L., W. Anderson, "A Simple Experimental Procedure for Stress Intensity Factor Calibration," *Engineering Fracture Mechanics*, 1969, Vol. 1, pp. 565-568.

17. Tetelman, A. S., "Acoustic Emission and Fracture Mechanics Testing of Metals and Composites," Contract DAH-04-68-C-0008, TR No. 7, July 1972.
18. Bell, R. L., "Acoustic Emission Transducer Calibration -- Transient Pulse Method," Dunegan/Endevco Corp., TRDE-73-3.
19. Ono, K., "Acoustic Emission and Microscopic Deformation and Fracture Processes," Contract N00014-69-A-0200-4031, UCLA-ENG-7465, September 1974.
20. Wallace, R., "Acoustic Emission Technology Status Report -- 1972," Pratt & Whitney Aircraft FMDL 17432, 29 January 1973.
21. Harris, D. O. and R. L. Bell, "The Measurement and Significance of Energy in Acoustic Emission Testing," Dunegan/Endevco Corp., TRDE-74-3A, September 1974.
22. Copper, G. R. and C. D. McGillen, *Methods of Signal and Systems Analysis*, pp.131,362, Holt, New York, 1967.
23. Harris, D. O., "Analytical Techniques Relating Acoustic Emission to Fracture," Science Applications, Inc., SAI/SR-119-PA.